UNIVERSIDADE ESTADUAL DE CAMPINAS

Instituto de Física *Gleb Wataghin*

LUÍSA TOLEDO TUDE

RANDOM WALK AND BROWNIAN MOTION IN THE RELATIVISTIC AND IN THE QUANTUM REGIME

Passeio Aleatório e Movimento Browniano nos Regimes Relativístico e Quântico

Campinas

2020

LUÍSA TOLEDO TUDE

Random Walk and Brownian Motion in the Relativistic and in the Quantum Regime

Passeio Aleatório e Movimento Browniano nos Regimes Relativístico e Quântico

Dissertação apresentada ao Instituto de Física Gleb Wataghin da Universidade Estadual de Campinas como parte dos requisitos exigidos para a obtenção do título de Mestre em Física, na área de Física.

Dissertation submitted to the Gleb Wataghin Institute of Physics of University of Campinas in fulfillment of the requirements for the Master's degree in Physics, in the field of Physics.

Supervisor/Orientador: Marcos César de Oliveira

ESTE EXEMPLAR CORRESPONDE À VERSÃO FINAL DA DISSERTAÇÃO DE MESTRADO DEFENDIDA PELA ALUNA LUISA TOLEDO TUDE E ORIENTADA PELO PROF. DR. MARCOS CÉSAR DE OLIVEIRA.

Campinas
2020

Ficha catalográfica
Universidade Estadual de Campinas
Biblioteca do Instituto de Física Gleb Wataghin
Lucimeire de Oliveira Silva da Rocha - CRB 8/9174

Tude, Luisa Toledo, 1995-
T81r Random walk and Brownian motion in the relativistic and in the quantum regime / Luisa Toledo Tude. – Campinas, SP : [s.n.], 2020.

Orientador: Marcos César de Oliveira.
Dissertação (mestrado) – Universidade Estadual de Campinas, Instituto de Física Gleb Wataghin.

1. Movimentos brownianos. 2. Passeio quântico. 3. Relatividade (Física). 4. Temperatura. 5. Passeios aleatórios (Matemática). I. Oliveira, Marcos César de, 1969-. II. Universidade Estadual de Campinas. Instituto de Física Gleb Wataghin. III. Título.

Informações para Biblioteca Digital

Título em outro idioma: Passeio aleatório e movimento Browniano nos regimes relativístico e quântico
Palavras-chave em inglês:
Brownian movements
Quantum walk
Relativity (Physics)
Temperature
Random walks (Mathematics)
Área de concentração: Física
Titulação: Mestra em Física
Banca examinadora:
Marcos César de Oliveira [Orientador]
Marcus Vinicius Segantini Bonança
Renato Portugal
Data de defesa: 03-09-2020
Programa de Pós-Graduação: Física

Identificação e informações acadêmicas do(a) aluno(a)
- ORCID do autor: https://orcid.org/0000-0002-4058-2274
- Currículo Lattes do autor: http://lattes.cnpq.br/0497724905485404

MEMBROS DA COMISSÃO JULGADORA DA DISSERTAÇÃO DE MESTRADO DE **LUÍSA TOLEDO TUDE - RA 156456** APRESENTADA E APROVADA AO INSTITUTO DE FÍSICA "GLEB WATAGHIN", DA UNIVERSIDADE ESTADUAL DE CAMPINAS, EM 3 / 09 / 2020.

COMISSÃO JULGADORA:

- Prof. Dr. Marcos César de Oliveira – Orientador – DFMC/IFGW/UNICAMP
- Prof. Dr. Renato Portugal – LNCC
- Prof. Dr. Marcus Vinicius Segantini Bonança – DFMC/IFGW/UNICAMP

OBS.: Ata da defesa com as respectivas assinaturas dos membros encontra-se no SIGA/Sistema de Fluxo de Dissertação/Tese e na Secretaria do Programa daUnidade.

CAMPINAS
2020

À minha mãe.

Acknowledgments/Agradecimentos

Agradeço aos meus familiares e amigos de São José dos Campos, por todo o apoio e compreensão durante os meus anos de mestrado. Em especial agradeço à minha mãe, Marta, por sempre tentar me entender e me apoiar incondicionalmente e a meu pai e meu irmão por todas as conversas e conselhos.

Sou muito grata também aos amigos que conheci na UNICAMP e presenciaram de perto as fases que vivi até a conclusão desta etapa. Às pessoas que dividiam república comigo agradeço pelo compartilhamento, não só dos espaços físicos, mas também de momentos e aprendizados que vou levar sempre comigo. Sem a segurança e apoio de todas estas pessoas o processo de construção deste trabalho teria sido mais difícil e solitário.

Aos meus amigos Aline, Roberto, Davi, Marina, Pedro e Flávia agradeço pelos conselhos e discussões que envolveram diretamente o tema da dissertação. E aos professores com quem tive contato durante os anos de mestrado sou grata por todo o conhecimento que me ajudaram a adquirir.

Gostaria de agradecer também ao meu orientador professor Dr. Marcos César de Oliveira por toda ajuda e tempo que passou discutindo sobre os assuntos que permeiam esta dissertação e aos integrantes do meu grupo de pesquisa pelas conversas sobre física.

Por fim, gostaria de agradecer também ao financiamento do CNPq que possibilitou o desenvolvimento deste projeto.

Abstract

Brownian motion is defined as the irregular motion of particles immersed in a fluid and can be obtained by the continuum limit of the simple random walk. From the position probability density function of a particle subjected to that motion, information about the fluid, such as its temperature, can be obtained. In this work, we analyze the Brownian motion in the relativistic regime. Previous proposals for position and velocity probability distributions of the Brownian particle are analyzed and, particularly, we propose our own approach to the problem based on the Jaynes maximal entropy principle. In addition, we analyze quantum walks, its asymptotic limit, and the concept of temperature for two and three-state quantum walks. We calculate the Gibbs temperature of the three-state quantum walk and checked that in the asymptotic limit it also respects the definition of entanglement temperature. We also study the frontier of quantum and random walks through decoherence, the connection between quantum walks and relativistic dynamics by means of the continuum limit, and the mathematical connections between the diffusion and Schrodinger equation and between the telegraph and Dirac equation.

Resumo

O movimento Browniano é definido como movimento irregular de partículas imersas em um fluido e pode ser obtido a partir do limite continuo do passeio aleatório simples. A partir da função densidade de probabilidade de posições de uma partícula sujeita a tal movimento, informações sobre o fluido, tal como sua temperatura, podem ser obtidas. Neste trabalho analisamos o movimento Browniano no regime relativístico. Propostas de distribuição de probabilidade de posição e velocidade da partícula Browniana são analisadas e, em particular, propomos nossa própria abordagem para o problema, embasada no princípio de máxima entropia de Jaynes. Além disso analisamos passeios quânticos, seu limite assintótico e o conceito de temperatura em passeios de dois e três estados. Calculamos a temperatura temperatura de Gibbs para o passeio de três estados e checamos que no limite assintótico esta tambem respeita a definição de temperatura de emaranhamento. Também estudamos a fronteira entre passeios quânticos e passeios aleatórios através de decoerência, a conexão entre passeios quânticos e a dinâmica relativística através do limite continuo e a conexão matematica entre as equações de difusão e de Schrodinger e entre as equações do telegrafo e de Dirac.

Contents

CHAPTER 1

Introduction

The Scottish botanist Robert Brown (1773-1858), when studying pollen particles suspended on water, noticed an irregular motion. In 1828 he published his work, Brown (1828), suggesting that the motion was due to the collisions with the smaller molecules of the liquid and not because it consisted of a living system, as it was believed at that time. This discovery was the starting point for a series of studies and experiments. However, it was only in 1905 that the so called Brownian motion was mathematically described. The explanation about the origin of the random motion of the Brownian particles played an important role in the acceptance of the existence of atoms and molecules, which is one of the most important human discoveries about Nature. The atomic theory is so relevant that the physicist Richard Feynman wrote the following words in his book Feynman Lectures of Physics, Feynman et al. (2011)

> *"If, in some cataclysm, all of scientific knowledge were to be destroyed, and only one sentence passed on to the next generation of creatures, what statement would contain the most information in the fewest words? I believe it is the atomic hypothesis (or the atomic fact, or whatever you wish to call it) that all things are made of atoms — little particles that move around in perpetual motion, attracting each other when they are a little distance apart, but repelling upon being squeezed into one another. In that one sentence, you will see, there is an enormous amount of information about the world, if just a little imagination and thinking are applied."*

In addition to the consolidation of the atomic theory, the discussion that involves Brownian motion and its connection with the diffusion theory has a fundamental role in the interpretation of several natural phenomena, such as the propagation of heat, the comprehension of noise in electrical systems, and the dynamics of

chemical reactions. Furthermore, the mathematical tools developed to describe the Brownian motion have application in many other areas of knowledge such as biology, economy, and engineering.

Naturally, when the special relativity theory was formulated, the physicists started to wonder what would be the consequences of that discovery for other fields of theoretical physics. Regarding the Brownian motion, it is straightforward that the usual distribution, obtained by a Markovian model, is not consistent, since it allows superluminal positions/velocities. Besides that, the molecular models that describe the behavior of the molecules of the fluid also needed to be reviewed. The relativistic generalization of Brownian motion and the thermodynamics of the medium it is immersed in generated an intense debate on the scientific community in the last decades. With this historical background in mind, one realizes that the field of relativistic Brownian motion is still in development and that the concepts related to relativistic diffusion will play an important role in future theoretical investigations. Some of the systems that can be approximated by the relativistic Brownian models, known today, are related to high energy collisions —quark-gluon plasma— and to thermalization and relaxation in astrophysics.

The description of Brownian motion can also be derived by the continuum limit of the simple random walk. The relativistic generalization of random walks does not provide many insights, but its quantum generalization does. A quantum walk is the quantum counterpart of random walks, and its applications concern developing faster search algorithms and simulation of analogous systems. With the increase of interest in the field of quantum computation, the theoretical and experimental domain of quantum walks became a key ingredient to the performance of quantum algorithms.

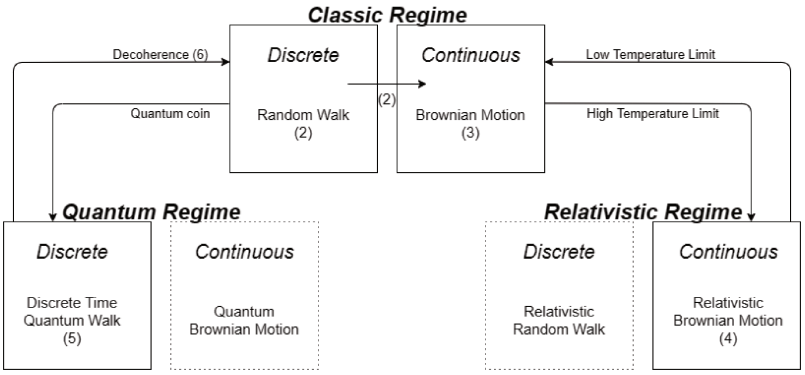

Figure 1.1: Diagram illustrating the topics that are analyzed in the dissertation.

In this work, we are interested in the relations between discrete and continuous stochastic processes and the classical, relativistic, and quantum regimes. Particularly, we are also interested in what concerns the temperature of the processes. The dissertation is divided into three main parts, one dedicated to each regime (classical, relativistic, and quantum). Figure 1.1 displays an illustrative scheme of the main topics covered in the dissertation. The solid squares present the subjects discussed by us, while the subjects inside the dotted squares are not

part of the scope of the dissertation. The numbers between parentheses indicate the chapters where we analyze the topics. In the next two chapters of the dissertation (2, 3) we cover the classical non-relativistic aspect of Brownian motion and random walks. The second chapter is devoted to the introduction of some important definitions and some approaches to connect the simple random walk and Brownian motion, i.e, the asymptotic, and continuum limits. The third chapter concerns the Brownian motion and we present different approaches that lead to the same probability density function of positions, a Gaussian distribution.

The relativistic regime is treated in chapter 4. Since it is not possible to derive a continuous relativistic Markov process in position space, the usual approaches found in the literature to analyze a relativistic version of Brownian particle are

- Derivation of a relativistic diffusion propagator in position space;
- Generalization of the Langevin equation.

In section 4.1 we analyze attempts to describe the motion using the first strategy and propose our own attempt. Our relativistic propagator, obtained by Jaynes principle, respects the limit of the speed of light and is equal to the propagator obtained by Dunkel et al. (2006) plus a constant. This difference is discussed in the conclusions of chapter 4. In section 4.2 using the second strategy we present the relativistic Langevin equation derived by Dunkel and Hanggi (2005) and analyze the generalization of the relativistic binary collision model through simulations. Our simulations seem to be in accordance with Jüttner distribution of velocities.

In what concerns the relativistic regime, at last, in chapter 5, we also analyze the mathematical resemblance via analytic continuation between differential equations that describe the evolution of the probability distribution of stochastic processes with quantum evolution as given by the Schrödinger and Dirac equations.

The analyses of the quantum regime begin in chapter 6. The main applications of the research of quantum walks involve building quantum algorithms. Search algorithms based on quantum walks are quadratically faster than classical algorithms due to the fact that the standard deviation of a quantum walk grows linearly with time, while for a classical random walk $\sigma \propto \sqrt{t}$. We begin in chapter 6 by making an overview of the definition of a discrete-time quantum walk on an infinite line and then, we study it as an open system, considering only the coin space. In that context, we look for the asymptotic limit and study the meaning of an entanglement temperature, i.e, a temperature associated with von Neumann's entropy. From that analysis, an original work was developed where we calculated the asymptotic reduced density matrix of a three-state quantum walk and the asymptotic temperature in an analogous way. We checked that for the two and three state quantum walk, in the asymptotic limit, the entanglement temperature is equivalent to the one of a Gibbs state. This happens because the system achieves a thermal equilibrium with its environment respecting the canonical ensemble.

We analyzed the limit between quantum and random walks through decoherence processes (chapter 7). In this part, our original contribution was the extension of decoherence models of the two-state quantum walk to

the three-state quantum walk. As in the two-state quantum walk, the decoherence makes the distribution of the three-state walk transit to a Gaussian, however by introducing the decoherence by broken links we see that the main property of the three-state quantum walk, which is the localization, is preserved.

In chapter 8 we analyzed the continuum limit of quantum walks with and without considering the interference term. Through the continuum limit of the discrete time quantum walk with the interference term, we studied the mathematical connections between quantum walks and the relativistic quantum equations that describe the motion of free particles. And finally in Chapter 8 we present our conclusions.

CHAPTER 2

Stochastic Processes and Random Walks

This chapter is devoted to the introduction of concepts of the stochastic theory and the definition and analysis of the random walk. The continuum and asymptotic limits of the random walk, presented in the last sections of the chapter, connect the discrete random process with its continuum version, the Brownian motion.

The concepts introduced here will gain physical meaning in later chapters, but the mathematical structure may have many other interpretations. This is why the theory of stochastic processes is useful in different areas of research, such as chemistry, biology, engineering, and economy.

2.1 Definitions

The main goal of this section is to set the definitions of the concepts we will use later on. Although we might have some intuition about some of these definitions and do not use them in a direct way, it is important to have them well established as we go through the calculations.

A **random variable** is a (measurable) function from the space of possible results of an experiment, ϵ, to the interval $I = [0,1] \in \mathbb{R}$,

$$X : \epsilon \xrightarrow[x \mapsto p(x)]{} I, \tag{2.1}$$

with the probability of the whole set being $p(\epsilon) = 1$.

A **stochastic process** is defined as a family of random variables $X = \{X_t, t \in T\}$, where the index t represents the random variable at different times. When the index t is discrete, we can classify the process as follows. It is said to be a **purely random process** if the conditional probability density of X_t does not depend on the values X_i, $i < t$, of the random variable at earlier times. In this case, the conditional probability density can be written

as

$$P(x_t|x_{t-1},..,x_1) = P(x_t). \tag{2.2}$$

A stochastic process is said to be a **Markov process** if the conditional probability density depends only on the last earlier time, such that

$$P(x_t|x_{t-1},..,x_1) = P(x_t|x_{t-1}). \tag{2.3}$$

If the process depends on the last two most recent values of x it is called a **second order Markov process**. Analogously, other higher order Markov processes can also be defined. The book *Principles of Random Walk*, Spitzer (1970), defines a **random walk** in the following way:

Let R be a d-dimension space of integers, such that if $x \in R$ we can write[1]

$$\mathbf{x} = (x^1, x^2, ..., x^d),$$

than for each $\mathbf{x}, \mathbf{y} \in R$ we define a real function, $\mathbb{P}(\mathbf{x}, \mathbf{y})$, called **transition function** of the random walk with the following property,

$$\begin{cases} 0 \leq \mathbb{P}(\mathbf{x}, \mathbf{y}) = \mathbb{P}(\mathbf{0}, \mathbf{y} - \mathbf{x}) \ ; \\ \sum_{x \in R} \mathbb{P}(\mathbf{0}, \mathbf{x}) = 1, \end{cases} \tag{2.4}$$

where $\mathbf{y} - \mathbf{x} = y^i - x^i$, $i = 1, 2, ..., d$. The property that $\mathbb{P}(\mathbf{x}, \mathbf{y}) = \mathbb{P}(\mathbf{0}, \mathbf{y} - \mathbf{x})$, is called spacial homogeneity and it shows that the transition function can be described by a single function $p(\mathbf{x}) = P(0, \mathbf{x})$, such that by consequence of Eq.(2.4),

$$\begin{cases} 0 \leq p(\mathbf{x}) \ ; \\ \sum_{\mathbf{x} \in R} p(\mathbf{x}) = 1. \end{cases} \tag{2.5}$$

Then a **random walk** is defined by a transition function, $p(\mathbf{x})$, that has the properties (2.5) defined for each $\mathbf{x}$ on R. This function represents the probability of a displacement $\mathbf{x}$ of a walker that walks on the elements of R. The spacial homogeneity means that the probability is invariant for spacial translations, i.e, the probability related to the movements of the walker depends only on the size of the step, but not on his previous location. Comparing the transition function of the random walk with the definition of a Markovian stochastic process it is easy to see that, by definition, a random walk is a stochastic Markov process.

Let us consider a random walker, who is initially at the origin of R. At each step he moves an amount $\mathbf{x_n}$, chosen from the probability $p(\mathbf{x})$ of Eq.(2.5), this means that the steps are **independent and identically distributed (iid)**. We can define a variable,

$$\mathbf{X_N} = \sum_{n=0}^{N} \mathbf{x_n}, \tag{2.6}$$

[1] The bold letters represent vectors on the d- dimensional space.

which is the position of the walker after N steps. To avoid confusion due to notation, from now on (in this chapter) we are always going to use capital letters to designate the position of the walker and small letters to the steps.

In figure 2.1 two types of random walks are presented; at figure a the path of (a) 1000 step simple walk in two dimensions is seen while on (b) we have a simulation of five Cauchy walks in one dimension. The second one is a random walk with transition function $\mathbb{P}(\mathbf{0},\mathbf{x}) = \frac{A_n}{a_n^2+x^2}$ (a_n is a positive sequence). Since the analysis of the simple random walk and its asymptotic limit is the main interest of this chapter, it will be better explained below.

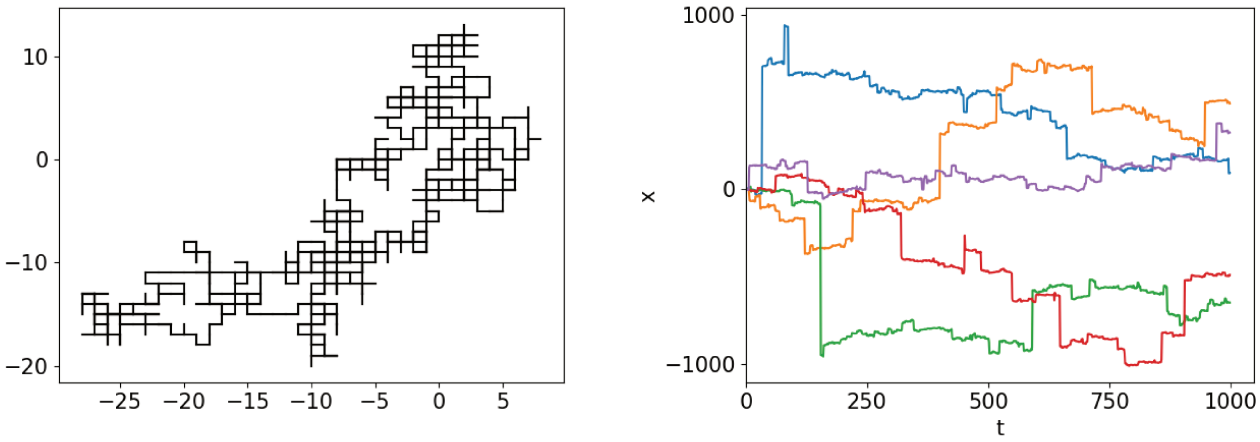

(a) Random walk.

(b) Cauchy walks.

Figure 2.1: Simulation of 1000 time steps for the simple random walk in two dimensions and for five Cauchy walks in one dimension.

We call simple random walks or Bernoulli's walks the random walks with transition function

$$\begin{cases} \mathbb{P}(\mathbf{0},\mathbf{x}) = \frac{1}{2d} & \text{if } |x| = 1; \\ \mathbb{P}(\mathbf{0},\mathbf{x}) = 0 & \text{otherwise,} \end{cases} \tag{2.7}$$

where $|\mathbf{x}|$ is the norm

$$|\mathbf{x}| = \left[\sum_{i=1}^{d} (x^i)^2 \right]^{1/2}. \tag{2.8}$$

In one dimension the simple random walk is equivalent to a walker that chooses which side he will take a step by flipping a coin. The exact solution of the probability distribution of the walker's position after N steps can be obtained by the following procedure, where, to simplify, we assume that the size of each step is 1. Suppose that after flipping the coin N times the walker took n steps to the right and $m = (N-n)$ to the left, then the distance he moved from the origin is

$$x = n - m = 2n - N \tag{2.9}$$

so $n = \frac{(x+N)}{2}$ and $m = \frac{(N-x)}{2}$. Therefore, if the coin is unbiased, the probability of having N steps, being n to the right and m to the left is $\frac{1}{2^N}$ times the number of sequences with n heads and m tails, i.e,

$$\mathbb{P}_N(X_N = x) = \left(\frac{1}{2}\right)^N \binom{N}{n} = \left(\frac{1}{2}\right)^N \binom{N}{\frac{N+x}{2}}, \tag{2.10}$$

where $\binom{N}{n} = \frac{N!}{n!(N-n)!}$ is the Newton binomial. Fig. 2.2 shows the probability distribution of the walker's position after 100 steps. It is interesting to notice that if the walker starts at the position zero, after an even number of steps the walker has zero probability of being at an odd position and after an odd number of steps the walker has zero probability of being at an even position.

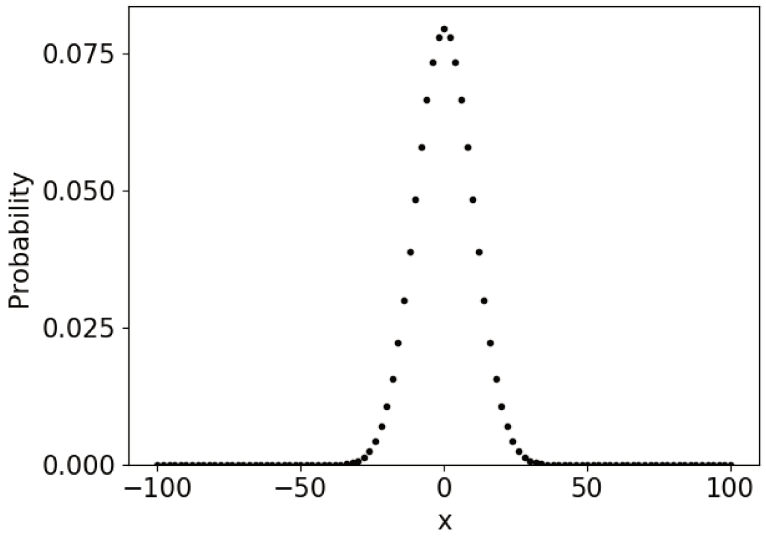

Figure 2.2: Probability distribution of the position of a walker that has initial position at the origin after 100 steps.

2.1.1 Moments and Cumulants

The **moments**, m_n, of a random variable, x, are defined as

$$\begin{aligned} m_1 &= \langle x \rangle, \\ m_2 &= \langle x^2 \rangle, \\ &\vdots \\ m_n &= \langle x^n \rangle. \end{aligned} \tag{2.11}$$

In a multi-dimensional setting, the moments are written as tensors

$$m_n^{(j_1, j_2, \ldots, j_n)} = \langle x_{j1}, x_{j2}, \ldots, x_{jn} \rangle. \tag{2.12}$$

The moments can be used to define physical coefficients such as the **drift** , D_1, and **diffusion**, D_2, coefficients

$$\begin{aligned} D_1 &= \frac{m_1}{\tau} \\ D_2 &= \frac{m_2}{2\tau}, \end{aligned} \tag{2.13}$$

where τ is the time variable. The moments of a variable with distribution $P(x)$ can be obtained using the **moment generating function**, $\hat{P}(k)$. In one dimension this function is given by (Mandel and Wolf (1995)),

$$\hat{P}(k) = \langle e^{kx} \rangle = \int P(x) e^{kx} dx. \tag{2.14}$$

Therefore, by expanding the exponential as a power series and integrating term by term we can write

$$\hat{P}(k) = \sum_{n=0}^{\infty} \frac{k^n m_n}{n!}, \tag{2.15}$$

and the moments are found to be $m_n = (-i)^n \dfrac{\partial^n \hat{P}}{\partial k^n}(0)$. To define the moment generating function of a discrete random variable we replace the integral by a sum over n,

$$\hat{P}(k) = \sum_{x=0}^{\infty} P(x) e^{kx}. \tag{2.16}$$

This equation generates the same moments as the continuous one.

The **characteristic function**, $\hat{C}(k)$, is defined as the Fourier transform of the probability distribution

$$\hat{C}(k) = \langle e^{ikx} \rangle = \int P(x) e^{ikx} dx. \tag{2.17}$$

When $P(x)$ is square integrable, the inverse Fourier transform also exists

$$P(x) = \frac{1}{2\pi} \int \hat{C}(k) e^{-ikx} dk. \tag{2.18}$$

Note that due to the similarity between the characteristic function and the moment generating function, the moments can be derived from the characteristic function on a analogous way. However it is important to point that the characteristic function exists even when the moments do not.

Cumulants are a certain nonlinear combinations of moments. They can be obtained considering a function known as **cumulant generating function**. It is defined as the logarithm of the moment generating function

$$\psi(k) = \log \hat{P}(k). \tag{2.19}$$

And the power series of $\psi(k)$ gives the coefficients known as cumulants, c_n,

$$\psi(k) = \sum_{n=1}^{\infty} \frac{c_n k^n}{n!}. \tag{2.20}$$

The first four cumulants are

$$\begin{aligned} c_1 &= m_1, \\ c_2 &= m_2 - m_1^2 = \sigma^2, \\ c_3 &= m_3 - 3m_1 m_2 + 2m_1^3, \\ c_4 &= m_4 - 3m_2^2 - 4m_1 m_3 + 12m_1^2 m_2 - 6m_1^4. \end{aligned} \tag{2.21}$$

We see that the first and second cumulants are the **mean** and **variance**, respectively. The third and fourth are called **skewness** and **kurtosis**. An important property of the cumulants is its additivity. If we define $\psi(\mathbf{k})$ to be the cumulant generating function of the steps displacement, i.e, the cumulant generating function associated to the transition function, and $\psi_N(\mathbf{k})$ the cumulant generating function associated to the probabilities of final position of a random walk, then

$$\begin{aligned} P_N(\mathbf{x}) &= \int e^{-i\mathbf{k}\cdot\mathbf{x}+N\psi(\mathbf{k})} \frac{d^d\mathbf{k}}{(2\pi)^d} \\ &= \int e^{-i\mathbf{k}\cdot\mathbf{x}+\psi_N(\mathbf{k})} \frac{d^d\mathbf{k}}{(2\pi)^d}, \end{aligned} \tag{2.22}$$

that is

$$\psi_N(\mathbf{k}) = N\psi(\mathbf{k}). \tag{2.23}$$

So the i-th cumulant tensor for the position after N steps is N times the i-th cumulant,

$$c_{i,N} = Nc_i. \tag{2.24}$$

Once the standard deviation (σ) is related to c_2 by $\sigma = \sqrt{c_2}$, and it measures the width of the distribution, after N steps σ_N will have evolved to $\sqrt{Nc_2} = \sigma\sqrt{N}$. And we see that the random walk with iid has square root scaling. This result is very important and will be better explored later on.

Another relevant definition is the one of **central-moments**, which are the expected value of a random variable of a specified integer power of the deviation of the random variable from the mean, i.e.:

$$V_x^{(m)} = \langle (x - \langle x \rangle)^m \rangle = \int (x - \langle x \rangle)^m p(x) dx. \tag{2.25}$$

It is easy to see that, for the simple and unbiased random walk the first three central moments are

$$\begin{aligned} V^{(0)} &= 1 \\ V^{(1)} &= 0 \\ V^{(2)} &= c_2 \end{aligned} \tag{2.26}$$

The third and fourth central-moments are related to skewness and kurtosis, respectively.

2.2 Asymptotic limit of the random walk

In this section, we derive some methods for approximate solutions of the random walk in the asymptotic limit ($N \to \infty$). The content of the analysis is based on the works of Rudnick and Gaspari (2004); Lawler and Limic (2010); Bazant (2000); García-Palacios (2004).

2.2.1 Rayleigh's Solution

The first time the term random walk was used was in 1905 by Karl Pearson in a letter to *Nature* (Bazant (2000)). He wanted to know the distribution of mosquitos on a infestation considering that at each time step the mosquito moves a fixed length at a random angle. Lord Rayleigh answered the letter showing that

$$P_N(R) \approx \frac{2R}{N} e^{-R^2/N}, \tag{2.27}$$

where $\mathbf{R}$ is the distance and N the number of steps. Let us derive a generalization of Lord Rayleigh result for an isotropic random walk with independent identically distributed (i.i.d.) displacements, where $p(\mathbf{x})$ is a transition function of the radial displacement $r = |\mathbf{x}|$ and there is no drift ($\langle \Delta \mathbf{x_N} \rangle = \mathbf{0}$). Therefore the following recursion relation, known as Bachelier's equation, applies

$$P_{N+1}(\mathbf{R}) = \int p(\mathbf{r}) P_N(\mathbf{R}\text{-}\mathbf{r}) d^d\mathbf{r}. \tag{2.28}$$

Eq. (2.28) states that the number of particles at a distance R is given by the number of particles that move from a previous position to another one that is at a distance R from the origin in the latest time step.

As N tends to infinity $P_N(\mathbf{r})$ varies on a length scale which is much larger than common values for r, so we can Taylor expand P_N inside the integral

$$\begin{aligned} P_{N+1}(\mathbf{R}) =& \int p(\mathbf{r}) \left[P_N(\mathbf{R}) - \mathbf{r}\cdot\nabla P_N(\mathbf{R}) + \frac{1}{2}\mathbf{r}\cdot\nabla\nabla P_N \cdot \mathbf{r} + \ldots \right] d^d\,\mathbf{r} \\ =& P_N(\mathbf{R}) - 0 + \frac{1}{2}\sum_i \sum_j \langle r_i r_j \rangle \frac{\partial^2 P_N}{\partial R_i \partial R_j} + \ldots \\ =& P_N(\mathbf{R}) + \frac{1}{2d}\langle \mathbf{r}\cdot\mathbf{r} \rangle \nabla^2 P_N(\mathbf{R}). \end{aligned} \tag{2.29}$$

Assuming the steps are taken at intervals τ such that $t = N\tau$, if we divide the expression by τ we have that

$$\frac{P_{N+1}(\mathbf{R}) - P_N(\mathbf{R})}{\tau} = \frac{\langle r^2 \rangle}{2d\tau} \nabla^2 P_N(\mathbf{R}). \tag{2.30}$$

Defining $P_N(R) = \rho(\mathbf{R}, N\tau)$, in the limit where $N \to \infty$, $\tau \to 0$, and so

$$\frac{\partial \rho}{\partial t} = D\nabla^2 \rho, \tag{2.31}$$

where $D = \frac{\langle r^2 \rangle}{2d\tau}$ is the diffusion coefficient, d is the dimension of the problem and (2.31) is the diffusion equation. To solve this partial differential equation with initial condition $\rho(\mathbf{R}, 0) = \delta(\mathbf{R})$ we take the Fourier Transform

$$\rho(\mathbf{k}, t) = \int e^{-i\mathbf{k}\cdot\mathbf{x}} \rho(\mathbf{x}, t) d^d\mathbf{x}, \tag{2.32}$$

$$\rho(\mathbf{x}, t) = \frac{1}{(2\pi)^d} \int e^{i\mathbf{k}\cdot\mathbf{x}} \rho(\mathbf{k}, t) d^d\mathbf{k}, \tag{2.33}$$

and obtain

$$\rho(\mathbf{R}, t) = \frac{e^{-\mathbf{R}^2/2\langle r^2 \rangle N}}{(2\pi\langle r^2 \rangle N/d)^{d/2}}, \tag{2.34}$$

or

$$P_N(\mathbf{R}) \approx \frac{e^{-d\,\mathbf{R}^2/4Dt}}{(4\pi D t)^{d/2}}. \tag{2.35}$$

We conclude that the long time limit of $P_N(\mathbf{R})$ for an isotropic random walk tends to a Normal distribution, as long as the second moment $\langle r^2 \rangle$ exists.

2.2.2 Recursion relation

Let us call the number of walks that start at x and end up at y, $C(N; x, y)$. Using the notation of section 2.1 $C(N; x, y) = \binom{N}{n}$. Clearly, this number depends on the number of walks whose paths passed to the neighborhood of that point. Therefore if the step size is l we can write

$$C(N; x, y) = C(N-1; x, y-l) + C(N-1; x, y+l). \tag{2.36}$$

To approximate this relation to a differential equation we write

$$\begin{aligned} C(N+1; x, y) =& C(N; x, y-1) + C(N; x, y+1) + 2C(N; x, y) - 2C(N; x, y) \\ =& l^2 \left[\frac{C(N; x, y-1) + C(N; x, y+1) - 2C(N; x, y)}{l^2} \right] + 2C(N; x, y) \\ \approx& l^2 \frac{\partial^2 C(N; x, y)}{\partial y^2} + 2C(N; x, y). \end{aligned} \tag{2.37}$$

We can replace the number of possible walks by the probability that after N steps a walker starting at x ends up at y, $P(N; x, y)$. To do that we use the fact that $C(N; x, y) = 2^N P(N; x, y)$, and

$$P(N+1; x, y) - P(N; x, y) = \frac{l^2}{2} \frac{\partial^2 P(N; x, y)}{\partial y^2}. \tag{2.38}$$

Now, taking the limit $N \to \infty$ and considering that $P(N; x, y)$ is a slowly varying function of N, we can approximate the left hand side of Eq. (2.38) to another derivative, arriving at

$$\frac{\partial P(N; x, y)}{\partial N} = \frac{l^2}{2} \frac{\partial^2 P(N; x, y)}{\partial y^2}, \tag{2.39}$$

which is again the diffusion equation, with Gaussian solution, analogous to Eq. (2.35).

$$P(N;x,y) = \frac{1}{\sqrt{2\pi N}} \exp\left[\frac{-(x-y)^2}{2l^2 N}\right]. \tag{2.40}$$

Comparing this two equations we can identify $N = 2Dt$ and by a simple calculation using the definition of c_2 of section 2.1.1 we arrive at the square root scaling again, that is, $\sigma = \sqrt{2Dt} = \sqrt{N}$.

2.2.3 Central Limit Theorem

The central limit theorem states that if $x_1, x_2, ..., x_N$ is a set of N independent random variables, each having the same probability $p(x)$ with mean μ and variance σ^2, both being finite, then the random variable defined as

$$\frac{\sum_{i=0}^{N} x_i - \mu N}{\sqrt{N}}, \tag{2.41}$$

has normal distribution with variance σ^2 as $N \to \infty$. Once we have enunciated the theorem, we shall proceed to its proof. Our method leads to a multidimensional generalization of this theorem, which is very convenient since we might treat random walk in dimensions greater than one.

Here we are interested in Markovian processes, that is, stochastic processes that are only influenced by its immediate past. In the case of a random walk this means that the probability distribution after N steps, P_N, depends only on the probability distribution of the former step, P_{N-1}. So we write

$$P_N(\mathbf{R}) = \int p_N(\mathbf{r}|\mathbf{R}-\mathbf{r}) P_{N-1}(\mathbf{R}-\mathbf{r}) d^d\mathbf{r}. \tag{2.42}$$

Using the property of spacial homogeneity of the transition function $p_N(\mathbf{r})$ we arrive at the Bachelier's equation again

$$P_N(\mathbf{R}) = \int p_N(\mathbf{r}) P_{N-1}(\mathbf{R}\text{-}\mathbf{r}) d^d\mathbf{r}. \tag{2.43}$$

Denoting $*$ for a convolution it is clear that $P_N = p_N * P_{N-1}$. Since the (2.28) is a recurrence formula

$$P_N = p_N * ... * p_2 * p_1 * P_0, \tag{2.44}$$

where $P_0 = \delta(\mathbf{x})$, is the initial position.

The Convolution Theorem states that the Fourier transform of a convolution of the multiplication of two functions is the multiplication of the Fourier transform of both functions, that is

$$\mathbb{F}[f * g(\mathbf{x})] = \mathbb{F}[f(\mathbf{x})]\mathbb{F}[g(\mathbf{x})]. \tag{2.45}$$

Therefore we can write for the Fourier transform of the probability P_N

$$\hat{P}_N(\mathbf{k}) = \hat{p_1}(\mathbf{k})\hat{p_2}(\mathbf{k})...\hat{p_N}(\mathbf{k}) = \prod_{i=1}^{N} \hat{p_i}(\mathbf{k}), \tag{2.46}$$

which for steps with identical probability distribution simplifies to $\hat{P}_N(\mathbf{k}) = (\hat{p}(\mathbf{k}))^N$. Using the inverse Fourier transform we obtain the PDF of the walker's position

$$P_N(\mathbf{X}) = \frac{1}{(2\pi)^d}\int e^{i\mathbf{k}\cdot\mathbf{X}}(\hat{p}(\mathbf{k}))^N d^d\mathbf{k}. \tag{2.47}$$

Is important to notice that there are two moment generating functions of interest, since $\hat{p}(\mathbf{k})$ is the characteristic function for the displacement x and $\hat{P}_N(\mathbf{k})$ for the position X_N. Therefore we can define a cumulant generating function for each one of this variables. For the steps this function is

$$\psi(\mathbf{k}) = \log\hat{p}(\mathbf{k}) = -ic_1\mathbf{k} - \frac{1}{2}\mathbf{k}\cdot c_2\cdot\mathbf{k} + ..., \tag{2.48}$$

and looking at Eq. (2.46) the additive property of section 2.1.1 is clear.

Now Let us analyze what shape the distribution tends to as $N\to\infty$. To do it we use **Laplace's Method**, which consists on using the fact that for a large N the dominant part of the integral (2.49),

$$P_N(\mathbf{X}) = \frac{1}{(2\pi)^d}\int_{\text{all }\mathbf{k}} e^{i\mathbf{k}\cdot\mathbf{X}+N\psi(\mathbf{k})}d^d\mathbf{k}, \tag{2.49}$$

is around the origin. Thus we can write

$$P_N(\mathbf{X}) \approx \frac{1}{(2\pi)^d}\int_{|\mathbf{k}|<\epsilon} e^{i\mathbf{k}\cdot\mathbf{X}+N\psi(\mathbf{k})}d^d\mathbf{k}. \tag{2.50}$$

Taylor expanding $\psi(\mathbf{k})$ around 0 leads to

$$P_N(\mathbf{X}) \approx \frac{1}{(2\pi)^d}\int_{|\mathbf{k}|<\epsilon} e^{i\mathbf{k}\cdot\mathbf{X}}e^{N(-ic_1\mathbf{k}-\frac{1}{2}\mathbf{k}\cdot c_2\cdot\mathbf{k}+...)}d^d\mathbf{k}, \tag{2.51}$$

and for sufficiently large N we can truncate the series after the second term.

$$P_N(\mathbf{X}) \approx \frac{1}{(2\pi)^d}\int_{\text{all }\mathbf{k}} e^{i\mathbf{k}\cdot(\mathbf{X}-Nc_1)}e^{\frac{N}{2}\mathbf{k}\cdot c_2\cdot\mathbf{k}}d^d\mathbf{k} \tag{2.52}$$

If c_2 is positive definite and symmetric, it is possible to define $\mathbf{w}\equiv\mathbf{k}\cdot\sqrt{Nc_2}$ such that $d^d\mathbf{w} = |\sqrt{Nc_2}|d^d\mathbf{k}$, where if $d>1$, $|\sqrt{c_2}|$ is the determinant of $\sqrt{c_2}$. Then Eq. (2.52) becomes

$$P_N(\mathbf{X}) \approx \frac{1}{(2\pi)^d N^{d/2}|c_2|^{-1/2}}\int e^{i(\mathbf{X}-Nc_1)\cdot(Nc_2)^{1/2}\cdot\mathbf{w}}e^{-\frac{\mathbf{w}^2}{2}}d^d\mathbf{w}. \tag{2.53}$$

Making use of the transformation $\mathbf{Z}\equiv\dfrac{\mathbf{X}-Nc_1}{\sqrt{Nc_2}}$ the integral reduces to

$$P_N(\mathbf{X}) \approx \frac{1}{(2\pi)^d N^{d/2}|c_2|^{-1/2}}\int e^{i\mathbf{Z}\cdot\mathbf{w}}e^{-\frac{\mathbf{w}^2}{2}}d^d\mathbf{w}, \tag{2.54}$$

which is the expression in terms of the multivariate Gaussian distribution. It can be seen as the product of d Gaussian distributions

$$P_N(\mathbf{X}) \approx \frac{1}{N^{d/2}|c_2|^{-1/2}}\int e^{iZ_1w_1}e^{-\frac{w_1^2}{2}}\frac{dw_1}{2\pi}\cdots\int e^{iZ_dw_d}e^{-\frac{w_d^2}{2}}\frac{dw_d}{2\pi}. \tag{2.55}$$

Those integrals are the inverse Fourier transform of the Gaussian, so we can write

$$P_N(\mathbf{X}) \approx \frac{1}{N^{d/2}|c_2|^{-1/2}} \left(\frac{e^{-\frac{z_1^2}{2}}}{\sqrt{2\pi}} \right) \cdots \left(\frac{e^{-\frac{z_d^2}{2}}}{\sqrt{2\pi}} \right). \tag{2.56}$$

Noticing that the transformation from $\mathbf{X}$ to $\mathbf{Z}$ creates a new random variable and calling its probability density function $\phi_N(\mathbf{Z})$ such that $P_N(\mathbf{X})d^d\mathbf{X} = \phi_N(\mathbf{Z})d^d\mathbf{Z}$ we have that

$$\phi_N(\mathbf{Z}) \approx \frac{e^{\frac{-\mathbf{Z}^2}{2}}}{(2\pi)^{d/2}}. \tag{2.57}$$

This is the result of the **Multidimensional Central Limit Theorem** (CLT). In one dimension, making another change from

$$Z = \frac{X - Nc_1}{\sqrt{Nc_2}} \to Z' = \frac{\sum_{i=0}^{N} x_i - \mu N}{\sqrt{N}} \tag{2.58}$$

we recover the result enunciated on the beginning of this section. And making the change of variables back to X we arrive at Eq. (2.40).

2.2.4 Edgeworth expansion

Now Let us see what is the result of the central limit theorem approximation in the one-dimensional case. Equation (2.51) becomes

$$P_N(x) \approx \frac{1}{2\pi} \int_{|k|<\epsilon} e^{ikx} e^{N(-ic_1k - \frac{1}{2}k^2c_2 + \frac{i}{3!}c_3k^3 + \ldots)} d^dk. \tag{2.59}$$

Making the changes of variables: $k = \dfrac{w}{\sigma\sqrt{N}}$ and $z = \dfrac{x - Nc_1}{\sigma\sqrt{N}}$ the new PDF is

$$\phi_N(z) \approx \frac{1}{2\pi} \int_{|k|<\epsilon} e^{iwz} e^{-\frac{w^2}{2}} e^{\left[\frac{(iw)^3\lambda_3}{3!\sqrt{N}} + \ldots \right]} d^dk, \tag{2.60}$$

where $\lambda_i = c_i/\sigma^i$, $i \in \mathbb{N}$. Taylor expanding the exponential on the right of the integral,

$$\phi_N(z) \approx \frac{1}{2\pi} \int_{|k|<\epsilon} e^{iwz} e^{-\frac{w^2}{2}} \left[1 + \left(\frac{(iw)^3\lambda_3}{3!\sqrt{N}} + \ldots \right) + \ldots \right] d^dk, \tag{2.61}$$

and since the Hermite polynomials are defined as

$$\frac{d^n}{dz^n} e^{-\frac{z^2}{2}} = (-1)^n H_n(z) e^{-\frac{z^2}{2}}, \tag{2.62}$$

and

$$\int_{-\infty}^{\infty} (iw)^n e^{-iwz} e^{-\frac{w^2}{2}} = (-1)^n \frac{d^n}{dz^n} \int_{-\infty}^{\infty} e^{-iwz} e^{-\frac{w^2}{2}}, \tag{2.63}$$

we can write the approximation for $\phi_N(z)$ on the asymptotic limit as

$$\phi_N(z) \approx \frac{e^{-\frac{z^2}{2}}}{\sqrt{2\pi}} \left[1 + \frac{\lambda_3}{3!\sqrt{N}} H_3(z) + \frac{\lambda_4}{4!N} H_4(z) + \frac{1}{2N} \left(\frac{\lambda_3}{3!} \right)^2 H_6(z) + O\left(\frac{z^6}{N^{3/2}} \right) \right]. \tag{2.64}$$

This relation, in one dimension, is called **Edgeworth expansion**. The analog expansion for more dimensions is called **Gram-Charlier expansion**.

Since the third momentum of symmetric distributions is an integral of an odd function, $\lambda_3 = 0$. Calculating $\sigma^2 = 1$ and $m_4 = 1$ we get from Eq. (2.21) that $\lambda_4 = -2$ for our case. This leads Eq. (2.64) to

$$\phi_N(z) \approx \frac{e^{-\frac{z^2}{2}}}{\sqrt{2\pi}}\left[1 - \frac{2}{4!N}H_4(z)\right]. \tag{2.65}$$

2.2.5 The Saddle Point Method

Another way of deriving the asymptotic limit of the probability density function (PDF) of the random walk is using the saddle point method. Considering a simple random walk in one dimension, that is, with transition function, $p(m)$, given by Eq. (2.7). The Bachelier's equation in its discrete form is

$$P_N(m) = \sum_{j=-\infty}^{\infty} p(j)P_{N-1}(m-j), \tag{2.66}$$

and the Fourier series of the transition function is

$$\hat{p}(k) = \sum_{m=-\infty}^{\infty} e^{ikm}p(m), \tag{2.67}$$

where k is a continuous variable, so

$$p(m) = \int_{\pi}^{\pi} e^{-ikm}\hat{p}(k)\frac{dk}{2\pi}. \tag{2.68}$$

Using Eq. (2.7) on the series we have

$$\hat{p}(k) = \sum_{m=-\infty}^{\infty} e^{ikm}\frac{1}{2}(\delta_{m,1} + \delta_{m,-1}) = \frac{1}{2}(e^{ik} + e^{-ik}) = \cos(k) \tag{2.69}$$

Due to the result of the convolution theorem, Eq. (2.46) , we can write $\hat{P}_N(k) = cos^N(k)$. Therefore

$$P_N(m) = \frac{1}{2\pi}\int_{-\pi}^{\pi} e^{-ikm}\cos^N(k)dk. \tag{2.70}$$

This integral can be evaluated using contour integration, which leads to the exact solution (2.10). On the other side, to find the asymptotic limit of the integral (2.70) we first use the fact that the integral kernel, $f(k) = e^{-ikm}\cos^N(k)$, is 2π-periodic and $f(k+\pi) = (-1)^{N+m}f(k)$ to rewrite it as follows

$$\begin{aligned} P_N(m) =& \frac{1}{2\pi}\int_{\frac{-\pi}{2}}^{\frac{3\pi}{2}} e^{-ikm}\cos^N(k)dk = \frac{1}{2\pi}\left(\int_{\frac{-\pi}{2}}^{\frac{\pi}{2}} + \int_{\frac{\pi}{2}}^{\frac{3\pi}{2}}\right)e^{-ikm}\cos^N(k)dk \\ =& \frac{[1+(-1)^{N+m}]}{2\pi}\int_{\frac{-\pi}{2}}^{\frac{\pi}{2}} e^{-ikm}\cos^N(k)dk \\ =& \frac{[1+(-1)^{N+m}]}{2\pi}\int_{\frac{-\pi}{2}}^{\frac{\pi}{2}} e^{-Nf(k,\eta)}dk, \end{aligned} \tag{2.71}$$

where $f(k,\eta) = ik\eta - \log[\cos(k)]$ and $\eta = m/N$. Now we can use the saddle point method on the last integral. The method consists of noticing that, as $N \to \infty$, the dominant contribution to the integral comes typically from the

point where $|e^f| = e^{\mathbb{R}\mathrm{e}f}$ attains its maximum. Of course, the imaginary factor can provide large cancellations, so to overcome this issue we use Cauchy's theorem to deform the path of the integral in such a way that $\mathbb{R}\mathrm{e}f$ attains its minimum at a point k_0 and grows quickly as we move away from it. Besides that, we also want that in at least a small section of the contour $\mathbb{I}\mathrm{m}f$ stays constant. Once the contour is chosen the rest of the procedure is analogous to Laplace's Method used in section 2.2.3, so we will jump some steps.

Let us begin finding the dominant contribution. It happens at the end points or at a saddle point, but in our case it is easy to see that the major contribution does not come from the end points, because $\log[\cos(\pm\pi/2)] \to -\infty$. Therefore Let us find the minimum of f,

$$\frac{df}{dk} = i\eta + \tan(k_0) = 0 \implies \tan[k_0(\eta)] = -i\eta. \tag{2.72}$$

Using the exponential form of the tangent and isolating k_0 we find that

$$k_0 = -\frac{i}{2}\log\left(\frac{1+\eta}{1-\eta}\right) + \pi l. \tag{2.73}$$

Where $l \in \mathbb{Z}$. Notice that the principal branch of the logarithmic is bounded for all η such that $|\eta| < 1$. The case where $|\eta| = 1$, however, needs to be handled separately, but that is not a big problem since we know that $P_N(m = N) = \frac{1}{2^N}$. Now, following the steps of the method we find $f(k_0,\eta)$ and $\frac{d^2 f(k_0,\eta)}{dk^2}$:

$$\begin{cases} f(k_0,\eta) = i\eta k_0 - \log[cos(k_0)] = \frac{\eta}{2}\log\left(\frac{1+\eta}{1-\eta}\right) + \frac{1}{2}\log(1-\eta^2), \\ \frac{d^2 f(k_0,\eta)}{dk^2} = -\sec^2 k_0 = 1-\eta^2. \end{cases} \tag{2.74}$$

Taylor expanding f in the last integral of Eq. (2.71) we arrive at

$$P_N(m) = \frac{[1+(-1)^{N+m}]}{2\pi} e^{-Nf(k_0,\eta)} \int e^{-\frac{1}{2}N(k-k_0)^2 \frac{d^2 f(k_0,\eta)}{dk^2}} dk, \tag{2.75}$$

where the solution of the integral is

$$\sqrt{\frac{2\pi}{N\left|\frac{d^2 f(k_0,\eta)}{dk^2}\right|}}. \tag{2.76}$$

Therefore we end up with the following **Globally Valid Solution**[2]

$$\phi_z \approx \frac{1}{\sqrt{2\pi\left(1-\frac{z^2}{N}\right)}} \exp\left[-\frac{z\sqrt{N}}{2}\log\left(\frac{\sqrt{N}+z}{\sqrt{N}-z}\right) - \frac{N}{2}\log\left(1-\frac{z^2}{N}\right)\right], \tag{2.77}$$

where, again, $z = m/\sqrt{N}$.

[2] For a more complete derivation see Bazant (2000)

2.2.6 Comparison between the methods

Since the Bachelier's equation is a statement that the distribution of the walk depends only on the last step, all the methods present in this section start from the same Markov hypotheses, and all the distributions converge to a Gaussian in the asymptotic limit. In order to compare the methods, the results were plotted together with the exact solution (Eq. (2.10)). Of course, for the comparison to make any sense it is necessary to plot the curves of probabilities of the same variables, that is, not to mix X and z. Therefore Eq. (2.10) and (2.40) were plotted together with Eq.(2.65) and (2.77) transformed to variable x.

Figures 2.3 shows the results for walks with 2, 6 and 60 steps, respectively. Another important factor to take into account is the difference of normalization of the discrete and continuous probability distributions - probability density function. To compare both distributions we had to divide the exact solution by 2 as if we were considering histograms with interval 2. As we can see, for $N = 2$, although the Gaussian approximation is

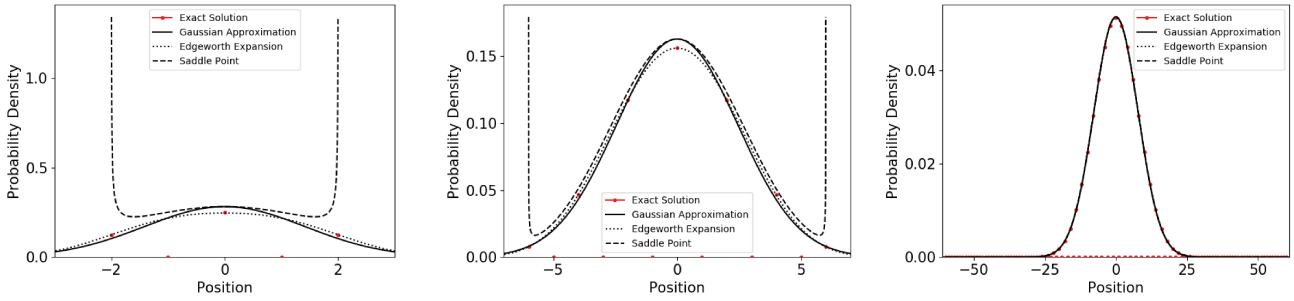

(a) $N = 2$ (b) $N = 6$ (c) $N = 60$

Figure 2.3: Comparison between the methods of approximation explained in this section and the exact solution of a Bernoulli random walk after different number of steps.

reasonable, Edgeworth expansion is the best. For $N = 6$ the Edgeworth expansion is still the best, but the other ones start to fit better. The saddle point approximation blows up at $x \approx \pm 6$.

At last, for $N = 60$ we notice that all approximated solutions fit the exact one perfectly, and they are almost indistinguishable. As expected as N gets larger the approximations are better.

2.3 Continuum Limit

In this last section, we derived an asymptotic approximation for the simple random walk. Now, to see what happens on the continuum limit. We define $\rho(X, N\tau)$ as the continuum approximation for $P_N(X)$ - where $\tau = t/N$ is the time between steps - and consider the problem in one dimension.

Recalling the Bachelier's Equation (2.28) - Markov hypotheses - and Taylor expanding $P_N(R-r)$ we have

$$\begin{aligned} P_{N+1}(R) &= \int p(r)P_N(R-r)dr \\ &= \int_{-\infty}^{\infty} p(r) \sum_{n=0}^{\infty} \frac{(-r)^n}{n!} \frac{d^n}{dR^n}[P_N(R)]dr \\ &= \sum_{n=0}^{\infty} \frac{(-1)^n}{n!} \langle r^n \rangle \frac{d^n}{dR^n}[P_N(R)] \\ &= P_N(R) + \sum_{n=1}^{\infty} \frac{(-1)^n}{n!} \langle r^n \rangle \frac{d^n}{dR^n}[P_N(R)]. \end{aligned} \tag{2.78}$$

In the last line we use the fact that $\langle r^0 \rangle = \int_{-\infty}^{\infty} p(r)dr = 1$. Rearranging the terms and dividing both sides of the equation by τ we have

$$\frac{P_{N+1}(R) - P_N(R)}{\tau} = \sum_{n=1}^{\infty} \frac{(-1)^n}{n!\tau} \langle r^n \rangle \frac{d^n}{dR^n}[P_N(R)]. \tag{2.79}$$

Now calling $D_n = \frac{\langle r^n \rangle}{n!\tau}$ and using the new variable ρ we arrive at a partial differential equation

$$\frac{\partial \rho(R,t)}{\partial t} = \sum_{n=1}^{\infty} (-1)^n D_n \frac{\partial^n}{\partial R^n}[\rho_N(R,t)]. \tag{2.80}$$

This equation is known as **Kramers-Moyall expansion** for coefficients D_n that do not depend on the position, R, (Risken (1996)). Its general form is

$$\frac{\partial \rho(R,t)}{\partial t} = \sum_{n=1}^{\infty} (-1)^n \frac{\partial^n}{\partial R^n}[D_n \rho_N(R,t)], \tag{2.81}$$

and it is possible to show that this expansion is of order 1, 2 or ∞. This demonstration is presented in appendix A.1. In the case when it has order 2 we call it **Fokker-Planck equation**.

$$\frac{\partial p(x,t)}{\partial t} = -\frac{\partial}{\partial x}[D_1(x,t)p(x,t)] + \frac{1}{2!}\frac{\partial^2}{\partial x^2}[D_2(x,t)p(x,t)]. \tag{2.82}$$

The coefficients D_1 and D_2 are known as drift and diffusion coefficients, respectively. Stochastic processes with $D_1 = 0$ and D_2 constant are called **Wiener processes** and if both coefficients are constants but not null it is called a **Ornstein-Uhlembeck process**.

Despite being useful, this form of Kramers-Moyal expansion is not the most correct form of expansion, since errors are introduced on first order continuous time derivative on time. To correct this errors let us consider the Taylor expansion of $\rho(x,t)$ around $t = N\tau$

$$\frac{P_{N+1}(R) - P_N(R)}{\tau} = \frac{\partial \rho}{\partial t} + \sum_{n=2}^{\infty} \frac{\partial^n \rho}{\partial t^n} \frac{\tau^{n-1}}{n!}, \tag{2.83}$$

which leads to the complete partial differential equation equivalent to Bachelier's equation

$$\frac{\partial \rho}{\partial t} + \sum_{n=2}^{\infty} \frac{\partial^n \rho}{\partial t^n} \frac{\tau^{n-1}}{n!} = \sum_{n=1}^{\infty} (-1)^n D_n \frac{\partial^n}{\partial R^n}[\rho_N(R,t)]. \tag{2.84}$$

Making a scaling analysis with some change of variables it is possible to recover the Central Limit Theorem. For the complete derivation, we refer to Bazant (2000).

Another useful form of Kramers-Moyal equation is the one which uses cumulants instead of moments as coefficients. It can be obtained expanding the time derivatives in function of position derivatives and identifying terms of momentum with cumulants, it is also done in Bazant (2000)

$$\frac{\partial \rho}{\partial t} = \sum_{n=1}^{\infty} (-1)^n \hat{D}_n \frac{\partial^n \rho}{\partial R^n}, \tag{2.85}$$

where

$$\hat{D}_n = \frac{c_n}{n!\tau}. \tag{2.86}$$

CHAPTER 3

Brownian Motion

Brownian motion is the name given to the irregular motion of particles immersed in a fluid. It was named after Robert Brown (1773-1858), a botanist that was studying the behavior of pollen particles suspended on the water surface with a microscope and noticed random movements. In 1828 he published his work Brown (1828), explaining that the origin of such motion was due to collisions of the pollen with the smaller particles of the liquid, and not because of some living force as it was believed until then. The molecules of the fluid are constantly moving due to thermal energy, so to predict the exact trajectory of a Brownian particle it would be necessary to know the momentum of all molecules of the fluid that collide with it. This is obviously impracticable, so to overcome this issue we make use of stochastic methods Risken (1996); Crispin W. (1994); Mandel and Wolf (1995). In this section, we present three different ways to approach the problem, all leading to the same solution: A Gaussian probability distribution of positions.

The discussion of stochastic processes launched by the discovery of Brownian motion caused an impact on many knowledge areas, such as physics, chemistry, biology, and economy. Due to its strong connection with diffusion, on physics, the study of Brownian motion led to advances in the interpretation of several natural phenomena - For example, heat propagation and noise in electric systems.

To analyze deterministically a particle suspended on a fluid we shall consider the damping force, $-\alpha v$ that acts on it. So according to second Newton's law

$$\dot{v} + kv = 0, \tag{3.1}$$

where m is the mass of the particle, v the velocity, $\dot{v}$ its time derivative, and $k = \dfrac{\alpha}{m}$, given in terms of the the

damping constant α. The solution of Eq. (3.1) is given by

$$v(t) = v(0)\exp^{-kt}. \tag{3.2}$$

This solution is valid only when the mass of the particle is sufficiently large so we can disregard the changes in velocity caused by thermal fluctuations. If we wish to consider the thermal phenomenon we have to add a fluctuation term, $F_f(t)$, called fluctuation force and define $\Gamma(t) = \frac{F_f(t)}{m}$, so that

$$\dot{v} + kv = \Gamma(t). \tag{3.3}$$

This equation is known as Langevin equation and $F_f(t)$ is a random force, known as Langevin force.

Before we start to present some of the possible approaches to the problem, we state two hypotheses that are always assumed to be true

- The motion of each of the Brownian particles is independent of the other ones. In this case, however, we are considering the motion of only one Brownian particle
- There is no correlation between events that happened at different times, i.e.,

$$\langle \Gamma(t_1)\Gamma(t_2)\rangle = q\delta(t_1 - t_2), \tag{3.4}$$

  where $q = \dfrac{2kK_BT}{m}$ can be obtained with the solution of (3.3) and the equipartition theorem.

In the next sections we will present Einstein's and Langevin's approaches to find the position probability density function of the Brownian motion (section 3.1) and the Binary collision model (3.2), which is an simple microscopic model, that is suitable for simulations and that can be generalized to the relativistic regime.

3.1 Einstein and Langevin Approaches

In 1905 Einstein (1905) published an article where the Brownian motion was treated in the following way. Let N be the total number of suspended particles, dn the number of particles with displacement between Δ and $\Delta + d\Delta$ and $f(x,t)$ the number of particles per unit volume. The number of particles that are between the planes x and $x+dx$ at time $t+\tau$ are the ones that were at a distance Δ from the x plane at time t and moved Δ on the interval τ, where Δ can be any distance. This is the same as writing

$$f(x,t+\tau)dx = dx\int_{-\infty}^{\infty} f(x+\Delta,t)p(\Delta)d\Delta, \tag{3.5}$$

in terms of the probability distribution $p(\Delta)$. Taylor expanding $f(x,t+\tau)$ and $f(x+\Delta,t)$, expression (3.5) becomes

$$f(x,t) + \tau\frac{\partial f}{\partial t} + \ldots = f(x,t)\int_{-\infty}^{\infty} p(\Delta)d\Delta + \frac{\partial f(x,t)}{\partial x}\int_{-\infty}^{\infty}\Delta p(\Delta)d\Delta + \frac{\partial^2 f(x,t)}{\partial x^2}\int_{-\infty}^{\infty}\frac{\Delta^2}{2}p(\Delta)d\Delta + \ldots. \tag{3.6}$$

Since $p(x) = p(-x)$ and the probability $p(\Delta)$ is normalized the integrals of expression (3.6) are

$$\begin{aligned} \text{For } k=0: &\int_{-\infty}^{\infty} p(\Delta)d\Delta = 1; \\ \text{For odd } k: &\int_{-\infty}^{\infty} \Delta^k p(\Delta)d\Delta = 0; \\ \text{For } k=2: &\int_{-\infty}^{\infty} \Delta^2 p(\Delta)d\Delta = 2\tau D_2, \end{aligned} \tag{3.7}$$

where the last expression is used to define the coefficient D_2. Hence, considering only the first two terms in the left hand side of the equation we find

$$f(x,t) + \tau\frac{\partial f}{\partial t} = f(x,t) + \frac{\partial^2 f(x,t)}{\partial x^2}D_2\tau + \ldots \implies \frac{\partial f}{\partial t} = D_2\frac{\partial^2 f(x,t)}{\partial x^2} + \ldots. \tag{3.8}$$

This expression is called **Diffusion equation**. We can identify D_2 with the diffusion coefficient of the Fokker Planck equation. The normalized solution is known to be

$$f(x,t) = \frac{N}{\sqrt{4\pi D_2}}\frac{\exp^{\frac{-x^2}{4D_2 t}}}{\sqrt{t}}. \tag{3.9}$$

At this point we call the attention to the similarity between this approach and the Rayleigh's and Recursion methods, presented in chapter 2, in the sense that all three approaches start from a Markovian expression and Taylor expansion of it around zero.

Figure (3.1) shows the distribution of positions obtained by the solution of the diffusion equation for different times, with the initial condition being a delta function on position zero, i.e, the initial position of the Brownian particle is completely known.

Treating now the case where there is only one Brownian particle, if we suppose that the diffusion coefficient is time independent and substitute the solution found for $f(x,y)$ in the definition of second moment, we get

$$\langle x^2\rangle = \int dx x^2 f(x,t) = \int dx x^2 \frac{1}{\sqrt{4\pi D_2}}\frac{\exp^{\frac{-x^2}{4D_2 t}}}{\sqrt{t}} = 2D_2 t. \tag{3.10}$$

By symmetry, it is clear that $\langle x\rangle = 0$. Therefore, from equations (3.9) and (3.10) we can note that the particles on Brownian Motion are set to a normal distribution and that the coefficient D_2 is related to the variation of the curve width with time. In his paper Einstein finds an expression for the diffusion coefficient by using the fact that in the dynamic equilibrium the Helmholtz free energy does not change. Langevin, on the other hand found an equivalent result using equation (3.3). Solving it for v and taking the mean value of both sides the fluctuation term vanishes, that is,

$$v(t) = v_0 e^{-kt} + e^{-kt}\int F(t')e^{kt'}dt' \implies < v(t) >= v_0 e^{-kt}. \tag{3.11}$$

The variance of v is $(\Delta v)^2 =< v^2 > - < v >^2 = \frac{C}{2k}$, where C is an integration constant. So considering a Wiener process for the long time limit $< v >= 0$, so using the equipartition theorem

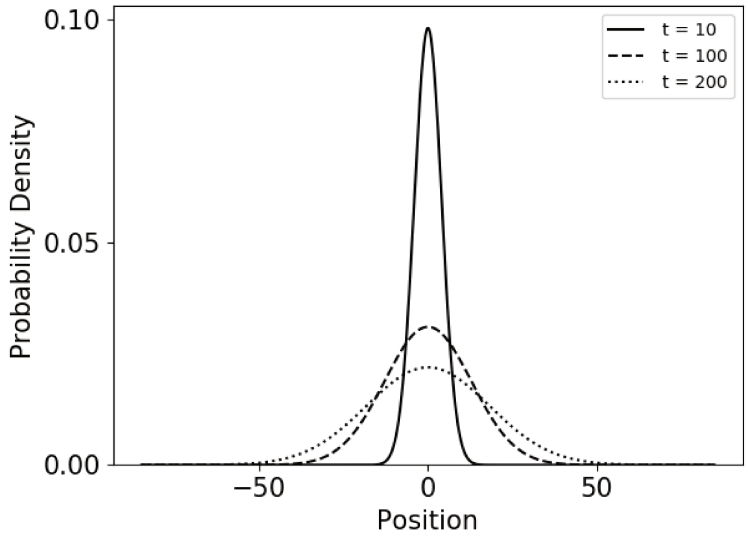

Figure 3.1: Probability density function of Brownian particle position after 30, 100 and 500 time units. Initial condition is $(x_0, t_0) = (0,0)$.

$$< v^2 >= \frac{C}{2k} = \frac{k_B T}{m} \implies C = \frac{2k k_B T}{m}. \tag{3.12}$$

Now, analogously calculating the first and second position moments we find that at the long time limit $< x^2 >= \frac{2t k_B T}{mk}$. Comparing it with equation (3.10) we obtain

$$D_2 = \frac{k_B T}{mk}. \tag{3.13}$$

Considering that the Brownian particle is a small sphere, the damping constant k is $-6\pi\eta a$, where η is the fluid viscosity and a the particle diameter. Therefore, in principle, we can calculate the diffusion coefficient from measurable parameters.

There is a large class of stochastic processes that can be described by an equation analogous to Langevin's , that is, equations with one stochastic (q) and one deterministic (A) term, such as

$$\frac{dx}{dt} = A(x,t) + q(t). \tag{3.14}$$

If $< q(t) >= 0$ and $< q_i(t) q_j(t') >= g(t)\delta(t - t')$ we call it a Gaussian process. Those can be subdivided in the Wiener and Ornstein-Uhlembeck processes, which have already been explained in the previous section.

Now it is clear that the investigation of Brownian motion via the Fokker-Planck equation, by Einstein's approach or Langevin Equation lead to the same results. Fokker-Planck equation (2.82) is actually a more general result that can be used on a wide range of stochastic problems. Based on those results, we made the simulations, displayed in figure (3.2), for one and two dimensions.

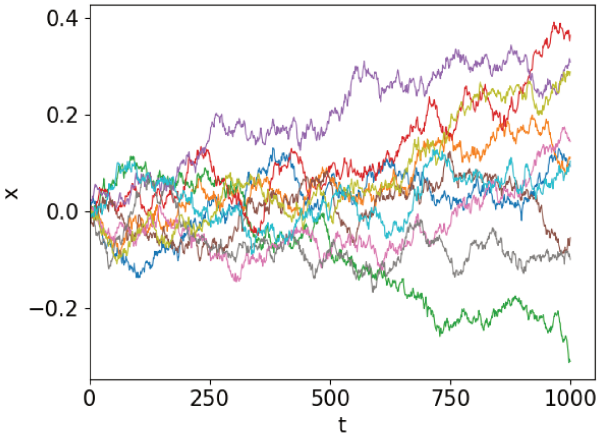

(a) 10 Brownian particles in one dimension

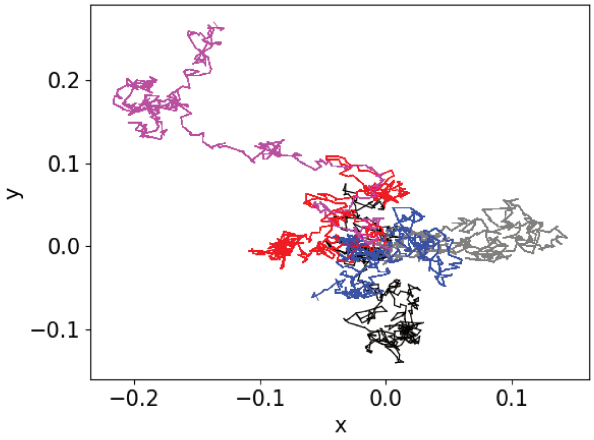

(b) 5 Brownian particles in two dimensions

Figure 3.2: Simulation of the motion made by considering that the displacements at each time step are Gaussian distributed and the direction (or angle in the two dimensional case) of displacement are uniformly distributed.

3.2 Binary Collision Model

Brownian motion can be described by microscopic models as well (Dunkel (2008)). The approach to obtain a Langevin equation from this type of model consists in making a model of the interactions between the Brownian particle and the medium and eliminate the degrees of freedom of the heat bath. Particularly, in the Binary Collision model it is presupposed that the collisions between the Brownian particle and the molecules of the heat bath are elastic. This means that the total energy and momentum are conserved. Using capital letters referring to the Brownian particle and small letters to the molecules of the bath (with r designating the medium molecule) this condition is expressed as

$$\begin{aligned} E + e_r &= E_{\text{final}} + e_{\text{final},r}; \\ P + p_r &= P_{\text{final}} + p_{\text{final},r}; \end{aligned} \tag{3.15}$$

The solution to the system of equations is

$$\Delta P = P_{\text{final}} - P = \frac{2MP_r}{M+m} - \frac{2Pm}{M+m}, \tag{3.16}$$

which describe the momentum variation due to one collision. Let us consider the momentum variation of the Brownian particle, $\delta P(t) = P(t+\delta t) - P(t)$, in an interval, δt, sufficiently large so that at least one collision happens. Assuming that the collisions occurring in the interval are independent events, we find

$$\delta P(t) \approx \sum_r \Delta P_r I_r(t, \delta t) \tag{3.17}$$

where the variable I indicates if there was a collision with the molecule indexed by 'r' in the interval, δt, or not, i.e.

$$I_r = \Theta(X - x_r)\Theta(x_r' - X') - \Theta(x_r - X)\Theta(X' - x_r') = \begin{cases} 1 & \text{Collision occurred;} \\ 0 & \text{No collision occurred.} \end{cases} \tag{3.18}$$

Substituting ΔP_r and considering $M >> m$, we find

$$\delta P(t) \approx -2\left[\sum_r \frac{m}{M} I_r\right] P(t) + 2\sum_r p_r I_r. \tag{3.19}$$

Interpreting the first term as the friction and the second one as noise, the equation (3.19) is equivalent to Langevin equation (3.3). Although equation (3.19) may look complicated, because it uses the velocity of the molecules of the fluid, those can be easily obtained by a velocity PDF that properly describes the fluid, i.e, Maxwell-Boltzmann distribution.

The Binary Collision model was used to simulate Brownian motion. Figure 3.3 displays the result of the simulations. In figure 3.3(a) the path of three Brownian particles in a two dimensional space is displayed. The histogram on figure 3.3(b) accounts for the velocity occurrences after 50 collisions. The parameters used in the simulation were

$$\begin{aligned} m &= 10^{-22}\text{g}; \\ M &= 10^{-15}\text{g}; \\ a &= \sqrt{\frac{K_B T}{m}} = 100\text{m/s}, \end{aligned} \tag{3.20}$$

To see the code of the simulation we refer to A.7. Note that, as expected, the shape of the histogram is consistent with a Gaussian distribution.

In addition to the numerical results, it is also possible to obtain a Langevin equation, similar to (3.14) for the momentum

$$\frac{dP(t)}{dt} = -k(P)P + \Gamma(t), \tag{3.21}$$

with $\langle \Gamma(t_1)\Gamma(t_2)\rangle = q(P)\delta(t_1 - t_2)$. Then, the specific function $q(P)$ and $k(P)$ need to be found using the features of our model and bath. The function $q(P)$ is defined by $q(P) = k(P)MK_B T$ — this is a generalization of eq. (3.4). The function $k(P)$, on the other hand, can be found by the following criterion

$$\left\langle \left.\frac{dP(t)}{dt}\right|_{P(t)=p} \right\rangle = \left\langle \left.\frac{\delta P(t)}{\delta t}\right|_{P(t)=p} \right\rangle, \tag{3.22}$$

where the left hand side is obtained by the Langevin equation

$$\left\langle \left.\frac{dP(t)}{dt}\right|_{P(t)=p} \right\rangle = -\left[k(p)p - \frac{dp}{dt}MK_B T\right]. \tag{3.23}$$

The right hand side is obtained by Taylor expanding I_r around $\delta t = 0$,

$$I_r(t, \delta t) \approx \frac{\delta t}{2}|v_r - V|\delta(x_r - X), \tag{3.24}$$

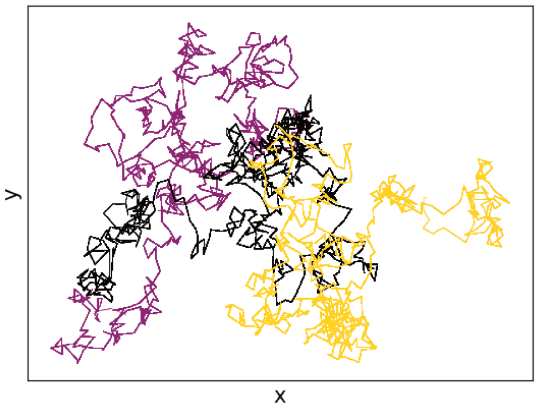

(a) Simulation of three Brownian particles.

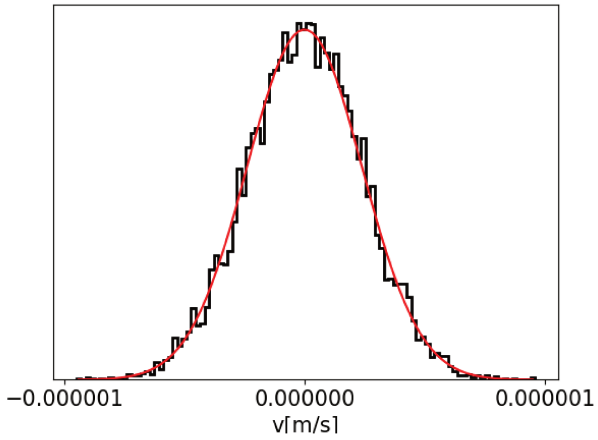

(b) Histogram of velocities after 50 collisions made with 10000 simulations.

Figure 3.3: Results of the simulations using binary collision model. The red Gaussian is depicted for comparison.

and calculating the mean of both sides of expression (3.19). This can be done by noticing that the expectation values of the form $\langle G(x_r, v_r) I_r(t, \delta t)\rangle$ can be calculated as

$$\langle G(x_r, v_r) I_r(t, \delta t)\rangle = \frac{\delta t}{2L} \int_{-\infty}^{\infty} dv_r G(x_r, v_r) |v_r - V| \psi_{MB}(v_r), \tag{3.25}$$

where L is the one-dimensional volume of the container and $\psi_{MB}(v_r)$ is the Maxwell Boltzmann distribution. Here we will simple name[1]

$$\left\langle \frac{\delta P(t)}{\delta t}\bigg|_{P(t)=p} \right\rangle = \mathcal{K}(p). \tag{3.26}$$

Therefore, the coefficient $k(p)$ can be found by solving the following ordinary differential equation

$$-k(p)p + \frac{dk(p)}{dp} MK_B T = \mathcal{K}(p). \tag{3.27}$$

The initial condition to $k(p)$ must be given so that the asymptotic behavior of the distribution is correct. Then, once $k(p)$ is found, the Langevin-type equation (3.21) is completely defined.

This model provides the general idea of the approximations required to obtain the Langevin equation from microscopic considerations and the knowledge of the asymptotic distribution of the real physical process. When compared to other microscopic models, the binary collision model has the advantage that it can be generalized to the relativistic regime (see section 4.2.2).

[1] For a more detailed calculation of this mean drift force $\mathcal{K}(p)$ we refer the reader to Dunkel and Hanggi (2009).

CHAPTER 4

Relativistic Regime

In chapter 3, Einstein's and Langevin's approaches to describe the Brownian motion were presented. Although each approach uses a different track, both of them point out that the position probability density function of the Brownian particle is Gaussian. This is also in accordance with the central limit theorem, however as the name points out, the theorem is an approximation valid for the central region of the distribution. In fact, the Gaussian solution is not always applicable, particularly when the relativistic regime for velocities is assumed. The problem is that as $x \to \infty$, the probability $P(x) \to 0$, but for $ct < |x| < \infty$, $P(x) \neq 0$. In other words, a normal distribution implies that the Brownian particle can have superluminal velocity. Figure (4.1) illustrates the issue.

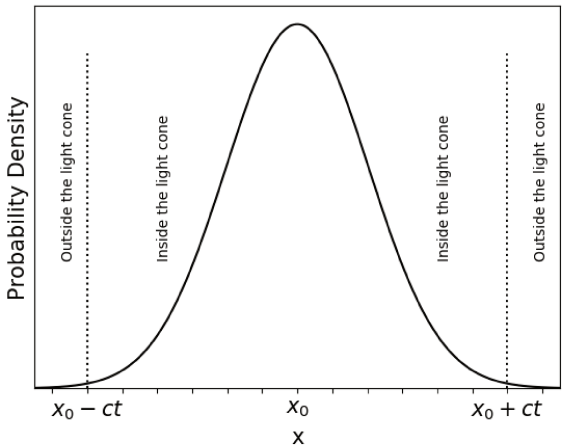

Figure 4.1: Illustration of why the Gaussian distribution is not in accordance with relativity. The figure is out of scale and should be interpreted only as a graphic illustration of the problem.

Another way of seeing the problem of superluminal locations is through the evolution of the variance. Figure 4.2 shows the evolution of the position variance with respect to time, i.e, $\sigma^2 = 2Dt$. The red curve represents the variance of a light wave propagation, $\sigma^2 = (ct)^2$. We see that for $t < \frac{2D}{c}$ the variance of the Gaussian is larger than the variance of the light. This means that the mean width of the Gaussian is out of the light cone, or in other words, the non-relativistic result implies that there is at least 32% of chance to find the particle with velocity larger than that of light for those small times ($t < 2D/c$). Note that a curve being inside the light cone in fig 4.2 does not imply that the distribution is in accordance with relativity. It means that the full width at half-maximum is inside the light cone, but does not carry any information about the tails of the distribution.

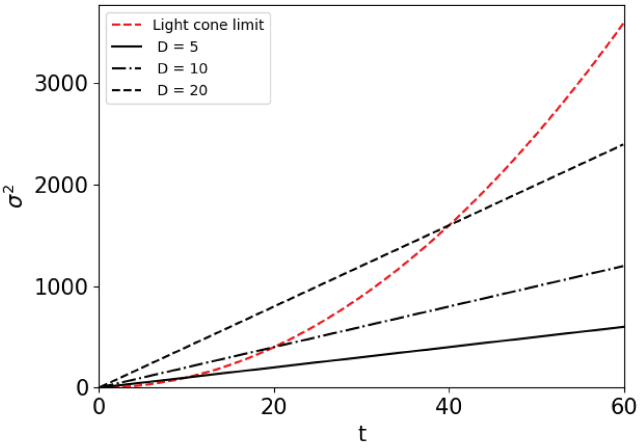

Figure 4.2: Comparison between the variance of a light wave propagation and diffusion propagation, for three different values of diffusion propagators.

In principle, the problem can be seen as an approximation problem, in the sense that Einstein's derivation of the diffusion equation and the demonstration of the central limit theorem at some point appeal to an approximation valid in the central region of the distribution. However, the answers we want to find studying relativistic Brownian motion are not just with respect to the tail problem of the Gaussian solution, but also how does the whole distribution change in the relativistic regime, i.e, what is the position probability density function of a Brownian particle immersed on a fluid with high thermal energy. Despite the difficulties imposed, the generalization of the theory of stochastic processes to a relativistic domain has been extensively discussed in the literature (Rudberg (1957); Debbasch (2004); Debbasch et al. (1997); Dunkel and Hanggi (2009); Dudley (1966); Hakim (1968)). Particularly, in the works of Dudley (1966) and Hakim (1968), it was demonstrated that a non-trivial Lorentz invariant Markov process in Minkowski space-time does not exist. This means that we can't find a process with non-constant, non-vanishing velocity in Minkowski space-time by assuming the Markovian Hypothesis [1]. An equivalent statement against the Markovian hypotheses was derived in the work of Dunkel

[1] The demonstration of this proposition is rather complicated and uses definitions that would take too much space to be presented

et al. (2006), where the authors showed that a solution to relativistic Brownian motion cannot be obtained from the limit of a "relativistic random walk" as in the non-relativistic case. The proof is easily seen in the light of the Central Limit Theorem (CLT) and we repeat it bellow.

Let us consider a 1-dimensional walk where each step occurs on a discrete time interval τ_i. The position variable after N steps is

$$X(t) = x_0 + \sum_{i=1}^{N} v_i \tau_i, \tag{4.1}$$

where v_i is the constant velocity of the 'walker' on an interval τ_i. The mean velocity along a path with N steps is defined as

$$V_N(t) = \frac{X(t) - x_0}{t} = \frac{1}{t} \sum_{i=1}^{N} \tau_i v_i = \frac{1}{N} \sum_{i=1}^{N} v_i, \tag{4.2}$$

where $t = \sum_{i=1}^{N} \tau_i$. Therefore, if the variables v_i are identically and independently distributed (iid), with zero mean and finite variance, the CLT states that the distribution of $Z_N = \sqrt{N} V_N$ converges to a Gaussian, as shown in section 2.2.3. Hence, if we keep t fixed as $N \to \infty$, the mean velocity V_N goes to zero and the first equality of eq.(4.2) implies that $X(t) = x_0$. This means that the particle effectively does not move. Since for a relativistic system the velocity is always bounded, the variance of v_i is also bounded and we conclude that the only way to escape from CLT consequences is to demand the process to be non Markovian. In other words, **it is impossible to find a non-trivial, continuous, relativistic Markov process in position space from the continuous limit**.

The consequences of this result are very strong since the Markovian hypothesis is the starting point of some very important tools used in the treatment of stochastic processes and in the approaches described in chapter 3. In order to circumvent this issue, there are two possible strategies. One can consider a non-Markovian approach to generalize the diffusion equation or a Markovian generalization of the Brownian motion can be constructed in phase space, i.e, considering not only position and time variables but also the momentum.

In this chapter, we will analyze the relativistic Brownian motion using both strategies. The first strategy will be studied in section 4.1, where we analyze three different approaches to derivate a relativistic generalization of the diffusion propagator:

- The Telegraph equation;
- The generalized Diffusion Propagator;
- The propagator obtained by the maximization of entropy.

The results of the three approaches are consistent with the limits imposed by relativistic theory and approach the classical distribution in the asymptotic limit. The fist two were already presented in the literature,

here, therefore we content ourselves in just enunciate it here and the reader with more interest in the subject can find the demonstration in the references.

while the third represents our own contribution. The comparison between the resultant propagators is also discussed. Since we are always considering that position of the particle at initial time ($t_0 = 0$) is $x_0 = 0$ with probability 1, the propagator $p(x,t|x_0,t_0)$ also represents the probability distribution $p(x,t)$,

$$p(x,t) = \int_{-\infty}^{\infty} dx_0 p(x,t|x_0,t_0)\delta(x_0). \tag{4.3}$$

The second strategy is present at section 4.2, where we show an attempt to generalize Langevin's equation made by Dunkel and Hanggi (2005) and the generalization of the binary collision model (Dunkel and Hanggi (2009)). The attempt to make a relativistic generalization of the Langevin equation is not unique. There are other works that use different additive noise and a drift term, if the reader is interested in knowing these other models we suggest the papers by Dunkel and Hanggi (2009); Debbasch (2004); Debbasch et al. (1997). The advantage of approaching the problem through Langevin's equations is that the stochastic dynamics, due to the interactions with the reservoir, is more clear. Because of that, a knowledge of the properties of the heat bath is required to derive Langevin's equations in the relativistic regime. Particularly, on the binary collision model, we made a simulation of the motion of the Brownian particle considering the hypotheses that the collision between the Brownian particle and the molecules of the fluid are elastic and that the fluid molecules respect Jüttner's distribution. This led to a distributions of velocities (for the Brownian particle) that also converges to Jüttner's (see Appendix A.3), this is a good indication for the validity of the model.

The relativistic Brownian motion has application in modeling the thermalization process of quark-gluon plasma produced in heavy-ion collisions, in the analyses of ultra-relativistic plasma beam collisions, and in the general understanding of relativistic thermodynamics, Dunkel (2008). Once the right generalization of the diffusion equation is found, if one writes its solution in a moving reference frame with respect to the rest frame of the fluid, the standard deviation of this distribution can be used to find the temperature transformation, because $\sigma^2 \propto T$. Particularly, if the distribution of positions of the Brownian particle on the point of view of a moving observer, with respect to the lab frame, has a smaller (bigger) variance then the distribution from the point of view of the rest frame of the fluid we could conclude that a body looks colder (hotter) for a moving observer. For more on the issue of temperature transformations, we referee to Appendix A.4.

4.1 Relativistic Diffusion

As it was already mentioned, there are two suitable strategies to derivate the PDF's of the stochastic motion of a relativistic Brownian particle. This section is dedicated to approaches that generalize the diffusion equation and/or propagator. Since those models analyze the problem in Minkowski space-time the resultant PDF cannot be Markovian, in other words, the distributions necessarily do not respect Chappman-Kolmogorov equation

$$P(x,t|x_0,t_0) = \int dx_1 P(x,t|x_1,t_1)P(x_1,t_1|x_0,t_0), \tag{4.4}$$

for some value of $t_1 \in (t_0, t)$.

4.1.1 Telegraph equation (TE)

One of the alternatives to the diffusion equation is the telegraph equation. This equation presents applicability in the descriptions of several phenomena besides diffusion, such as on the transmissions of electrical signals, heat wave propagation, and the continuum limit of the model of the persistent random walk. An analytic continuation connects the telegraph and Dirac equations in an analogous way that the diffusion and Schrodinger equations are connected. The TE can be obtained considering one more term on Einstein derivation of diffusion equation (3.6) or by the model of persistent random walk. The usual form of the telegraph equation is

$$\frac{1}{h}\frac{\partial p}{\partial t} + \frac{\partial^2 p}{\partial t^2} = v^2 \frac{\partial^2 p(x,t)}{\partial x^2}, \tag{4.5}$$

where h is an additional relaxation time parameter and v a velocity parameter, both being positive. Notice that considering only the first term on the right hand side of equation (4.5) it becomes the diffusion equation and considering only the second term it becomes the wave equation. For $h > 0$, the TE is a differential linear hyperbolic equation and its solution can be obtained by applying a Fourier and Laplace transform, on x and t, respectively on both sides of equation, Masoliver and Weiss (1999). If $q(w,s)$ is the Fourier-Laplace transform of $p(x,t)$, solving the differential equation to the variable q we find

$$q(w,s|x_0) = \frac{(s+1/h)e^{-iwx_0}}{s(s+1/h)+v^2w^2}. \tag{4.6}$$

Applying the inverse Fourier-Laplace transform, we get

$$\begin{aligned} p(x,t|x_0) &= \frac{e^{(-\frac{t}{2h})}}{2}[\delta(x-x_0-vt)+\delta(x-x_0+vt)] \\ &\quad + \frac{e^{\left(\frac{-t}{2h}\right)}}{8vt}\left[I_0(\phi)+\frac{I_1(\phi)}{2h\phi}\right]\Theta(vt-|x-x_0|) \end{aligned} \tag{4.7}$$

where $\phi = \frac{\sqrt{v^2t^2-(x-x_0)^2}}{2vt}$, and I_0, and I_1 are modified Bessel functions.

The solution (4.7) has the shape of a Gaussian truncated by the Heaviside function ($\Theta(x) = 1$ for $x > 0$ and $\Theta(x) = 0$ if $x < 0$) on points located on a distance vt of the initial position x_0. In each of these points, there is a delta function with an amplitude that decays with time. An interesting feature of the solution is that it has a shape composed by a union of the solutions of wave and diffusion equation, i.e., the central region of the PDF has a Gaussian shape truncated at the limits $x = \pm vt$ with delta functions at that limiting position decaying with time. Figure (4.3) shows the solution of the telegraph equation with a sharp Gaussian initial condition used to approximate the delta initial distribution. This approximation is useful to allow the computational calculation of the solution of the differential equation and to allow us to visualize the behavior of the distribution without

having to force the drawn of delta functions on the graph. We see that, for a fixed h, in small times the wave-like behavior is strong and as we increase the time, the diffusive behavior is more present, making the distribution to approach the Gaussian shape.

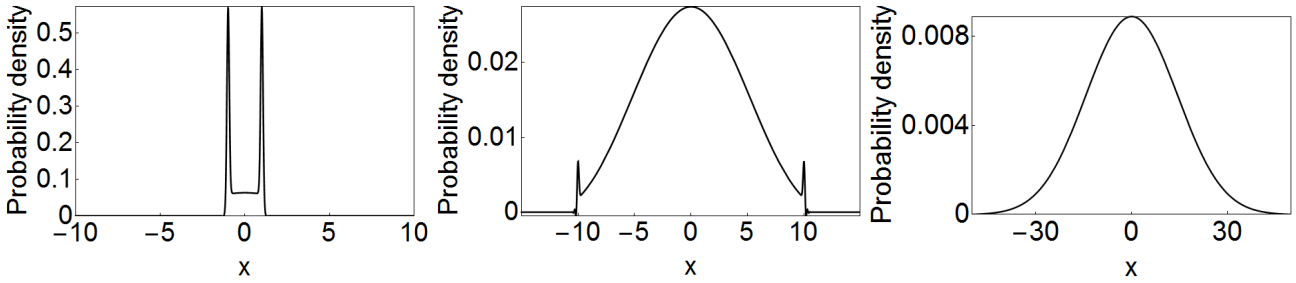

(a) $t = 1$. (b) $t = 10$. (c) $t = 100$.

Figure 4.3: Solution of the Telegraph Equation for a sharp Gaussian initial condition. The distribution is not normalized and natural units are being considered ($h = 1$, $v = c = 1$).

The standard deviation of the probability density function can be obtained calculating the first and second moments of the distribution. Since the solution is symmetric, the first moment is $m_1 = \langle x \rangle = x_0$. The second moment is found by multiplying both sides of expression (4.5) by x^2 and integrating. This leads to

$$\frac{d^2 m_2}{dt^2} + \frac{1}{h}\frac{dm_2}{t} = 2v^2. \tag{4.8}$$

Considering the following initial conditions

$$\begin{cases} m_2(0) = x_0^2; \\ \left.\frac{dm_2}{dt}\right|_{t=0} = 0, \end{cases} \tag{4.9}$$

we find

$$\sigma^2(t) = m_2(t) - m_1^2(2) = 2v^2 h[t - h(1 - e^{-t/h}))]. \tag{4.10}$$

Fig 4.4 displays the variance as a function of time for different values of the parameter h - we considered $v = 1$ in all cases.

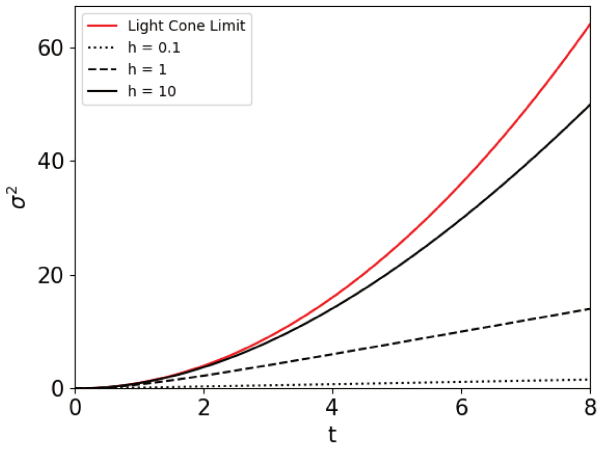

Figure 4.4: Variance of the the position distribution of the solution of the Telegraph equation for different values of h

Since the solution truncates on the light cone, it does not contradict relativity theory. In 1970 van Kampen showed (Kampen (1970)), using a theoretic microscopic model, that the TE can be recovered, but this approximation fails in the neighborhood of the diffusion fronts formed by the delta functions. Besides that, another argument against using TE to describe the relativistic Brownian motion is that the singularities due to the delta function do not describe massive particles in a reasonable way because it would indicate that a big amount of particles would have a great amount of energy.

Therefore, we can conclude that although the TE gives an distribution that doesn't allow particles to be out of the light cone, the distribution shouldn't be used to describe massive particles.

4.1.2 Relativistic Diffusion Propagator

An alternative method to find the PDF of the relativistic Brownian motion was proposed by Dunkel et al. (2006). The approach consists of writing the non-relativistic diffusion propagator in terms of action integration and then generalizing it to the relativistic case by switching the action to its relativistic version.

Let us consider a non-relativistic particle that is in position x_0 at time t_0 and travels to x at time t. The particle can have collisions with the particles in the fluid it is immersed, but we consider that its speed, v, as in a scattering problem, remains approximately constant between the collisions. The action of the particle in this path is given by the integral of its kinetic energy. So the action per mass is

$$a(x|x_0) = \frac{1}{2}\int_{t_0}^{t} dt' v(t')^2. \tag{4.11}$$

The minimum value to the action corresponds to the case where there is no collision during the period $t_1 - t_0$.

So $v = \frac{x-x_0}{t-t_0}$, and

$$a_{\mathtt{min}}(x|x_0) = \frac{(x-x_0)^2}{2(t-t_0)}. \tag{4.12}$$

On the other hand, the maximum value of the action is unlimited. Therefore the propagator can be written as

$$p(x|x_0) \propto \int_{a_{min}}^{a_{max}} da e^{-\frac{a}{2D}} = -2D[exp(-a_{max}/2D) - exp(-a_{min}/2D)], \tag{4.13}$$

where $p(x|x_0)$ respects the normalization condition.

To obtain the relativistic generalization we just need to find the expressions of the integral limits, i.e., of $a_+ \equiv a_{max}$ and $a_- \equiv a_{min}$. The relativistic action based on the proper time of the particle is given by

$$a(x|x_0) = -c^2 \int_{t_0}^{t} dt' \left(1 - \frac{v(t')^2}{c^2}\right)^{1/2}, \tag{4.14}$$

and analogous to the non-relativistic case the minimum value of the action is obtained substituting $v = \frac{x-x_0}{t-t_0}$:

$$a_-(x|x_0) = -c^2 \left[(t-t_0)^2 - \left(\frac{x-x_0}{c}\right)^2\right]^{1/2}. \tag{4.15}$$

The maximum action for this case, on the other side, is limited by the velocity of light. From eq. (4.14) we see that $a_{max} = 0$ for this case. Then the relativistic propagator is

$$p(x|x_0) = \frac{2D}{N}[e^{-a_-/2D} - 1], \tag{4.16}$$

where N is the normalization constant. This diffusion process is non-Markovian and (4.16) is the same for higher dimensions. Moreover, the solution does not allow superluminal velocities and does not present singularities like the solution of the telegraph equation. Figure (4.5) shows the resultant PDF of this approach, considering the initial state as $\delta(x-0)$. Note that on the long time limit the resultant distribution converges to a standard Gaussian density function.

It is convenient to mention that (4.13) is part of a major class of diffusion processes defined by

$$p_w(x|x_0) = \frac{1}{N}\int_{a_-}^{a_+} da w(a). \tag{4.17}$$

The non-relativistic diffusion process has $w(a) = e^{-a/2D}$, so it is a natural choice to denote the function $w(a)$ of the relativistic case in the same way, but there is still some arbitrariness on that choice. Making a graph of the evolution of the variance of distribution (4.16) in time we see that, unlike the Gaussian distribution, for small times the propagation behavior does not generate a variance larger than the light wave variance. Figure 4.6 (a) shows, in black, this result for different values of the diffusion coefficient D. The red curve is the variance of a light wave propagating in the vacuum, displayed for comparison. On the other hand, figure 4.6 (b) shows that the long time limit behavior of the variance of the distribution found by the relativistic propagator method is a constant line parallel to the line correspondent to the non-relativistic result. For smaller values of D, the difference between both variances is smaller, this is a consequence of the fact that in the low-temperature limit the relativistic distribution converges to the Gaussian one faster.

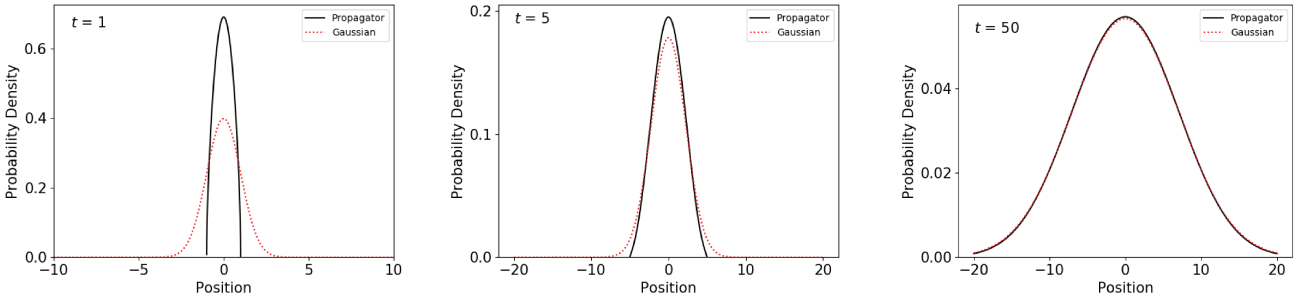

(a) $t = 1$. (b) $t = 5$. (c) $t = 6$.

Figure 4.5: Probability density function of positions of the relativistic Brownian motion obtained by the propagator approach considering the initial probability as $p(x, t = 0) = \delta(x)$ is shown for different times. The curves in red represent the non relativistic result with same variance and are displayed for comparison. The unities considered are such that $c = 1$, i.e, natural unities and the diffusion coefficient D was taken to be 0.8.

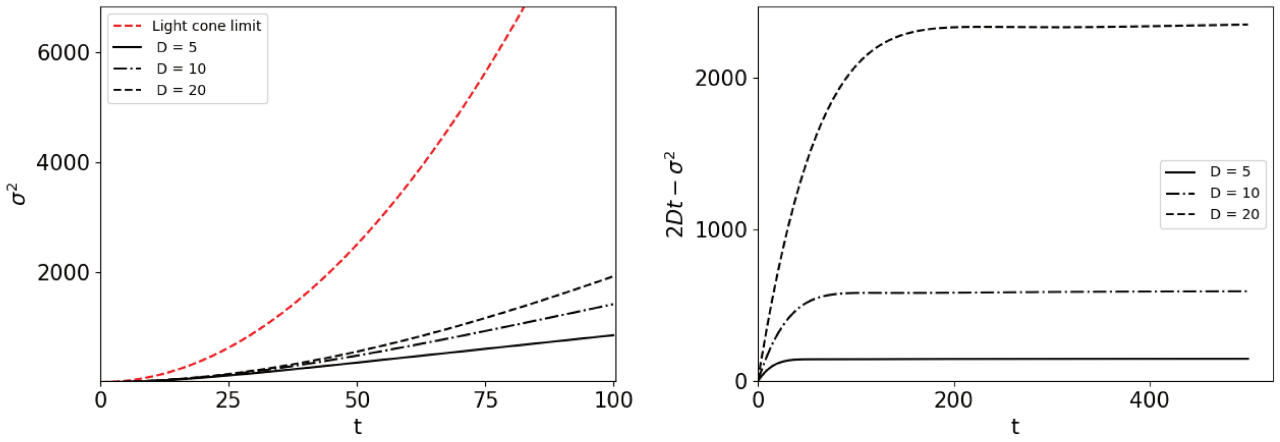

(a) Evolution of the variance. (b) Evolution of $2Dt - \sigma^2$.

Figure 4.6: Behavior of the variance for the relativistic distribution obtained in this section. In figure (a) the variance of a light wave propagating in vacuum is displayed in red for comparison with the evolution of the variance for different diffusion coefficients. And in figure (b) the difference between the variance of the relativistic and non-relativistic case is plotted.

4.1.3 Entropy maximization

Qiuping A. Wang showed in his papers Wang (2005a, 2006, 2004, 2005b) some evidence that suggests an equivalence between maximization of Shannon entropy and minimum action principle for stochastic processes. Here we first give a summary of his calculations and then use the method proposed in the papers to calculate the position probability distribution of a Brownian particle in the non-relativistic and relativistic

regimes.

It is well known that if the initial point (A) on the phase space of a deterministic system is known then there is only one possible trajectory that the system can assume. That is the least (or extreme) action trajectory. On the other hand, for a stochastic system, there will be many possible trajectories between two fixed points, with different times paths, $t_{AB}(k)$. Here we use the index k to indicate the path. Figure (4.7) illustrates the variety of trajectories in a two-dimensional phase space, being the analysis valid to systems with N bodies in a three-dimensional space, that is, with a $6N$ dimensional phase space.

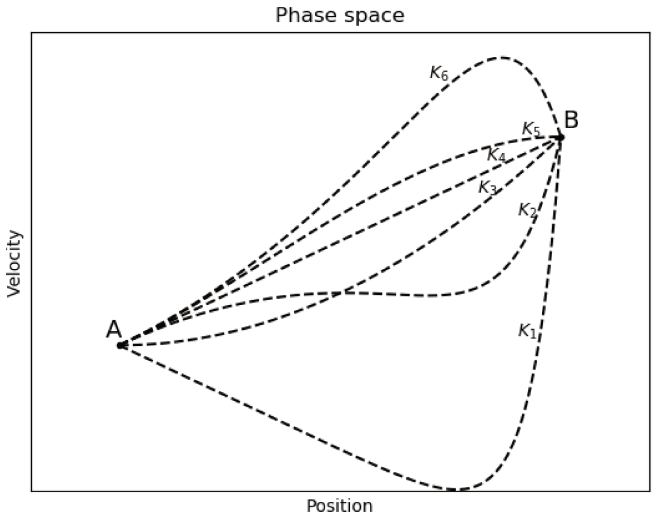

Figure 4.7: Illustration of paths on phase space.

Denoting $p_{AB}(k)$ the path probability of the system going from A to B, through the trajectory k, as given by

$$p_{AB}(k) = \frac{L_k}{L}, \tag{4.18}$$

where from the total of L trajectories made by the system in experiments, L_k is the number of systems that follow trough path k. Supposing that each path that goes from A to B is uniquely defined by its action, it is possible to find an expression for $p_{AB}(k)$ as a function of the action of path k.

Before starting the calculation to find $p_{AB}(k)$, it is important to set some definitions. The action of a path between points A and B, $A_{AB}(k)$, is defined as

$$A_{AB}(k) = \int_{t_{AB}(k)} \mathscr{L}_k(t)\,dt, \tag{4.19}$$

where $\mathscr{L}$ is the Lagrangian of the system. The Shannon entropy related to the path probability $p_{AB}(k)$ is

$$H_{AB}(k) = -\sum_k p_{AB}(k) \ln p_{AB}(k). \tag{4.20}$$

We will maximize the entropy under two constrains. The fist one is that $p_{AB}(k)$ is normalized

$$1 = \sum_k p_{AB}(k), \tag{4.21}$$

and the second is set by the mean action, A_{AB}

$$A_{AB} = \sum_k p_{AB}(k) A_{AB}(k). \tag{4.22}$$

This means that the mean value of action is fixed. Now using Lagrange multiplier's method to extremize the Shannon entropy, as explained in appendix A.2, we write

$$\delta[-H_{AB} + \lambda \sum_k p_{AB}(k) + \eta \sum_k p_{AB}(k) A_{AB}(k)] = 0, \tag{4.23}$$

where λ and η are Lagrange multipliers. Deriving the whole expression with respect to $p_{AB}(k)$, and rearranging terms we get the path probability

$$p_{AB}(k) = \frac{e^{-\eta A_{AB}(k)}}{Q}. \tag{4.24}$$

Where Q is the normalization constant.

It can be proven that if $\eta > 0$, the path distribution is stable with respect to action fluctuation of paths, Wang (2005a). This means that if we cut all paths from A to B in half then the sum of the entropy of the two groups does not increase with virtual changes of the two groups of paths. In this case, equation (4.24) implies that the most probable paths are the ones with the least action. This can be interpreted as proof that the choice of the mean action as a constraint implies a connection between the Jaynes Entropy Principle and the principle of least action. However, it is important to point out that the principle of least action states that the path taken by the system is the one for which the action is stationary to first order, not necessarily least. Therefore, it might seem like the connection points out to a restriction in the principle, but it does not. Equation (4.24) states that a stochastic system that has a stationary entropy will have a distribution where paths of least action occur with higher probability.

At this point, it is important to reinforce the meaning of path probability. $p_{AB}(k)$ is the probability of the system to go from the point A to B of phase space (when both are fixed) through the k trajectory. However, since in our analyzes of the Brownian motion we are interested in knowing the position PDF of the Brownian particle after a fixed time interval (τ), i.e., the probability that a particle that leaves point x_a (fixed) of the coordinates space will get to an arbitrary point x_b, the path probability by itself, does not have much useful information. The approach proposed by Wang (2006) to calculate the position PDF, $p_{B|A}$ (Probability of finding the particle at position X_b knowing that it was initially in x_a), is to maximize the Shannon entropy again, but now using the entropy that concerns the choice of final position, that is,

$$H_A = -\sum_b p_{B|A} \ln p_{B|A}. \tag{4.25}$$

Using as constraints the normalization of $p_{B|A}$ and the mean action $A_A = \sum_b p_{B|A} A_{AB}$ and following Lagrange's multipliers method we arrive at the following probability distribution,

$$p_{B|A} = \frac{e^{-\alpha A_{AB}}}{Z}, \tag{4.26}$$

where Z is the normalization constant and α is the Lagrange multiplier. Thus, using Wang's approach the only thing left for us to do is to calculate A_{AB}. Note that until now, no specification about the action was made, so eq. (4.26) is valid to any regime. Moreover, the problem of finding the position PDF of a particle in relativistic or non-relativistic Brownian motion consists in the calculation of the mean value of action through all possible paths between points x_a and x_b. Let's start by the non-relativistic case.

We used path integral to calculate the mean (4.22) over all possible paths between x_a and x_b (see appendix A.5). The result obtained was

$$p_{B|A} = \sqrt{\frac{\alpha m}{2\pi\tau}} e^{-\alpha A_{min}}, \tag{4.27}$$

where m is the particle's mass and A_{min} is the least action between x_a and x_b,

$$A_{min} = \frac{m(x_b - x_a)^2}{2\tau}. \tag{4.28}$$

Calculating the variance of final positions, $\sqrt{\langle x_b^2\rangle - \langle x_b\rangle^2}$ and equating it to $\sqrt{2D\tau}$, where D is the diffusion coefficient, we conclude that

$$\alpha = \frac{1}{2mD}. \tag{4.29}$$

This result matches the solution of the diffusion equation, which is a great indication of the validity of the method to be further extended to the relativistic regime.

Now, the extension to the relativistic case is straightforward, in the sense that we just need to find the mean value of action through all possible paths between points x_a and x_b.

The relativistic Lagrangian of a free particle is given by

$$\mathscr{L} = -mc^2\sqrt{1 - \frac{v^2}{c^2}}, \tag{4.30}$$

where v is the velocity of the particle, c the velocity of light and the action of a path, k, is written as the integral of the Lagrangian in an interval of time. As in the non relativistic case, to calculate the mean action through all possible paths between x_a and x_b, we could, in principle, consider that those trajectories are composed by small segments where the particle moves with constant speed. Therefore

$$\begin{aligned} A_{AB} = \frac{1}{Q}\lim_{\tau\to 0}\int\int\ldots\int -mc^2\left[\sqrt{\tau^2 - \frac{(x_1-x_0)^2}{c^2}} + \sqrt{\tau^2 - \frac{(x_2-x_1)^2}{c^2}} + \ldots + \sqrt{\tau^2 - \frac{(x_n-x_{n-1})^2}{c^2}}\right] \\ \times \exp\left[\phi mc^2\left(\sqrt{\tau^2 - \frac{(x_1-x_0)^2}{c^2}} + \sqrt{\tau^2 - \frac{(x_2-x_1)^2}{c^2}} + \ldots + \sqrt{\tau^2 - \frac{(x_n-x_{n-1})^2}{c^2}}\right)\right] dx_1\ldots x_{n-1}, \end{aligned} \tag{4.31}$$

where τ is the discrete time interval. The problem with this approach is that, as discussed in the beginning of this chapter, it is impossible to describe a non-trivial continuum relativistic Markov process. Thus, we should look for a non-Markovian process and when we calculate path integrals we are implicitly assuming the system to be Markovian. However, assuming by analogy to the non relativist case, that if we could find a method of summing over all possible paths that did not require the system to be Markovian we would also find that the mean action is $A_{AB} = A_{\min} + \text{constant}$. That would imply that the probability $p_{B|A}$ is proportional to $e^{-\phi A_{\min}}$, with ϕ being a Lagrange multiplier, i.e,

$$p_{B|A} = \frac{1}{Z}\exp\left(\phi mc^2\sqrt{(t-t_0)^2 - \left(\frac{x-x_0}{c}\right)^2}\right). \tag{4.32}$$

This assumption is in accordance with the non-relativistic limit, in the sense that the distribution tends to a Gaussian if $v \ll c$.

This method generates a PDF that does not allow superluminal velocities, i.e, $p(x > ct) = 0$, but it is not a consistent PDF since, for small times, $p(x = ct) \neq 0$, i.e, the distribution is, somehow, displaced upwards. Figure 4.8 shows the distribution for different times. Note that our result approximates the result obtained

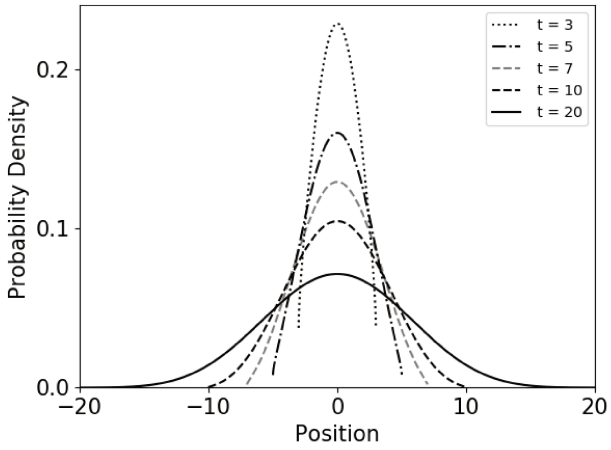

Figure 4.8: Probability density function obtained by the method of maximization of entropy for the position of the Brownian particle considering five different times.

by the method of generalization of the relativistic propagator. The difference is only due to the subtraction of 1, in the method of section 4.1.2. We can assign the difference to the fact that while their result consider $-e^{-\mathbb{A}_{\max}} + e^{-\mathbb{A}_{\min}} = e^{-\mathbb{A}_{\min}} - 1$ our generalization leads to $e^{-\mathbb{A}_{\min}}$. This suggests that our generalization is probably not taking into account a shift due to the contribution of the maximum action. Figure 4.9 shows the probability density function (4.32) displaced, i.e, $p_{B|A} - 1/Z$.

From figures 4.8 and 4.9 we see that our result is not reasonable for small times, however, as the time increases the difference between the propagator found by us and the one found in section 4.1.2 gets negligible.

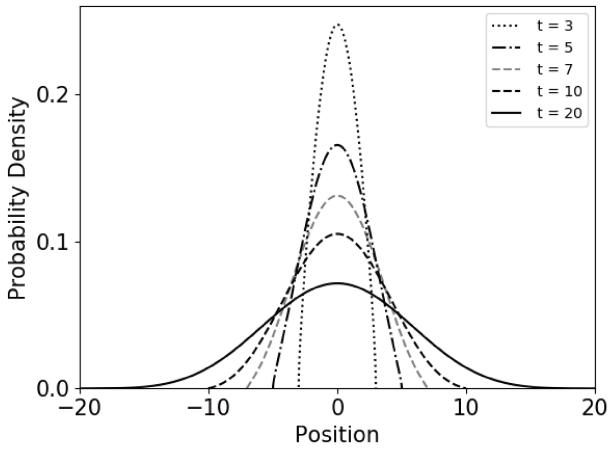

Figure 4.9: Probability density function obtained by the method of maximization of entropy for the position of the Brownian particle dislocated upwards. Note that this is the same PDF as the one found in section 4.1.2

This can be explained by the fact that the method of maximization of entropy is only valid in the equilibrium limit, when the distribution is stationary. Therefore, our result is formally correct only for large times, where it is in accordance with the equilibrium assumption. Yet, it is highly satisfactorily for describing the behavior for the variance of the distribution function at all times. Figure 4.10 displays the variance of the distribution as a function of time and the difference between the variance of the position distribution and the Gaussian. We see that the variance of the distribution is in accordance with the relativistic limit and that on the long time limit the variance grows linearly with time.

In face of the results obtained, it is remarkable that, at least for stochastic processes, the principle of least action, and the principle of maximal entropy (at equilibrium) are connected.

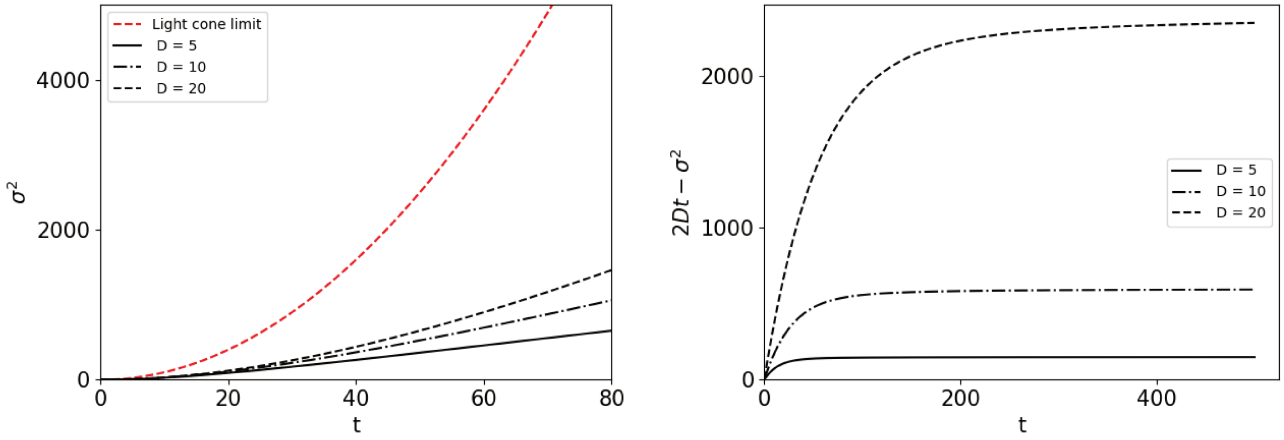

(a) Evolution of the variance.

(b) Evolution of $2Dt - \sigma^2$

Figure 4.10: Behavior of the variance for the relativistic distribution obtained in this section. In figure (a) the variance of a light wave propagating in vacuum is displayed in red for comparison with the evolution of the variance for different diffusion coefficients. And in figure (b) the difference between the variance of the relativistic and non-relativistic case is plotted.

4.2 Relativistic Brownian Motion in phase space

In the last section, we discussed three approaches to derive propagators for the relativistic diffusion. Since the strategies considered only position and time variables, the resultant propagators had to be non-Markovian. This section is devoted to models that treat Relativistic Brownian motion in the phase space, and the non-Markovian restriction does not apply to this case.

Generalized Langevin equations can form a useful tool to model the motion of particles in a random medium. Comparing with the approach of trying to find a relativistic diffusion propagator, this strategy has a more direct dependence with the fluctuation force. This means that it can be easily modified to model the motion of the Brownian particle in different types of baths. In some sense, we can also say that the microscopic features of the bath are less hidden (Dunkel and Hanggi (2009)).

We first present the relativistic Langevin equation obtained by Dunkel and Hanggi (2005) and then we discuss a derivation of a relativistic binary collision model (Dunkel and Hanggi (2009)), used as a simple microscopic model of the Brownian motion. As in the non-relativistic case, the relativistic binary collision model also leads to an equation for the momentum variation that can be heuristically interpreted as a Langevin equation.

Despite the fact that the main result of the chapter is the derivation of the propagator with the method of maximization of entropy, this section is presented for completeness, i.e, to show approaches that use the second strategy (Brownian motion in phase space) to describe the problem. Our contribution in this part of the work

are restrained to the histograms of the velocity of the Brownian particle made out of simulations of the Binary collision model.

4.2.1 Generalized Langevin Equation

Since the distribution of Brownian Motion can be derived using the Langevin equation, a possible approach to find its relativistic generalization is by trying to generalize the Langevin equation either. We worked on an attempt of generalization of the Langevin equation that used the four-vector of force instead of the usual non-relativistic version of the second law of Newton. However after gaining knowledge of the work of Dunkel and Hanggi (2005), we concluded that the challenge of making such a generalization had been overcame by the authors. For this reason, and for completeness, we will present here a brief summary of the paper. The authors use the fact that on the proper reference frame of the Brownian particle the relativistic equations must reduce to Newtonian equations, therefore, writing, on the covariant form, the equations of motion on a reference frame that is in temporary rest with respect to the particle is possible to generalize, term by term, the Langevin equation.

To generalize the viscosity force term, we write the coefficient of viscosity using an analogy with the pressure tensor known on relativistic hydrodynamics of perfect fluids (Cf. Weinberg (1972)) as

$$\nu^{\alpha}_{\beta} = \nu\left(\eta^{\alpha}_{\beta} + \frac{u^{\alpha}u_{\beta}}{c^2}\right), \tag{4.33}$$

where $(\eta^{\alpha\beta}) = (\eta_{\alpha\beta}) = \mathrm{diag}(-1,1)$ is the (1+1)-dimensional Minkowski metric tensor, ν is the viscous coefficient measured on the rest frame of the particle, c is the speed of light and u^{β} is the velocity of the particle. The relativistic Langevin equation found by the authors was

$$dp^{\alpha}(\tau) = -\nu^{\alpha}_{\beta}(p^{\beta}(\tau) - mU^{\beta})d\tau + w^{\alpha}, \tag{4.34}$$

where U^{β} is the (1+1)-velocity of the heat bath and $w^{\alpha}(\tau) = dW^{\alpha}(\tau)$ is the stochastic increment, characterized by

$$\begin{aligned} \langle w^{\alpha}(\tau)\rangle &= 0 \\ \langle w^{\alpha}(\tau)w^{\beta}(\tau')\rangle &= \begin{cases} 0, & \tau \neq \tau'; \\ D^{\alpha\beta}, & \tau = \tau', \end{cases} \end{aligned} \tag{4.35}$$

where $D^{\alpha\beta}$ is the stochastic term the characteristic correlation factor of a Wiener process. It is generalized to a correlation tensor on a similar way to the viscosity coefficient,

$$D_{\alpha\beta} = 2Dd\tau\left(\eta_{\alpha\beta} + \frac{u_{\alpha}u_{\beta}}{c^2}\right). \tag{4.36}$$

On the non relativistic limit ($|v| << c$) the usual Langevin equation is recovered.

Once the Generalized Langevin equation (4.34) is obtained the problem is apparently solved. However, since it is a stochastic differential equation there are different interpretations of the integral of the random term that leads to different Fokker-Planck equations. In the original paper, besides the usual interpretations known as Itô and Stratonovich stochastic differential equations, the authors propose a third discretization rule, known as Hänggi-Klimontovich interpretation, see appendix A.6. The momentum density functions found solving each Fokker-Planck equation are

$$\begin{aligned} P_I(p) &= C_I\left(1+\frac{p^2}{m^2c^2}\right)^{-1/2}\exp\left(-\beta\sqrt{1+\frac{p^2}{m^2c^2}}\right);\\ P_S(p) &= C_S\left(1+\frac{p^2}{m^2c^2}\right)^{-1/4}\exp\left(-\beta\sqrt{1+\frac{p^2}{m^2c^2}}\right);\\ P_{HK}(p) &= C_{HK}\exp\left(-\beta\sqrt{1+\frac{p^2}{m^2c^2}}\right), \end{aligned} \tag{4.37}$$

where the indexes I, S and HK stands to Itô, Stratonovich and Hänggi-Klimontovich discretization rules and the normalization constants are denoted by $C_{I/S/HK}$. The parameter β, defined by Einstein relation, is a measure of the ration between the rest mass and the thermal energy of the Brownian particle,

$$K_B T = \frac{mc^2}{\beta} = \frac{D}{mv}. \tag{4.38}$$

Although all three results provide distributions without superluminal solutions, the Hänggi-Klimontovich approach stands out from the others as the resultant distribution is equivalent to the Jüttner distribution presented in the appendix A.3. To see that, we change the variable of expressions (4.37) to find the velocity distributions by

$$\mathbb{P}(v) = P(p(v))\left|\frac{\partial P}{\partial v}\right|, \tag{4.39}$$

where $p(v) = mv\gamma(v)$, γ being the Lorentz factor. Figure (4.11) displays the three probability distributions of the velocity of the Brownian particle for three different values of β. The results show that in the low-temperature limit, ($\beta >> 1$), all three solutions approach a Gaussian profile, and as the temperature increases the differences between the distributions are accentuated. The last Hänggi-Klimontovich interpretation seems to be more interesting than the other two, due to the fact that it leads to a Jüttner distribution. However, which one is the correct physical interpretation is an open question that probably depends of the microscopic structure of the environment that the Brownian particle is embedded in.

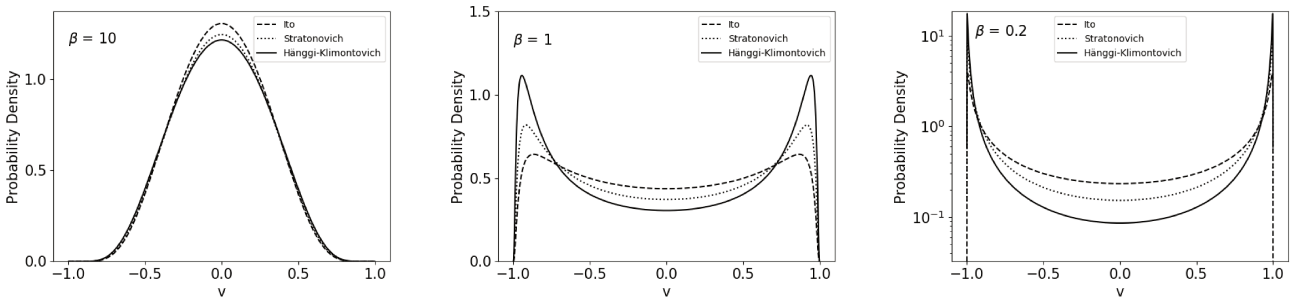

(a) $\beta = 10$. (b) $\beta = 1$. (c) $\beta = 0.2$.

Figure 4.11: Probability density function of the velocity of the Brownian particle considering three values of parameter β. Here we consider natural units.

4.2.2 Relativistic Binary Collision Model

As demonstrated in section 3.2, the Binary collision model can be used to obtain a Langevin-type equation from the microscopic features of the problem. This section concerns the generalization of the binary elastic collision model to the relativistic case. Despite being a simple model for the system, it can work as an alternative procedure to simulate the behavior of the Brownian motion at this regime Dunkel (2008).

The assumptions of the model are the same as the ones for its non relativistic counterpart. Therefore the notation for mass, momentum and energy are, as well, the same. Let us consider an elastic collision between the Brownian particle and a molecule of the fluid, such that the total momentum and energy of the system are conserved,

$$\begin{aligned} M_i &= M_f; \\ m_i &= m_f; \\ E_i + e_i &= E_f + e_f; \\ P_i + p_i &= P_f + p_f. \end{aligned} \tag{4.40}$$

In this case, however, the momentum is given by $p = mv\gamma(v)$, the energy by $e = (m^2c^4 + p^2c^2)^{1/2}$ and the velocities of the particles of the fluid respect the Jüttner distribution (Appendix A.3). Solving the system of equations we find the variation of the momentum of the Brownian particle due to the collision with the r-molecule of the fluid,

$$\Delta P_r = -2\gamma(u_r)^2 \frac{e_r}{E_+ e_r} P + 2\gamma(u_r)^2 \frac{E}{E + e_r} p_r, \tag{4.41}$$

where $u(p,P) = \frac{P+p}{E+e}$. Note that equation (4.41) becomes (3.19) at low velocities. The variation of momentum

for the Brownian particle during the interval δt can e approximated by

$$\begin{aligned}\delta P(t) &= P(t+\delta t) - P(t) \\ &\approx -2\sum_{r=1}^{N}\gamma(u_r)^2\frac{e_r}{E+e_r}P(t)I_r(t,\delta t) + 2\sum_{r=1}^{N}\gamma(u_r)^2\frac{E}{E+e_r}p_r I_r(t,\delta t),\end{aligned} \tag{4.42}$$

where I is the same as for the non relativistic case. As in the non-relativistic version of the model, we can heuristically identify the first term of eq. (4.42) as the 'friction' and the second one as the 'stochastic force'.

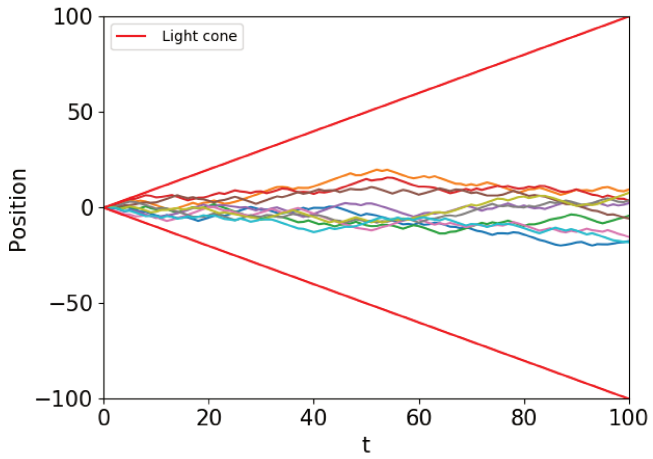

Figure 4.12: Path of ten Brownian particles in one dimension, simulated using relativistic binary collision model. The path of a light propagating wave is displayed for comparison.

We employ this model to simulate the motion of 10 Brownian particles ($M/m = 10^6$) in one dimension on a bath of inverse temperature $\beta = 1$. We considered that the particle suffers one single collision at each time step ($dt = 1$). Fig. 4.12 shows the position as a function of time for each of the simulations. They were calculated by considering that the particle has a constant velocity between collisions. Note that the positions of the particles stay inside the light-cone limit at all times. For small times the positions reach close to the limit allowed by relativity and for long times the particles keep localized on the central region, far from the frontier of the light cone.

To analyze the behavior of the velocity distribution of the Brownian particles we made the histograms presented in figure 4.13 of the velocity of the particle after 100 collisions, considering 1000 runs of the simulation — to see the code of the simulation we refer to A.7 . We see that the result of the model, indeed, seems to exclude superluminal velocities. Furthermore, the distribution of velocities of a particle in a 'cold' bath has the usual shape of a Gaussian, while the for hotter baths, e.g. when $\beta = 1$ the distribution has a bi-stable character. The Jüttner distribution is also depicted in red, for comparison. We see that for all three values of β the relativistic velocity distribution is a good fit for the histogram.This is an indication that the Brownian particle is achieving thermal equilibrium with the fluid. The results are, apparently, in accordance with the distributions obtained

by the solution of the generalized Langevin equation, figure 4.11.

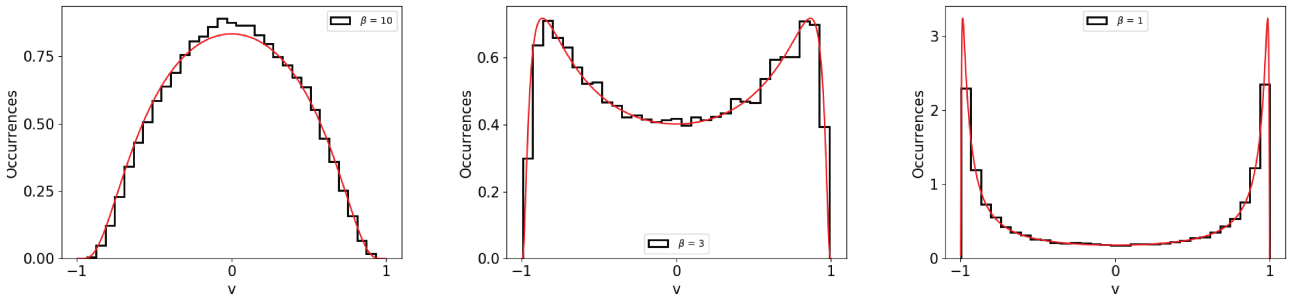

(a) $\beta = 10$. (b) $\beta = 5$. (c) $\beta = 1$.

Figure 4.13: The histogram of the velocity of the Brownian particle after 100 collisions. The units are such that $c = 1$, i.e, natural units.

At last, to compare these results with the other previous models we also made a graph of the position variance as a function of time, fig.4.14. The variance was obtained by a sample of size 1000 and the variance of a light wave propagating in the vacuum is displayed to help comparisons. Again we see that the curves are in accordance with the speed limit.

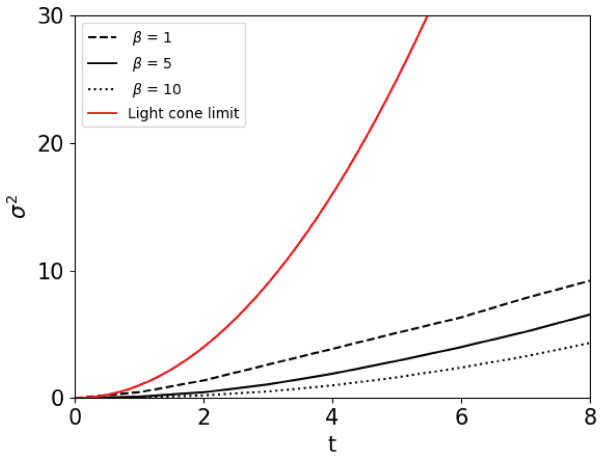

Figure 4.14: Variance of the the position distribution of relativistic Brownian motion in view of the relativistic binary collision model.

Since this model is a relativistic extension of binary collision model, it is possible to derive a relativistic Langevin equation using an analogous procedure to the one used in section 3.2. The Langevin equation is again

$$\frac{dP(t)}{dt} = -k(P)P + \Gamma(t),$$

with $\langle \Gamma(t_1)\Gamma(t_2)\rangle = q(P)\delta(t_1 - t_2)$. However, now the coefficient $q(t)$ is given by a relativistic version of the one

obtained the previously. This is done by switching the mass for the energy (Dunkel and Hanggi (2009))

$$q(P) = 2k(P)E(P)K_B T. \tag{4.43}$$

Demanding the same condition as in the non-relativistic case, $\left\langle \frac{dP(t)}{dt}\Big|_{P(t)=p} \right\rangle = \left\langle \frac{\delta P(t)}{\delta t}\Big|_{P(t)=p} \right\rangle$, we find that the coefficient $k(p)$ respects the following differential equation

$$-k(p)p + K_B T \frac{d}{dp}[k(p)E(p)] = \mathcal{K}(p). \tag{4.44}$$

Once again, if the solution of the ordinary differential equation is obtained, the function $k(p)$ allows the Langevin equation to be completely defined for the system. However sometimes the solution can be hard or even impossible to be found. In this case, one has to appeal to approximations. In any case the method allow us to find a Langevin equation from the previous knowledge of the fluid and assumptions related to the interactions between the Brownian particle and the molecules of the medium.

4.3 Conclusions

As explained in the introductory part of the chapter, it is impossible to find a relativistic non-trivial, continuous Markov process in position space. Due to this imposition, we studied in this chapter two strategies to analyze relativistic Brownian motion. First, we analyzed approaches of non-markovian generalization of diffusion propagator and then we analyzed models that take into account relativistic Brownian motion in phase space.

Concerning the first strategy, three approaches where proposed. Figure 4.15 shows a comparison between the PDFs obtained in section 4.1 and the Gaussian distribution, where we considered $h = v = D = 1$ because this parameters generate a Gaussian with the same variance in the asymptotic limit ($t \to \infty$). From figure 4.15 we can infer that, in fact, all methods tend to a Gaussian in the asymptotic limit. For small times the distributions have notable differences. The solution to the Telegraph equation imposes a big probability of finding the particle with the speed of light and this is not suitable for a particle with mass. Thus, we conclude that the best options for the generalized relativistic diffusion propagators are the ones obtained by Dunkel et al. (2006) and by our approach of maximization of entropy. As we already discussed, both results are equal apart from a constant shift, which is due to a contribution of the maximum action. Since our approach is only valid for the equilibrium, where the distribution, in fact, has the maximum entropy and in that regime the difference between both approaches are negligible we can affirm that our result is in accordance with Dunkel's .

In section 4.2 we first analyzed a method to obtain a relativistic generalization of the Langevin equation by generalizing term by term equation 3.3. Then we used a microscopic model to simulate the relativistic Brownian motion by considering elastic collisions between the Brownian particle and the particles of the bath. Both

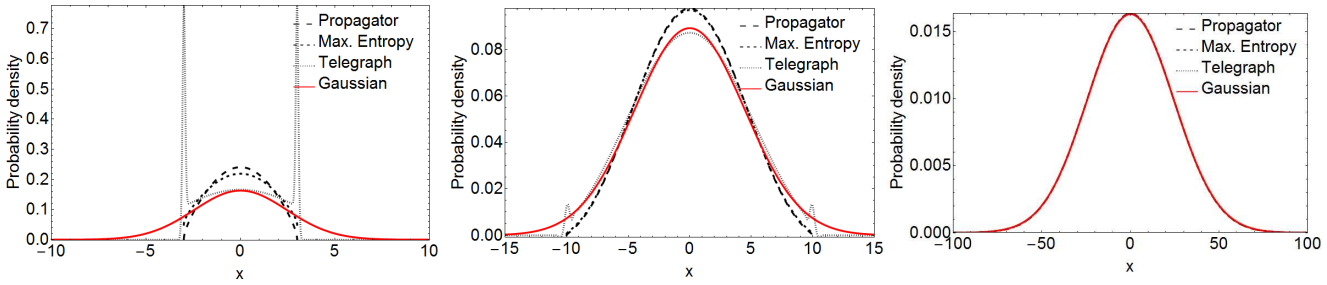

(a) $t = 3$. (b) $t = 10$. (c) $t = 100$.

Figure 4.15: Comparison between the position PDF's derived in the chapter. Natural units are being considered.

approaches lead to a stationary distribution that is in accordance with Jüttner distribution of velocities. This is a good indicator of the validity of the methods, however, the real features of those methods depend on the nature of the medium that the Brownian particle is embedded in.

CHAPTER 5

Connection Between the Relativistic Stochastic Equations and Quantum Mechanics

It is well known that the diffusion equation is connected to the Schrodinger's equation by an analytic continuation. In fact, this connection inspired the generalization of Wiener's integral (Appendix A.5) to a new description of quantum mechanics via Feynman's path integrals. In this chapter, we present connections between a relativistic version of the Schrodinger's equation, a "relativistic diffusion equation" and an analogous connection between Dirac and the telegraph equations. Those connections are shown here to demonstrate the mathematical resemblance between differential equations of the quantum, relativistic quantum, and classical stochastic regimes. These connections are also useful because, knowing them, one can look for the solution of a new mathematical issue in a relativistic context in the literature of the stochastic theory. The resemblances also may directly allow one to use the results of the stochastic simulations to investigate of analogous relativistic systems.

We assert here and reinforce it in other parts of the section, that there is no reasonable physical argument to believe that just because an analytic continuation of Schrodinger's equation leads to the diffusion equation, this could be generalized to the relativistic regime. In fact, the result of section 5.1 shows the opposite, since the "relativistic diffusion equation" derived by the analytic continuation of Schrodinger's equation does not respect the limits imposed by the relativistic theory.

5.1 Analytic Continuation of the Relativistic Schrodinger's Equation

A different approach to find a 'relativistic' generalization of the diffusion equation was developed by Baeumer et al. (2010). As mention before, Schrodinger's equation is connected to the diffusion equation by an analytic

continuation. To see that we write the first one as

$$i\hbar\frac{\partial\psi}{\partial t} = \frac{-\hbar^2}{2m}\Delta\psi, \tag{5.1}$$

where m is the rest mass, $\frac{\hbar^2\Delta}{2m} = \frac{\mathbf{p^2}}{2m}$ and $\mathbf{p}$ is the moment. Then the analytic continuation $\tau = it$ leads to the classical diffusion equation,

$$\hbar\frac{\partial\psi(x,\tau)}{\partial\tau} = \frac{\hbar^2}{2m}\Delta\psi(x,\tau), \tag{5.2}$$

with the diffusion coefficient being $D = \hbar/2m$. The main idea of this approach is to extrapolate this idea to the relativistic context, i.e, to consider a relativistic version of Schrodinger's equation and make the same transformation. To obtain this relativistic version we simply change the kinetic energy, $\frac{\mathbf{p^2}}{2m}$, from equation (5.1) to its relativistic form $\sqrt{\mathbf{p^2}c^2 + m^2c^4} - mc^2$, leading to

$$i\hbar\frac{\partial\psi}{\partial t} = E\psi = [\sqrt{\mathbf{p^2}c^2 + m^2c^4} - mc^2]\psi = [\sqrt{-\hbar^2c^2\nabla + m^2c^4} - mc^2]\psi, \tag{5.3}$$

Making the same analytic continuation, $\tau = it$, the relativistic Schrodinger's equation becomes

$$\frac{\partial\psi(x,\tau)}{\partial\tau} = [mc^2 - \sqrt{\hbar^2c^2\nabla + m^2c^4}]\psi(x,\tau). \tag{5.4}$$

Substituting $m' = \frac{mc^2}{\hbar}$ and $t = \tau$ we have

$$\frac{\partial\psi(x,t)}{\partial t} = [m' - \sqrt{m'^2 - c^2\nabla}]\psi(x,t). \tag{5.5}$$

Which is - by considering that the connection of the non-relativistic case is also valid in this case - the relativistic diffusion equation. Note that the expression contains a fractional derivative operator, $\nabla^{1/2}$. There are two ways to contour this problem. The first one is by taking the Fourier transform and using the fact that if $\hat{\psi}(k,t) = \int e^{-i\mathbf{k}\cdot\mathbf{x}}\psi(x,t)dx$ is the Fourier transform of $\psi(x,t)$, then the transform of $\Delta\psi(x,t)$ is $-|\mathbf{k}|\hat{\psi}(k,t)$. This leads to

$$\hat{\psi}(k,t) = \exp[t(m' - \sqrt{m'^2 - c^2|\mathbf{k}|^2})], \tag{5.6}$$

that is the Fourier transform of a known probability density function called normal inverse Gaussian distribution (NIG).

The second way to deal with the problem is by finding an equivalent differential equation that does not have fractional derivatives. To get to this equation we first take the Fourier transform with respect to the spacial variable and the Laplace transform with respect to the time variable. This leads equation (5.5) to

$$s\bar{\psi}(k,s) - \hat{\psi}_0(k) = [m' - \sqrt{m'^2 - c^2|\mathbf{k}|^2}]\bar{\psi}(k,s), \tag{5.7}$$

where $\bar{\psi}(k,s)$ is the Fourier-Laplace transform of $\psi(x,t)$. Rearranging terms we obtain

$$\bar{\psi}(k,s) = \frac{\hat{\psi}_0(k)}{s - m' + \sqrt{m'^2 - c^2|\mathbf{k}|^2}}. \tag{5.8}$$

Multiplying the right hand side by $\frac{s-m'-\sqrt{m'^2-c^2|\mathbf{k}|^2}}{s-m'-\sqrt{m'^2-c^2|\mathbf{k}|^2}}$ leads to

$$\bar{\psi}(k,s)=\frac{[s-m'-\sqrt{m'^2-c^2|\mathbf{k}|^2}]\hat{\psi}_0(k)}{s^2-2m's-c^2|\mathbf{k}|}, \tag{5.9}$$

that can be reorganized as

$$-[s^2\bar{\psi}(k,s)-s\hat{\psi}_0(k)-(m'-\sqrt{m'^2-c^2|\mathbf{k}|^2})\hat{\psi}_0(k)]+2m'[s\bar{\psi}(k,s)-\hat{\psi}_0(k)]=-c^2|\mathbf{k}|\hat{\psi}_0(k). \tag{5.10}$$

Finally, dividing the whole expression by $2m'$ and inverting the Fourier-Laplace transform we arrive to

$$-\frac{1}{2m'}\frac{\partial^2}{\partial t^2}\psi(x,t)+\frac{\partial}{\partial t}\psi(x,t)=\frac{c^2}{2m'}\Delta\psi(x,t). \tag{5.11}$$

This differential equation is mathematically equivalent to the relativistic diffusion equation (5.5), but does not contain any fractional calculus operator. The solution is given by Baeumer et al. (2010), as

$$\psi(x,t)=\int_0^\infty p(x,\tau)h(\tau,t)d\tau, \tag{5.12}$$

where $p(x,\tau)$ is a Gaussian distribution

$$p(x,\tau)=\frac{\exp\left(-\frac{x^2}{2c^2t/m'}\right)}{\sqrt{2\pi c^2 t/m'}}, \tag{5.13}$$

and $h(\tau,t)$ is given by

$$h(\tau,t)=\frac{t}{\tau}\frac{\exp\left(-\frac{(t-\tau)^2}{2\tau/m'}\right)}{\sqrt{2\pi\tau/m'}}. \tag{5.14}$$

Figure (5.1) shows the normal inverse Gaussian distribution, equation (5.12), for different values of mass and time. Note that for small times the relativistic process approximates a Cauchy process and for long times the distribution approximates a Gaussian. Analyzing the distribution for different masses we also find a transition to the Cauchy distribution for small masses, m' and, to the non-relativistic result for larger masses.

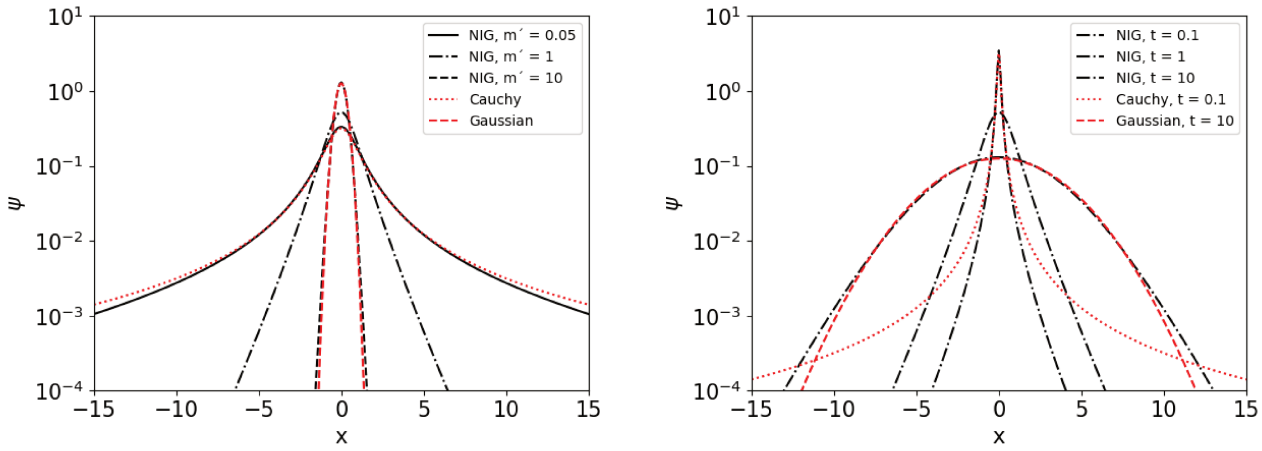

(a) Different values of m' and $t = 1$.

(b) Different values of t and $m' = 1$.

Figure 5.1: The graphs show the solution of the relativistic diffusion equation. The Cauchy and Gaussian distributions are also shown for comparison.

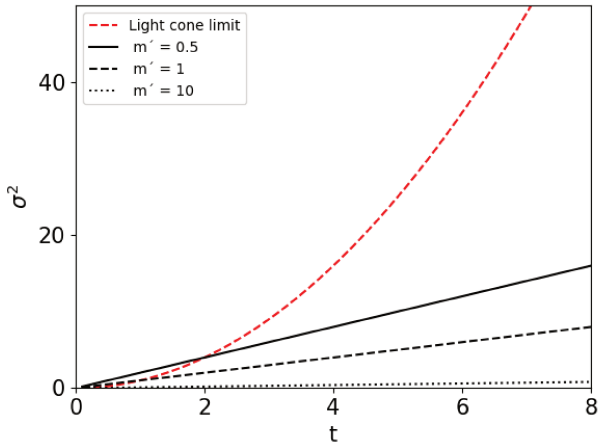

Figure 5.2: Variance evolution of the probability density function of relativistic Brownian motion obtained by the analytical continuation of relativistic Schrodinger equation, considering the initial probability as $p(x, t = 0) = \delta(x)$ is displayed in black for different values of parameter m'. The variance of light wave propagating in vacuum is presented in red for comparison.

An important feature of this distribution is that the behavior of the variance is the same as the one of Brownian motion, i.e, it grows linearly with time, $\sigma^2 = \dfrac{t}{m'}$. Figure 5.2 shows this result for different values of m'.

From fig. 5.1 and 5.2 we see that the model does not present the sharp fronts of the telegraph equation, but it does not exclude the superluminal positions. Therefore it is not a good candidate to be used on a relativistic version of Brownian motion. This result was somewhat expected, since there is no reason to believe that the

connection between the diffusion equation and Schrodinger's equation would also exist in the relativistic limit.

5.2 Analytic Continuation of the Dirac Equation

As demonstrated in the last section the Schrodinger's equation is connected to the diffusion equation by an analytic continuation. This continuation can be implemented by imaginary time, as in section 5.1, but also by other transformations as imaginary $\hbar$ and imaginary mass. This fact is connected to the fact that Wiener's and Feynman's integrals are also different only by an analytic continuation (see Appendix A.5). Gaveau et al. (1984) extended these connections to the relativistic case and demonstrated that the Dirac equation is connected to the Telegraph's equation also by an analytic continuation.

Let us again consider a particle moving in a line with velocity v that from time to time changes its direction of motion. Suppose that the reversal of direction is Poisson distributed, i.e., the probability of changing the direction in the time interval dt is $a\,dt$. The master equation for this process is given by

$$P_{\pm}(x, t+\Delta t) = P_{\pm}(x \mp \Delta x, t)(1 - a\Delta t) + P_{\mp})(x \pm \Delta x, t)a\Delta t, \tag{5.15}$$

where $P_+(x,t)$ and $P_-(x,t)$ correspond to the probability of the particle being in position x at time t moving to the right and left, respectively. After some calculations, dividing the expression by $\Delta x \Delta t$ and taking the limits of $\Delta x \to 0$ and $\Delta t \to 0$, we find that

$$\frac{\partial P_{\pm}}{\partial t} = -a(P_{\pm} - P_{\mp}) \mp v\frac{\partial P_{\pm}}{\partial x}, \tag{5.16}$$

where $v = \dfrac{\Delta x}{\Delta t}$. That are two coupled equations. To decouple them, we isolate the probability with respect to one of the directions and substitute it in the other coupled equation. This results in

$$\frac{\partial^2 P_{\pm}}{\partial t^2} - v^2\frac{\partial^2 P_{\pm}}{\partial x^2} = -2a\frac{\partial P_{\pm}}{\partial t}, \tag{5.17}$$

which is the Telegraph equation, again. Gaveau et al. (1984) demonstrated the connection between equation 5.16 and the Weyl representation of the Dirac equation,

$$i\hbar\frac{\partial \psi}{\partial t} = mc^2\sigma_x\psi - ic\hbar\sigma_z\frac{\partial \psi}{\partial x}. \tag{5.18}$$

This is done by the transformation $u(x,t) = \exp(imc^2 t/\hbar)\psi(x,t)$. This leads to

$$\frac{\partial u_{\pm}}{\partial t} = \mp c\frac{\partial u_{\pm}}{\partial x} - \frac{imc^2}{\hbar}(u_{\pm} - u_{\mp}), \tag{5.19}$$

where the indexes + and − refer to the first and second components on the spinor, u, respectively. Identifying $c \leftrightarrow v$ and $\dfrac{imc^2}{\hbar} \leftrightarrow a$ we see that the connection is indeed valid. The continuation can also be made by taking the imaginary time, then v will have the imaginary factor as well, since $v = \frac{dx}{dt}$. The mathematical resemblance extends to the path integral formulations, where the sum over paths are identical, but for an imaginary factor i.

The conclusion we can take from those connections is that, mathematically, the structure of Brownian motion is related to Schrodinger's equation the same way that a Poisson's process is related to the Dirac equation. Does this mean that the telegraph equation is the right candidate for a relativistic diffusion equation? Not necessarily. This conclusion would represent an arbitrary extrapolation of the mathematical resemblance. First, because we would have to assume that the Dirac equation is the correct relativistic extension of Schrodinger equation, and not the relativistic Schrodinger's equation presented in the last section, or other relativistic equation like Klein Gordon equation, for example, without mentioning masses and velocities. Secondly, we would need to assume that the connection between Schrodinger and the diffusion equation is also valid in the relativistic context, that is, the relativistic Brownian motion is described by an equation that is an analytic continuation of a relativistic version of Schrodinger's equation. We should be careful when interpreting the mathematical resemblances studied in this and in the last section to not attribute more meaning then they already carry. However, the analogy between both structures can be very useful to solve quantum mechanical problems with small changes in the tools developed to the study of classical problems. Those types of connections are very important to provide a better mathematical understanding of the quantum-classical-relativistic limits.

Once the relativistic regime has already been discussed, we devoted the next chapters to the analyzes of the quantum generalization of the simple random walk.

CHAPTER 6

Quantum Walks

Quantum Walks form a wide group of dynamical systems that represent the time evolution of a walker on a graph. Those are mainly divided in the Discrete-Time Quantum Walks (DTQW) and Continuous-Time Quantum Walks (CTQW). In this work our main interest is related to Discreet Time Quantum Walks on a one-dimension infinite lattice, therefore most part of the chapter is devoted to the introduction and analysis of thermodynamic properties of this type of quantum walks. For completeness, in appendix A.8, we also present an overview of the continuous-time quantum walk.

The study of Quantum Walks started as a generalization of the classical random walks to quantum systems. However, some of their properties attracted the attention of researchers to the possibility of using them as a mathematical tool to build quantum algorithms. Among those properties we can cite:

- The quantum walk in one dimension spreads ballistically, i.e, quadratically faster than the random walk. This characteristic will be more emphasized in the next sections.
- The mixing time — amount of time taken to reach the limiting distribution — of a quantum walk is quadratically faster than its classical counterpart.
- A quantum walk can have a hitting time smaller than the random walk, i.e, the time to reach a chosen site can be small.
- It has been proved that Quantum Walks, under particular conditions, can be used to implement a model of universal computation - Childs (2009); Lovett et al. (2009).

- The quantum walk can be used to simulate analogous systems, such as relativistic quantum mechanical systems See Chapter 8).

In the next sections, we will first give an overview of discrete-time quantum walks (Portugal (2013)) and analyze the asymptotic limit of the coin state. Particularly, we prove that if a quantum walk respects the master equation used to model quantum Brownian motion, in the asymptotic equilibrium the Hamiltonian of the coin system depends on the initial conditions. Then, in sections 6.3 and 6.4 we analyze the thermodynamics of the quantum walks calculating its entanglement entropy and temperature. As expected, our numerical results imply that, in the asymptotic limit, the entanglement temperature converges to Gibbs temperature. At last, in section 6.5, the calculations are extended to a three-state quantum walk, which is a quantum walk that accounts also for the possibility that the walker stays at the same site. Our contribution related to this part of the work consists of the analytic calculation of the reduced asymptotic density matrix of the coin and the calculation of entropy and temperature of this type of walk. We conclude that in this case the entanglement temperature also converges to a Gibbs temperature when the system is in equilibrium with the bath.

6.1 Discrete time Quantum walk: Overview

The Quantum Walk on the line is the quantum version of the simple random walk studied in Chapter 2. Therefore its dynamics can be described by two operators, one representing the coin toss and the other, the shift of the walker on the line. The difference between the random walk and its quantum version is that in the second case the coin toss does not give a classical result such as heads or tails, but a superposition of both. In that way, instead of taking a step to the right or to the left, the walker step is a superposition of both directions. Figure 6.1 illustrates this difference using a Galton board.

The system is composed by a coin and a walker, therefore its Hilbert space is written as $\mathscr{H} = \mathscr{H}_C \otimes \mathscr{H}_P$, where $\mathscr{H}_C$ is the coin Hilbert space and $\mathscr{H}_P$ the Hilbert Space associated with the positions of the walker in the one dimensional infinite lattice. The state of the system at any time can be described as a spinor

$$|\psi(t)\rangle = \sum_{n=-\infty}^{\infty} \begin{pmatrix} a_n(t) \\ b_n(t) \end{pmatrix} |n\rangle\,, \tag{6.1}$$

where a_n and b_n are the wave components correspondent to left and right chirality, respectively, i.e, with the two possibles states of the coin.

As in its classical counterpart, each time step of the Quantum Walk dynamics is composed by two operations. A rotation in the coin (chirality) space (C), followed by a shift (Sh) operation. Using the variable $\gamma \in [0, \pi/2]$

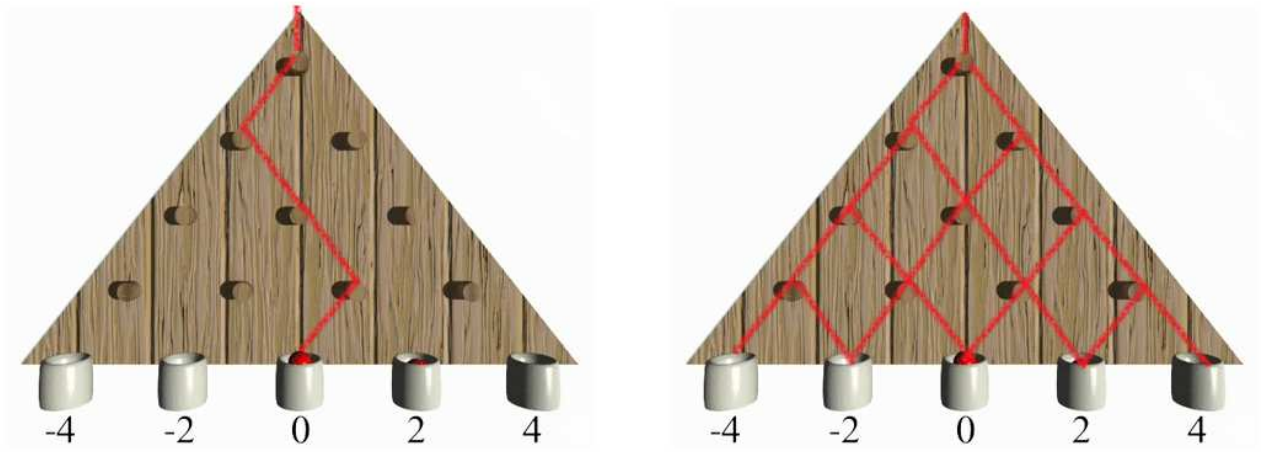

(a) Random Walk

(b) Quantum walk

Figure 6.1: Illustration of Random (a) and Quantum (b) Walk. Figure modified from Silberhorn (2020)

to determine the bias of the coin, the first operator can be written as

$$C = \begin{pmatrix} \cos\gamma & \sin\gamma \\ \sin\gamma & -\cos\gamma \end{pmatrix}. \tag{6.2}$$

If $\gamma = \pi/4$ the coin is know as the Hadamard coin. On the other hand, the shift operator is

$$\mathrm{Sh} = \left(\sum_{n=-\infty}^{\infty} |n-1\rangle\langle n| \otimes |L\rangle\langle L| \right) + \left(\sum_{n=-\infty}^{\infty} |n+1\rangle\langle n| \otimes |R\rangle\langle R| \right). \tag{6.3}$$

Therefore, using these two unitary operators the dynamics can be summarized to

$$|\psi(t)\rangle = (\mathrm{Sh}(C \otimes \mathbb{I}))^t |\psi(0)\rangle = U|\psi(0)\rangle, \tag{6.4}$$

where $\mathbb{I}$ stands for the identity in position space, and t is the time parametrized as the number of time steps. In order to give some intuition about the evolution of the walk for the reader let us calculate here the first steps of a Hadamard walk with initial condition

$$|\psi(0)\rangle = \begin{pmatrix} 1 \\ 0 \end{pmatrix} |0\rangle = |L\rangle \otimes |0\rangle. \tag{6.5}$$

The firs step leads to

$$|\psi(1)\rangle = \mathrm{Sh}(C \otimes \mathbb{I})|L\rangle \otimes |0\rangle = \mathrm{Sh}\left[\frac{|L\rangle + |R\rangle}{\sqrt{2}} \right] \otimes |0\rangle = \frac{1}{\sqrt{2}}(|L\rangle \otimes |-1\rangle + |R\rangle \otimes |1\rangle). \tag{6.6}$$

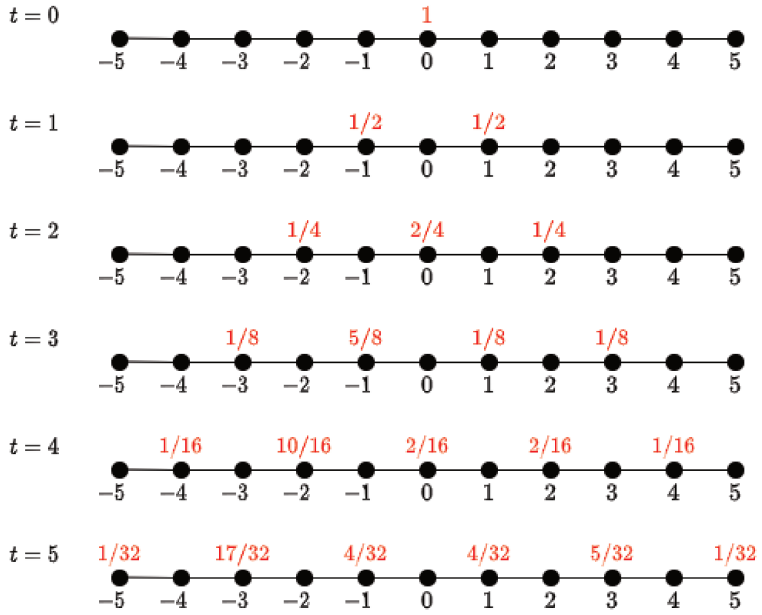

Figure 6.2: illustration of the fist five steps of the quantum walk with initial condition $|L\rangle \otimes |0\rangle$

Analogously the states at the next four steps are

$$
\begin{aligned}
|\psi(2)\rangle &= \frac{1}{2}(|L\rangle \otimes |-2\rangle + (|L\rangle + |R\rangle) \otimes |0\rangle - |R\rangle \otimes |2\rangle);\\
|\psi(3)\rangle &= \frac{1}{2\sqrt{2}}(|L\rangle \otimes |-3\rangle + (2|L\rangle - |R\rangle) \otimes |-1\rangle - |L\rangle \otimes |1\rangle + |R\rangle \otimes |3\rangle);\\
|\psi(4)\rangle &= \frac{1}{4}(|L\rangle \otimes |-4\rangle + (3|L\rangle + |R\rangle) \otimes |-2\rangle + (-|L\rangle + |R\rangle) \otimes |0\rangle + (|L\rangle - |R\rangle) \otimes |2\rangle - |R\rangle \otimes |4\rangle);\\
|\psi(5)\rangle &= \frac{1}{4\sqrt{2}}(|L\rangle \otimes |-5\rangle + (4|L\rangle + |R\rangle) \otimes |-3\rangle - 2|R\rangle \otimes |-1\rangle - 2|R\rangle \otimes |1\rangle + (2|R\rangle - |L\rangle) \otimes |5\rangle + |R\rangle \otimes |5\rangle).
\end{aligned}
\tag{6.7}
$$

With those states we can obtain the position probabilities distribution, displayed in red on figure 6.2, by summing the two chirality contributions, i.e., using that $P(n,t) = |a_n(t)|^2 + |b_n(t)|^2$. Note that for $t < 3$ the probability distribution is identical to the probability of the random walk. After that, the interference starts to make the distribution differ from the classical one. At $t = 3$ the distribution also starts to get asymmetric, this is due to the fact that the Hadamard operator acts differently in the states $|L\rangle$ and $|R\rangle$. Therefore, since the initial condition is $|L\rangle \otimes |0\rangle$, there are more cancellations of the terms of right chiralities. To obtain a symmetrical distribution we need to superpose the distribution of the walks starting with both coin states. We do that by considering $\frac{1}{\sqrt{2}}(|L\rangle - i|R\rangle)|0\rangle$ as the initial condition.

By analysing the procedure used to calculate the state after the first five time steps we see that the action of the coin and shift operators can be summarized in the following recurrence relation for the chirality amplitudes

$$
\begin{aligned}
a_n(t+1) &= a_{n+1}(t)\cos\gamma + b_{n+1}(t)\sin\gamma,\\
b_n(t+1) &= a_{n-1}(t)\sin\gamma - b_{n-1}(t)\cos\gamma.
\end{aligned}
\tag{6.8}
$$

Using that relation the quantum walk with Hadamard coin was simulated. Figure 6.3 shows the position probability density function of the walker for $t = 100$.

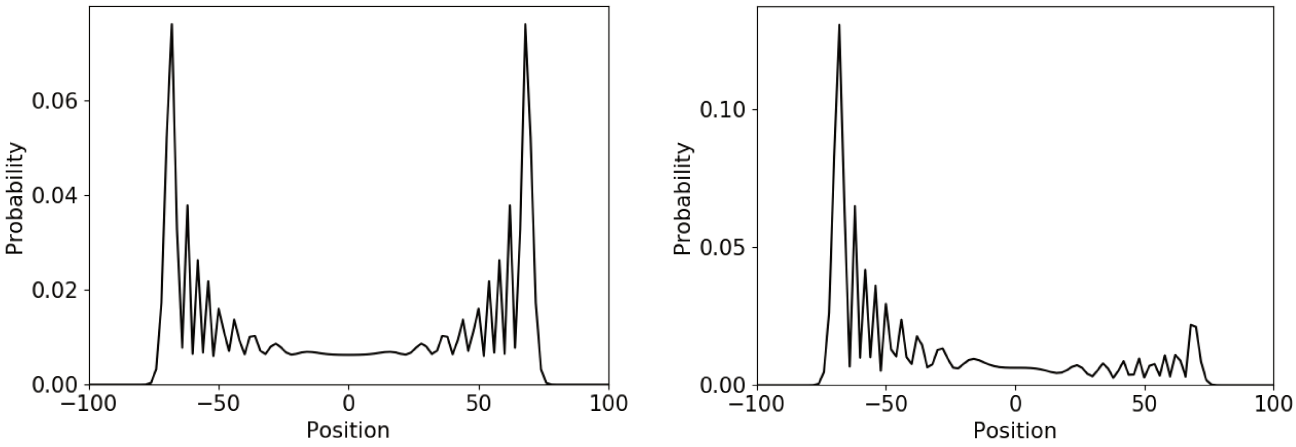

(a) $|\psi(0)\rangle = \frac{1}{\sqrt{2}}(|L\rangle - i\,|R\rangle)\,|0\rangle$.

(b) $|\psi(0)\rangle = |L\rangle \otimes |0\rangle$.

Figure 6.3: Probability distribution of the position of the walker after 100 steps. On (a) the initial condition generates a symmetric distribution, while on figure (b) the initial condition generates an asymmetric distribution.

One significant property of the discrete-time Quantum Walk that plays an important rule in the development of quantum search algorithms is its ballistic behavior, i.e., the fact that its standard deviation scales as $\sigma \propto t$ which is much faster than the classical case, where $\sigma \propto \sqrt{t}$. This difference can be seen clearly in figure 6.4 (a). Note that the slope of the line depends on the bias of the coin, γ.

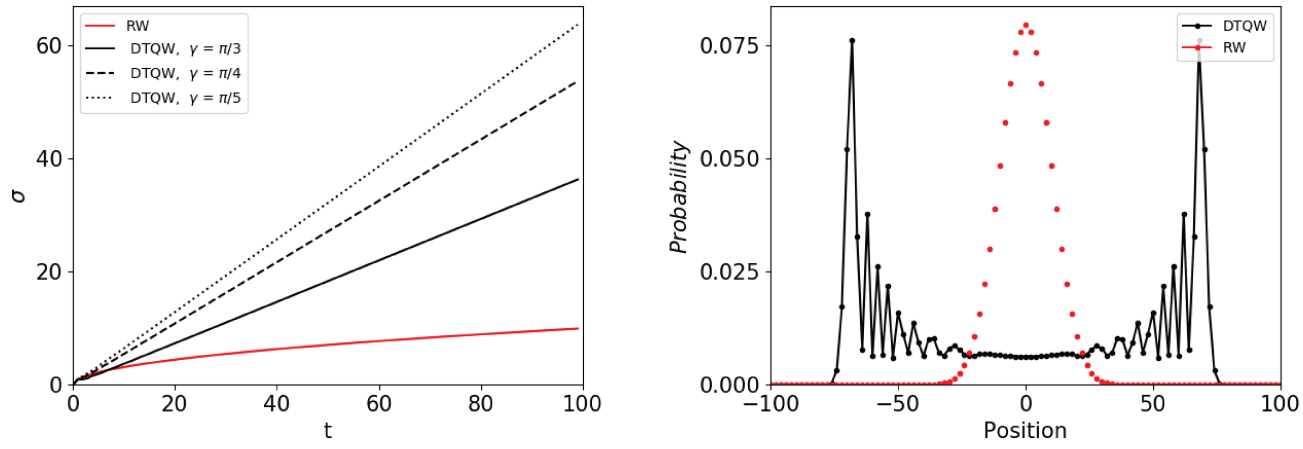

(a) Evolution of the standard deviation.

(b) Distribution of the quantum and random walk

Figure 6.4: Figure (a) compares the standard deviation of the classical and quantum walks and (b) is a comparison between both probability density functions in the symmetric case after 100 time steps.

To obtain the position probability distribution, such as shown in figure 6.3, the square of the amplitudes $a(x)$ and $b(x)$ are taken in account. Mathematically speaking, this means that to analyze the behavior of the walk on the position space only, a partial trace on the chirality space has to be done. The same can be made on the other way, that is, we can take the partial trace on position space to get a two dimensional density matrix and analyze the coin space. This approach is formalized by Romanelli (2010), where the global right and left chirality distributions were defined as

$$\begin{aligned} P_L(t) &= \sum_{n=-\infty}^{\infty} |a_n(t)|^2 \\ P_R(t) &= \sum_{n=-\infty}^{\infty} |b_n(t)|^2, \end{aligned} \tag{6.9}$$

and they represent the probabilities of the possible results of a measurement of the state of the coin. Using eq. (6.8) the evolution of the global chirality distributions is obtained,

$$\begin{pmatrix} P_L(t+1) \\ P_R(t+1) \end{pmatrix} = \begin{pmatrix} \cos\gamma^2 & \sin\gamma^2 \\ \sin\gamma^2 & \cos\gamma^2 \end{pmatrix} \begin{pmatrix} P_L(t) \\ P_R(t) \end{pmatrix} + \mathbb{R}e(Q(t)) \sin 2\gamma \begin{pmatrix} 1 \\ -1 \end{pmatrix}, \tag{6.10}$$

where $Q(t) = \sum_{n=-\infty}^{\infty} b_n^*(t) a_n(t)$ is a interference term, responsible for the quantum effects that differentiate it from the random walk. If this term is left out, a classical Markovian process is recovered, Cf. Romanelli et al. (2003). Taking the limit of $t \to \infty$ in eq. (6.10) the asymptotic global chiralities are found to depend exclusively on the asymptotic value of Q:

$$\lim_{t\to\infty} \begin{pmatrix} P_L(t) \\ P_R(t) \end{pmatrix} \equiv \begin{pmatrix} P_{L,\infty}(t) \\ P_{R,\infty}(t) \end{pmatrix} = \frac{1}{2} \begin{pmatrix} 1 + 2\mathbb{R}e(Q_\infty)/\tan\gamma \\ 1 - 2\mathbb{R}e(Q_\infty)/\tan\gamma \end{pmatrix}, \tag{6.11}$$

and the reduced density matrix at time t is

$$\rho_c(t) = \mathrm{Tr}_n(|\psi(t)\rangle \langle\psi(t)|) = \begin{pmatrix} P_L(t) & Q(t) \\ Q(t)^* & P_R(t) \end{pmatrix}, \tag{6.12}$$

The advantage of considering the reduced space of the quantum walk is that the final state is not pure due to entanglement between the chirality and position space. This entanglement could be analyzed either way using the reduced state of position or chirality, but the first one has infinity dimensions while the second has only two – so, considering the reduced state of chirality can save much work in calculations. More aspects of the entanglement will be analyzed in sections 6.3 and 6.4.

6.2 Asymptotic Limit

There is a method developed by Nayak and Vishwanath (2000) to calculate analytically the chirality components of the state, $a(t)$ and $b(t)$, of a quantum walk with a Hadamard coin. Despite the complicated calculation, the idea is very simple. It consists in applying the Fourier transform on the position space, diagonalizing the

unitary matrix responsible for the dynamics in one time step and returning to the position space through the inverse Fourier transform. First we note that the state of the system can be written as

$$\begin{aligned}\psi(x,t+1) &= \begin{pmatrix} 0 & 0 \\ 1/\sqrt{2} & -1/\sqrt{2} \end{pmatrix}\psi(x-1,t) + \begin{pmatrix} 1/\sqrt{2} & 1/\sqrt{2} \\ 0 & 0 \end{pmatrix}\psi(x+1,t) \\ &\equiv M_+\psi(x-1,t) + M_-\psi(x+1,t),\end{aligned} \tag{6.13}$$

where the matrices M_+ and M_- are defined in eq. (6.13). Then consider the Fourier space of the position components of the state,

$$|k\rangle = \sum_{x=-\infty}^{\infty} e^{ikx}|x\rangle, \tag{6.14}$$

where $k \in \mathbb{R}$ and $k \in [-\pi,\pi]$. Therefore

$$\begin{aligned}\tilde{a}_k &= \langle k, L|\psi\rangle, \text{ and} \qquad \tilde{b}_k = \quad \langle k, R|\psi\rangle, \\ \tilde{a}_k &= \sum_x e^{-ikx}a_x, \text{ and} \quad \tilde{b}_k = \quad \sum_x e^{-ikx}b_x,\end{aligned} \tag{6.15}$$

where R and L stand for right and left, respectively. The total state can be written as

$$|\psi\rangle = \int_\pi^\pi \frac{dk}{2\pi}|k\rangle \otimes (\tilde{a}_k|R\rangle + \tilde{b}_k|L\rangle). \tag{6.16}$$

Using equations (6.13) and (6.14) we are able to write the evolution of the Fourier state

$$\tilde{\psi}(k,t+1) = M_+e^{ik}\tilde{\psi}(k,t) + M_-e^{-ik}\tilde{\psi}(k,t) = \quad \frac{1}{\sqrt{2}}\begin{pmatrix} e^{-ik} & e^{-ik} \\ e^{ik} & -e^{ik} \end{pmatrix}\tilde{\psi}(k,t). \tag{6.17}$$

The eigenvectors of this matrix are

$$|\Phi_k^{(1)}\rangle = \alpha_k\begin{pmatrix} u_k \\ v_k, \end{pmatrix} \quad |\Phi_k^{(2)}\rangle = \beta_k\begin{pmatrix} u_k \\ w_k \end{pmatrix}, \tag{6.18}$$

with

$$\begin{aligned}\alpha_k &= \frac{1}{\sqrt{2}}(1+\cos k^2 - \cos k\sqrt{1+\cos k^2})^{1/2}, \\ \beta_k &= \frac{1}{\sqrt{2}}(1+\cos k^2 + \cos k\sqrt{1+\cos k^2})^{1/2}, \\ u_k &= e^{-ik}, \\ v &= \sqrt{2}e^{-i\omega_k} - e^{-ik}, \\ w_k &= -\sqrt{2}e^{i\omega_k} - e^{ik}, \\ \sin\omega_k &= \frac{\sin k}{\sqrt{2}},\end{aligned} \tag{6.19}$$

and the eigenvalues are $\lambda_k^1 = e^{i\omega_k}$ and $\lambda_k^2 = e^{i(\pi+\omega_k)}$. Therefore, we can write the state vector as

$$|\tilde{\psi}(k,t)\rangle = U_k^t|\tilde{\psi}(k,0)\rangle = [(\lambda_k^1)^t|\Phi_k^{(1)}\rangle\langle\Phi_k^{(1)}| + (\lambda_k^2)^t|\Phi_k^{(2)}\rangle\langle\Phi_k^{(2)}|]|\tilde{\psi}(k,0)\rangle, \tag{6.20}$$

To return to the position space, the inverse Fourier transform has to be applied. This calculation can be done, at least numerically, to any value of time, however, it might be too time-consuming. On the other hand, the asymptotic limit solution is much simpler and can be solved using the method of stationary points. Abal et al. (2005) calculated the global chirality distributions as well as variable Q, for the asymptotic limit. Here we simply place the results, more details of the calculations can be seen on the reference. Considering a initial state localized on position $|0\rangle$, i.e,

$$|\psi(n,0)\rangle = \begin{pmatrix} \cos(\theta/2) \\ \sin(\theta/2)\, e^{i\phi} \end{pmatrix} |0\rangle \tag{6.21}$$

the global left chirality distribution is

$$P_{L,\infty} = \left(\frac{1}{2} - \frac{\sqrt{2}}{4}\right)(2 + \sqrt{2} + \cos\theta + \sin\theta\cos\phi), \tag{6.22}$$

the global right chirality distribution is $1 - P_L$ and the interference term is

$$Q_\infty = \left(\frac{1}{2} - \frac{\sqrt{2}}{4}\right)(\cos\theta + \sin\theta(\cos\phi - i\sqrt{2}\sin\phi)) \tag{6.23}$$

Those limits are in accordance with the relation found in eq. (6.11). In order to graphically see those results, the reduced density matrix eq. (6.12) can be written as a function of the Bloch vector and Pauli matrices

$$\rho_c = \frac{1}{2}(I + \mathbf{B}\cdot\sigma) = \frac{1}{2}\begin{pmatrix} 1 + B_z & B_x - iB_y \\ B_x + iB_y & 1 - B_z \end{pmatrix}. \tag{6.24}$$

Comparing (6.12) and (6.24) the Bloch vector is obtained in terms of P_L and Q

$$\mathbf{B} = 2(\mathbb{R}e(Q), -\mathbb{I}m(Q), P_L - 1/2). \tag{6.25}$$

Figure 6.5 shows the evolution of the Bloch vector as a function of time and the asymptotic solution calculated analytically, for an arbitrary initial condition. Both results have a good match.

To understand the asymptotic behavior of the Bloch vectors as a function of the initial condition the graphs shown in figure 6.6 were plotted. From them we can infer that in the limit of longer times the initial conditions ($\theta = \pi/4$, $\phi = \pi$) and ($\theta = 3\pi/4$, $\phi = 0$) generate states with the norm of Bloch vector ($|B| = \sqrt{B_x^2 + B_y^2 + B_z^2}$) tending to zero, i.e., maximally mixed. The final surface, made by the asymptotic limit of all initial conditions, is on a plane normal to the vector $(-1, 0, 1)$.

The final surface can indicate features about the Hamiltonian responsible for the dynamics of the system. To analyze that, let us consider that the reduced coin system can be modeled by the quantum Brownian motion as in the reference Romanelli (2011). Thus, the quantum Liouville equation can be reduced to the following master equation (for a more detailed demonstration we refer to Toda et al. (1991))

$$\frac{\partial \rho_c}{\partial t} = -\frac{i}{\hbar}[H_c, \rho_c] + \Gamma\rho_c, \tag{6.26}$$

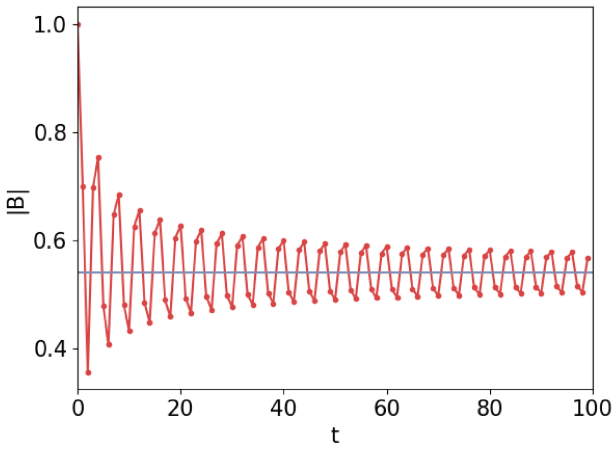

(a) Evolution of $|\mathbf{B}|$.

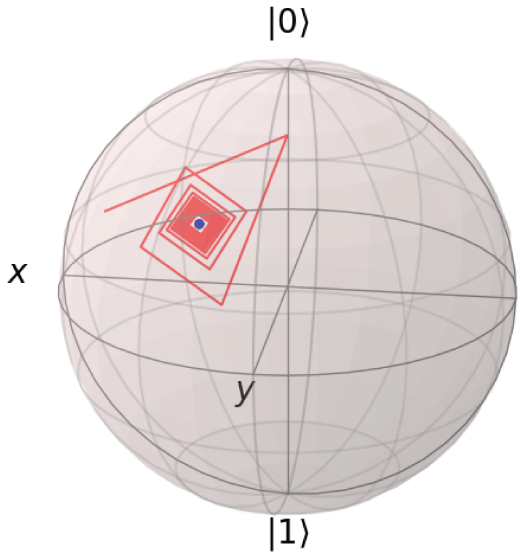

(b) Evolution of the Bloch vector.

Figure 6.5: Figure (a) shows the evolution of the norm of Bloch vector as a function of time and (b) shows the vector on the Bloch sphere as a function of time. The red dots shows the position of the vector and the blue dot/line is the asymptotic solution.The initial condition is the one of eq. (6.21) with $\theta = \pi/3$ and $\phi = \pi/5$.

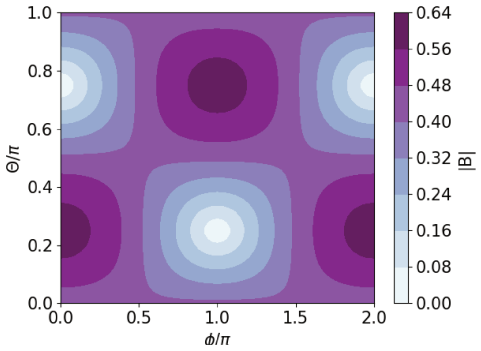

(a) Asymptotic values of $|\mathbf{B}|$.

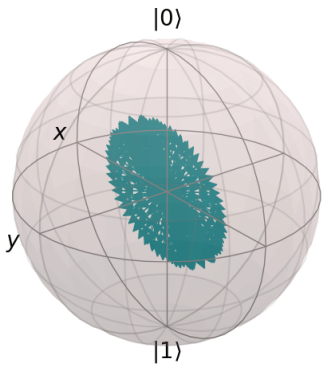

(b) Asymptotic Bloch vectors

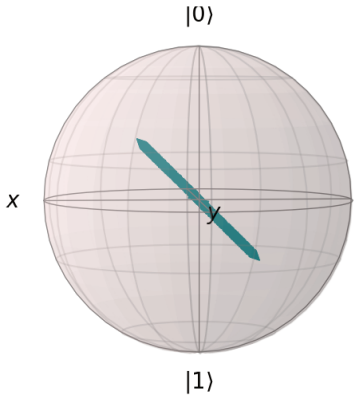

(c) Asymptotic Bloch vectors.

Figure 6.6: Map (a) shows the norm of the asymptotic limit of the Bloch vector as a function of the initial condition and (b) and (c) shows the final surface, made by the long time limit Bloch vectors of all initial conditions from different perspectives.

where H_c is the Hamiltonian of the reduced system and Γ is a Liouvillian representing the fluctuation and dissipation effects exerted effectively by the interaction of the coin and the walker as a noise exerted on ρ_c . The Hamiltonian can be associated to a magnetic field, $\mathbf{v}$, and written in terms of Pauli matrices

$$H = -\mathbf{v}\cdot\sigma. \tag{6.27}$$

This is possible because the set composed by the Pauli matrices with the identity are a basis for the space of 2×2 matrices. In this case, however, the identity does not have to be taken into account because it would only add a constant to the energy eigenvalues and we are interested on the energy gap between the two possible states.

By definition, if the system achieves equilibrium in the asymptotic limit, $\frac{\partial \rho_{c,\infty}}{\partial t} = 0$. However, Toda et al. (1991)(Pg. 88) also showed that if the asymptotic state is in accordance with the Canonical ensemble, then $\Gamma\rho_{c,\infty} = 0$ as well. This implies that $[H, \rho_{c,\infty}] = 0$, which implies that $\mathbf{B}_{\text{eq}}$ and $\mathbf{v}$ are parallel. The demonstration is very simple

$$\begin{aligned} 0 = [H,\ \rho_{c,\infty}] &= [\mathbf{v}\cdot\sigma, \frac{\mathbf{B}\cdot\sigma}{2}] = \sum_{i,j}[v_i\,\sigma_i,\ B_j\,\sigma_j] \\ &= \frac{1}{2}\sum_{i,j} v_i\,B_j[\sigma_i,\sigma_j] = \sum_{i,j} i\,v_i\,B_j\,\epsilon_{ijk}\,\sigma_k \\ &= \sum_k i\,(\mathbf{v}\times\mathbf{B})_k\,\sigma_k \end{aligned} \quad . \tag{6.28}$$

The Pauli matrices are a set of linearly independent matrices, therefore the only possibility that satisfies eq. (6.28) is $(\mathbf{v}\times\mathbf{B})_k = 0$ for every k. Looking again to the final surface of figure 6.6 we conclude that the effective Hamiltonian for the coin derived in that fashion depends on the initial conditions of the reduced system.

6.3 Entanglement Entropy

From figure 6.5 we can see that the Bloch vector starts at the surface of the sphere at the initial time and oscillates to a interior point, indicating that in the beginning of the walk the state was pure and as the time evolves it tends to a mixed state. This behavior is due to the entanglement between position and chirality spaces which can be quantified by the entanglement entropy, or von Neumann entropy

$$S = -\text{Tr}(\rho_c \log \rho_c). \tag{6.29}$$

In terms of the Bloch components this is written as

$$S = -\left(\frac{1+B}{2}\right)\log\left(\frac{1+B}{2}\right) - \left(\frac{1-B}{2}\right)\log\left(\frac{1-B}{2}\right). \tag{6.30}$$

For the case of the Hadamard walk, the entanglement entropy was calculated. Figure 6.7 shows the time evolution of the entropy for two different initial conditions. Although the convergence velocity is different for each initial condition, for all initial conditions the entropy has a convergence value. Figure 6.8 presents color maps with the values of the entropy depending on the initial conditions for different times. Comparing these maps with the one that shows the asymptotic limit of the entanglement entropy, fig. 6.9, we see that the calculations match again.

Another important feature to notice is that since the von Neumann entropy is a measure of how far from the pure state the system is, the maximum value of the entropy corresponds to the maximally mixed state, i.e.,

the state were both global chirality distributions are equal to $1/2$ ($|B| = 0$).

$$-\frac{1}{2}\log(\frac{1}{2}) - \frac{1}{2}\log(\frac{1}{2}) \approx 0.7. \tag{6.31}$$

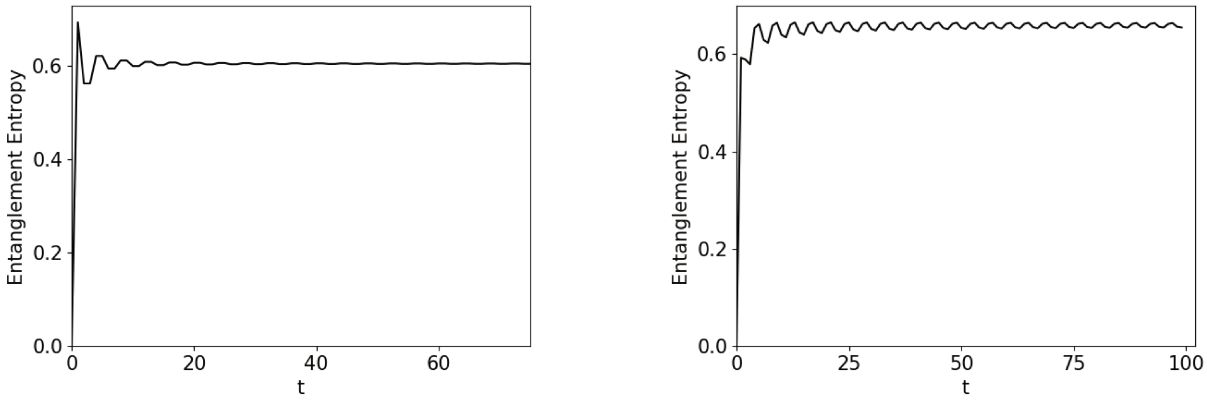

(a) Initial condition with $\gamma = \pi/2$ and $\phi = \pi/2$.

(b) Initial condition with $\gamma = \pi/4$ and $\phi = 5\pi/7$.

Figure 6.7: Evolution of the entanglement entropy of the discrete time quantum walk. The initial conditions were chosen randomly just to demonstrate how the entanglement entropy converges to an asymptotic limit.

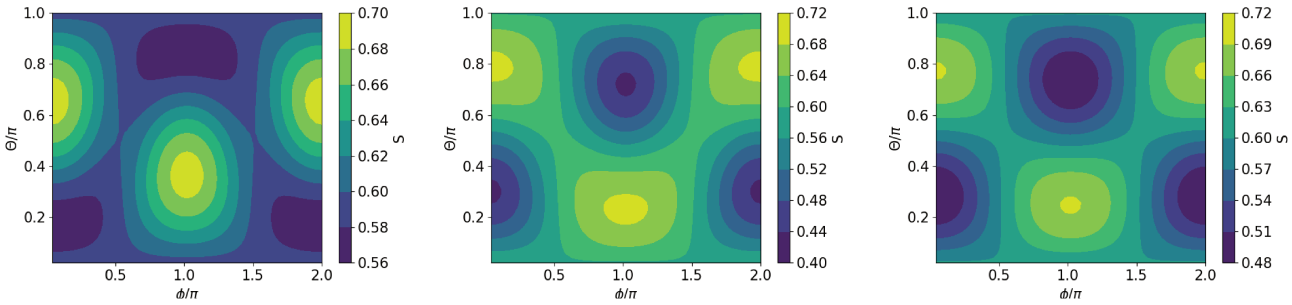

(a) $t = 10$.

(b) $t = 20$.

(c) $t = 102$.

Figure 6.8: Entanglement entropy of the discrete time quantum walk after 10, 20 and 100 time steps. All possible initial conditions are accounted for.

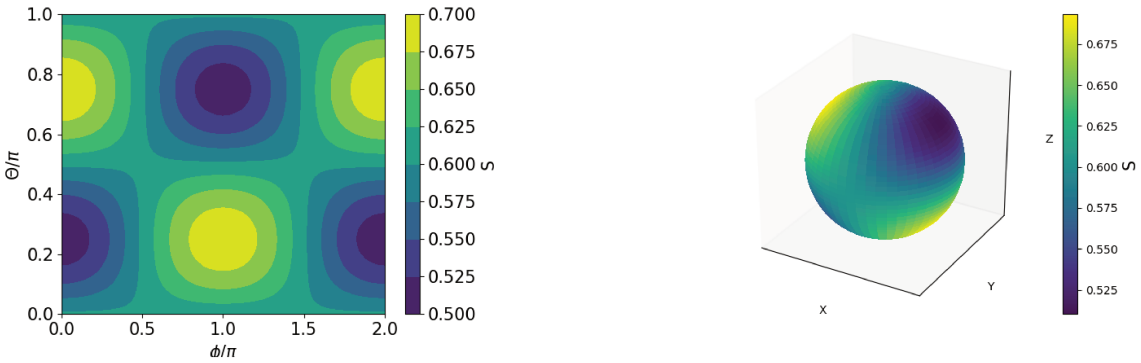

Figure 6.9: Asymptotic entanglement entropy for all possible initial conditions shown on a plane and on the surface of the Bloch sphere.

6.4 Temperature of Quantum Walks

A variable called entanglement temperature (T_E) can be defined with the help of the von Neumann entropy (Vallejo et al. (2020a)). In this section, we define this variable and discuss its physical meaning.

The expectation value of the energy of the system is

$$E = \langle H \rangle = \mathrm{Tr}(H\rho_c) = -\mathbf{B}\cdot\mathbf{v}. \tag{6.32}$$

An infinitesimal change of the internal energy is expressed as

$$dE = -d\mathbf{B}\cdot\mathbf{v} - \mathbf{B}\cdot d\mathbf{v}. \tag{6.33}$$

Eq. (6.33) can be seen as a statement of the first law of thermodynamics,

$$dE = \delta Q + \delta W, \tag{6.34}$$

where the energy change due to variations on the reduced state is identified as the heat variation, $\delta Q = -d\mathbf{B}\cdot\mathbf{v}$, and the energy change associated to the evolution of the Hamiltonian is the work, $\delta W = -\mathbf{B}\cdot d\mathbf{v}$.

In order to address a temperature to the two state open system we resort to the following definition of classical thermodynamics,

$$\frac{1}{T} = \frac{\partial S_{class}}{\partial E}, \tag{6.35}$$

where S_{class} stands for the thermodynamic entropy. Since the von Neumann entropy is the quantum extension of the statistical entropy - besides a k_B factor - we extend this definition for the quantum case switching one entropy for the other. To simplify the calculation we consider $k_B = 1$. Therefore writing the internal energy as $E = -v|B_{||}$, where $B_{||} = \mathbf{B}\cdot\hat{v}$ the definition of the entanglement temperature becomes

$$\frac{1}{T_E} = -\frac{1}{v}\frac{\partial S}{\partial B_{||}}. \tag{6.36}$$

From eq. (6.30) we have that

$$\frac{\partial S}{\partial B} = -\tanh B^{-1}, \tag{6.37}$$

and since $\frac{\partial B}{\partial B_{||}} = \frac{B_{||}}{B}$, the final expression for the entanglement temperature is

$$T_E = \frac{\epsilon B}{B_{||} \tanh B^{-1}} \tag{6.38}$$

where the eigenenergy is denoted by ϵ. Using eq. (6.38) the temperature of the quantum walk on the line was calculated for several initial conditions of the type presented in expression (6.21). Figure 6.10 shows the results in form of color-maps that map a temperature to each value of θ and ϕ of the initial condition. We see that, apart from two regions where the temperature achieves higher values -($\theta = 3\pi/2, \phi = 0$) and ($\theta = \pi/2, \phi = 0$) - , the rest of the initial conditions gives values of temperature per energy difference between 0 and 8.

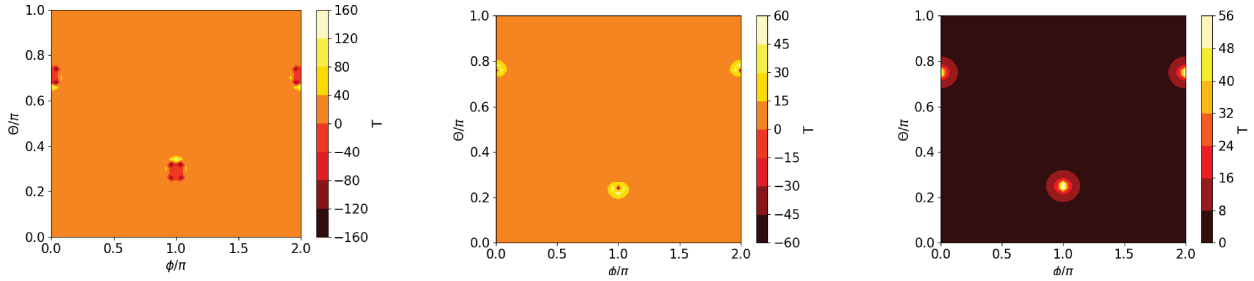

(a) $t = 10$. (b) $t = 100$. (c) Asymptotic limit.

Figure 6.10: Color maps of the temperature per energy of the quantum walk as a function of the initial conditions. The maps shows the temperature of the quantum walk after 10 time steps, 100 time steps and on the asymptotic limit.

Since we use the von Neumann entropy to calculate the temperature, it is clearly a measure of entanglement. However, is it possible to also address a thermodynamic meaning to this variable? The answer we defend here is that yes, it is. On Romanelli (2011) the temperature of the quantum walk was calculated assuming that in the asymptotic limit the reduced system is in equilibrium with its reservoir. The procedure was to assume the canonical ensemble for the system, and therefore, the eigenvalues of the asymptotic reduced density matrices can be written as

$$\lambda_{\pm} = \frac{e^{\pm\beta\epsilon}}{e^{\beta\epsilon} + e^{-\beta\epsilon}}, \tag{6.39}$$

where $\beta = 1/T_G$ is the inverse Gibbs temperature. Thus, inverting the expression, the temperature is obtained

$$T_G = \frac{2\epsilon}{\log\left(\frac{\lambda_+}{\lambda_-}\right)}. \tag{6.40}$$

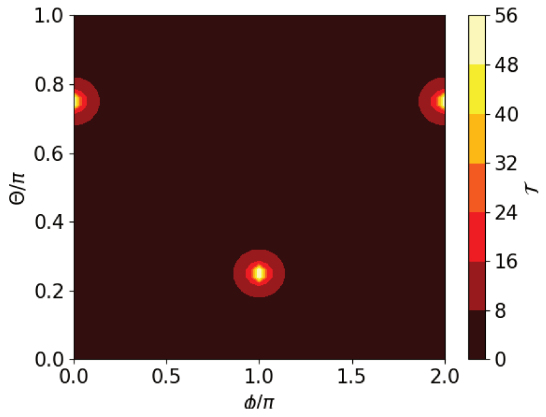

Figure 6.11: Color map of the temperature per energy of the quantum walk defined by eq.(6.40).

Figure 6.11 shows the absolute value of the asymptotic Gibbs temperature per energy calculated with this method, $\mathcal{T} = \left| \frac{2}{\log\left(\frac{\lambda_+}{\lambda_-}\right)} \right|$. As we can see the Gibbs temperature is equal to the entanglement temperature calculated with eq.(6.38) on the asymptotic limit, which proves that the entanglement temperature has a thermodynamic meaning and that the state of the reduced system goes to a Gibbs state when $t \to \infty$. Figure 6.12 shows that the difference between both results is at least of order 10^{-13}. This difference is probably due to computational errors, since it was shown analytically in (Vallejo et al. (2020a)) that definition (6.38) converges to (6.40) when the system (chirality) achieves equilibrium with the bath (walker).

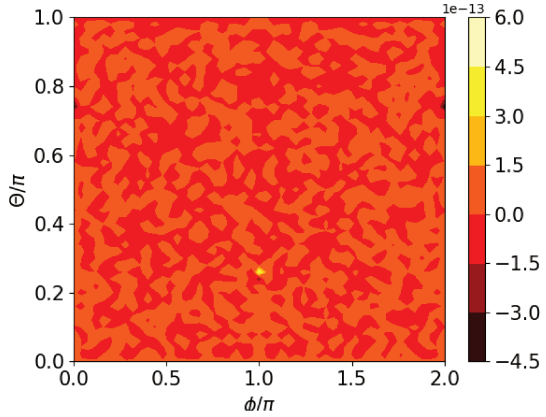

Figure 6.12: Color map difference between temperature calculated with both methods.

6.5 Three-state Quantum Walk

The principle of the three-state Quantum Walk, also known as the lazy quantum walk, is similar to the regular one-dimension Quantum Walk explained in the above sections. Therefore one will realize that the approaches we use to the analysis in this section are analogous to the ones used in the last sections. The main difference between the two and three state walks is that in the second case the chirality state space has three dimensions, therefore besides the possibilities of going to left or right, a probability of staying in the same place (site) is also taken into account. One can interpret this as a walk with a three-sided coin. The state of the system at time t is written as

$$|\psi(t)\rangle = \sum_{n=-\infty}^{\infty} \begin{pmatrix} a_n(t) \\ b_n(t) \\ c_n(t) \end{pmatrix} |n\rangle, \tag{6.41}$$

where the coefficients a_n, b_n and c_n correspond to the left (L), no movement (S) and right(R) chiralities, re-

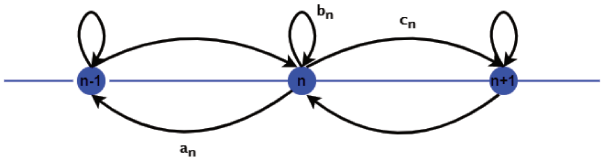

Figure 6.13: Diagram of three-state quantum walk.

spectively, as illustrates Fig.6.13. The operator we consider here to represent the action of the coin is

$$C = \frac{1}{3} \begin{pmatrix} -1 & 2 & 2 \\ 2 & -1 & 2 \\ 2 & 2 & -1 \end{pmatrix}, \tag{6.42}$$

known as Grover coin, and the shift operator is

$$\mathrm{Sh} = \left(\sum_{n=-\infty}^{\infty} |n-1\rangle \langle n| \otimes |L\rangle \langle L| \right) + \left(\sum_{n=-\infty}^{\infty} |n\rangle \langle n| \otimes |S\rangle \langle S| \right) + \left(\sum_{n=-\infty}^{\infty} |n+1\rangle \langle n| \otimes |R\rangle \langle R| \right). \tag{6.43}$$

The recurrence relations analogous to eq. (6.8) are

$$\begin{aligned} a_n(t+1) &= \frac{1}{3}(-a_{n+1}(t) + 2b_{n+1}(t) + 2c_{n+1}(t)), \\ b_n(t+1) &= \frac{1}{3}(2a_n(t) - b_n(t) + 2c_n(t)), \\ c_n(t+1) &= \frac{1}{3}(2a_{n-1}(t) + 2b_{n-1}(t) - c_{n-1}(t)), \end{aligned} \tag{6.44}$$

and the Global chirality probabilities are also defined in an analogous way to the two-state walk, eq. (6.9)

$$\begin{aligned} P_L(t) &= \sum_{n=-\infty}^{\infty} |a_n(t)|^2, \\ P_S(t) &= \sum_{n=-\infty}^{\infty} |b_n(t)|^2, \\ P_R(t) &= \sum_{n=-\infty}^{\infty} |c_n(t)|^2. \end{aligned} \tag{6.45}$$

Therefore, the recurrence relation of the GCP is easily obtained from eq. (6.4)

$$\begin{aligned} \begin{pmatrix} P_L(t+1) \\ P_S(t+1) \\ P_R(t+1) \end{pmatrix} &= \frac{1}{9}\begin{pmatrix} 1 & 4 & 4 \\ 4 & 1 & 4 \\ 4 & 4 & 1 \end{pmatrix}\begin{pmatrix} P_L(t) \\ P_S(t) \\ P_R(t) \end{pmatrix} + \frac{\mathbb{Re}[Q_1(t)]}{9}\begin{pmatrix} -4 \\ -4 \\ 8 \end{pmatrix} \\ &+ \frac{\mathbb{Re}[Q_2(t)]}{9}\begin{pmatrix} -4 \\ 8 \\ -4 \end{pmatrix} + \frac{\mathbb{Re}[Q_3(t)]}{9}\begin{pmatrix} -8 \\ -4 \\ -4 \end{pmatrix}, \end{aligned} \tag{6.46}$$

where the interference terms are

$$\begin{aligned} Q_1(t) &= \sum_{n=-\infty}^{\infty} a_n(t) b_n^*(t), \\ Q_2(t) &= \sum_{n=-\infty}^{\infty} a_n(t) c_n^*(t), \\ Q_3(t) &= \sum_{n=-\infty}^{\infty} b_n(t) c_n^*(t). \end{aligned} \tag{6.47}$$

Hence, the reduced density matrix is

$$\rho_c(t) = \begin{pmatrix} P_L(t) & Q_1(t) & Q_2(t) \\ Q_1^*(t) & P_S(t) & Q_3(t) \\ Q_2^*(t) & Q_3^*(t) & P_R(t) \end{pmatrix}. \tag{6.48}$$

Using these recurrence relations it is easy to simulate the position probability density function of the three-state quantum walk. Figure 6.14 shows the result of these simulations for two different initial conditions. It is possible to see that a different behavior emerges from this walk, which is localization for some initial conditions.

To deduce the asymptotic state of the walk, again a method similar to the one used to the two-state quantum walk is used. Considering the Fourier transform of the wave function of the system, $\tilde{\Psi}(k,t)$, the equation describing the dynamics of the walk is

$$\tilde{\Psi}(k,t+1) = \tilde{M}^t \tilde{\Psi}(k,0), \tag{6.49}$$

where in its diagonal form $\tilde{M}$ has two time dependent eigenvalues (λ_2, λ_3) and a constant one ($\lambda_1 = 1$) Inui et al. (2005); Falkner and Boettcher (2014). The constant eigenvalue is responsible for the main difference in behavior

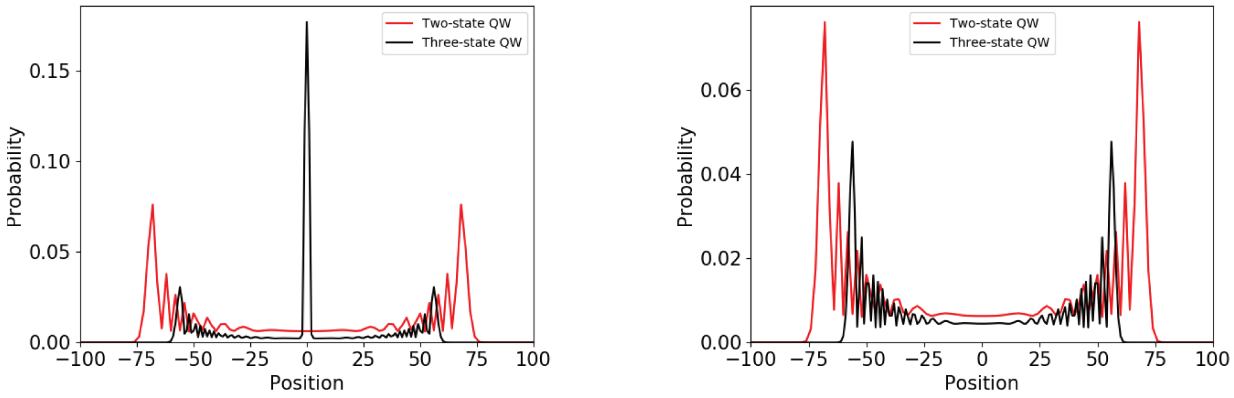

(a) $|\psi(0)\rangle = \left(\frac{i}{\sqrt{2}}, 0, \frac{1}{\sqrt{2}}\right)^T$ (b) $|\psi(0)\rangle = \left(\frac{1}{\sqrt{6}}, \frac{-2}{\sqrt{6}}, \frac{1}{\sqrt{6}}\right)^T$

Figure 6.14: The position probability density function of the lazy quantum walk for a initial condition that (a) generates localization and (b) for one that does not are depicted in comparison with the two-state quantum walk. All PDFs are calculated after 100 time steps.

of two and three state Quantum Walk, because it causes a localization around its initial position. Therefore using its diagonal form, the evolution operator $\tilde{M}$ can be written as follows

$$\tilde{M}^t = \tilde{M}_1 + \lambda_2^t \tilde{M}_2 + \lambda_3^t \tilde{M}_3. \tag{6.50}$$

The state vector is obtained performing the inverse Fourier transform. A more detailed explanation of this procedure can be found on Falkner and Boettcher (2014), where the asymptotic limit distribution was calculated with the matrices U_1, U_2 and U_3, defined on such a way that in the limit of $t \to \infty$ the state vector is

$$|\psi_n^\infty\rangle = (U_1 + U_2 + U_3)\,|\psi_0^0\rangle\,, \tag{6.51}$$

where $|\psi_0^0\rangle = \begin{pmatrix} a_n(0) \\ b_n(0) \\ c_n(0) \end{pmatrix} |0\rangle$ is the initial state of the walker. To perform the inverse Fourier transform on the time dependent parts of $\tilde{M}$ the method of stationary phase was used.

To obtain the asymptotic reduced density matrix of three-state Quantum Walks the numerical results of Falkner and Boettcher (2014), where the matrices $\tilde{M}_1$, $\tilde{M}_2$ and $\tilde{M}_3$ were calculated using the saddle point method, were strongly used, and they suggested that the cross terms of eq. (6.51) should not be considered on the calculation of the asymptotic density matrix, i.e,

$$\rho_\infty = |\psi_n^\infty\rangle\langle\psi_n^\infty| \approx U_1\,|\psi_0^0\rangle\langle\psi_0^0|\,U_1^\dagger + U_2\,|\psi_0^0\rangle\langle\psi_0^0|\,U_2^\dagger + U_3\,|\psi_0^0\rangle\langle\psi_0^0|\,U_3^\dagger. \tag{6.52}$$

The analytical form of ρ_∞ is too large to be displayed here, however, we present it in Appendix A.10. In order to test if the asymptotic limit was calculated correctly, we compare the evolution in time of the norm of the

generalized Bloch vector with the asymptotic value obtained for different initial conditions in fig. (6.15). The result suggests that the Bloch norm is indeed approaching the asymptotic value.

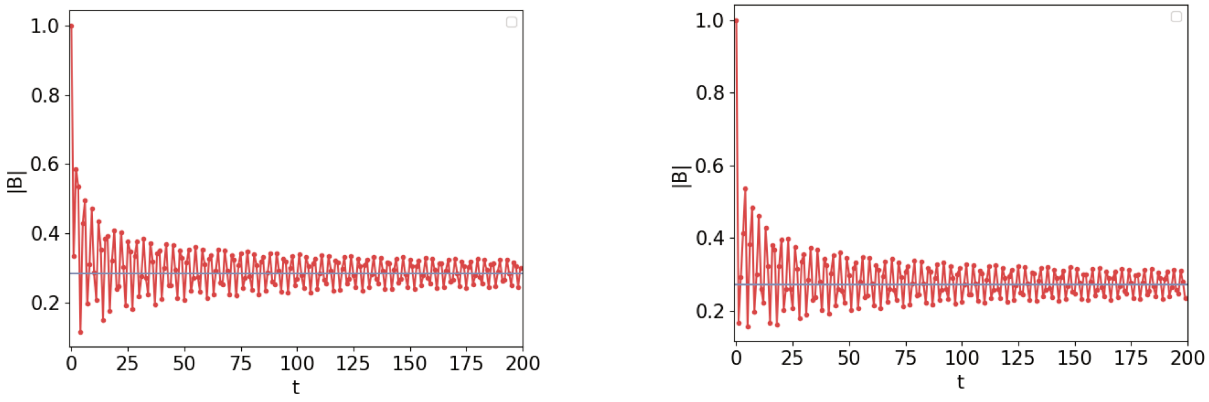

(a) $|\psi(0)\rangle = (0,0,i)^T$ (b) $|\psi(0)\rangle = \frac{1}{\sqrt{2}}(1,0,i)^T$

Figure 6.15: Evolution of the norm of the generalized Bloch vector is presented in red for two different initial conditions. The blue line is the asymptotic limit calculated by eq. (6.52).

If we consider that the reduced system also respects the master equation (6.26), due to the same arguments presented in the two-state quantum walk case, we have that $[H, \rho_{c,\infty}] = 0$. Since the reduced space has three dimensions we will use the Gell-Mann matrices[1], Ozols and Mancinska (Accessed in 08/2020); Kimura and Kossakowski (2004), $\lambda = (\lambda_1, \lambda_2, \lambda_3, \lambda_4, \lambda_5, \lambda_6, \lambda_7, \lambda_8)$ and the identity, $\mathbb{I}$ as a basis. Therefore the reduced density matrix can be written as

$$\rho_{c,\infty} = \frac{1}{3}(\mathbb{I}\mathrm{d} + \sqrt{3}\mathbf{B}\cdot\lambda), \tag{6.53}$$

and the Hamiltonian is $H = -\mathbf{v}\cdot\lambda$. Hence,

$$\begin{aligned} 0 = [H, \rho_{c,\infty}] &= \frac{-\sqrt{3}}{3}[\mathbf{v}\cdot\lambda, \mathbf{B}\cdot\lambda] = \frac{-1}{\sqrt{3}}\sum_{i,j}[v_i\lambda_i, B_j\lambda_j] \\ &= \frac{-1}{\sqrt{3}}\sum_{i,j} v_i B_j [\lambda_i, \lambda_j] = \frac{-2i}{\sqrt{3}}\sum_{i,j,k} v_i B_j f_{ijk}\lambda_k, \end{aligned} \tag{6.54}$$

where f_{ijk} are structure constants. Since the Gell-Mann matrices are linearly independent, eq. (6.54) leads to a system of eight equations, for which $\mathbf{v} \propto \mathbf{B}$ is a solution. This suggests that in equilibrium the generalized Bloch vector is parallel to the field associated with the Hamiltonian. This time, however, it is not possible to visualize the vectors because the generalized Bloch sphere is a 8-sphere. What we can depict is the norm of the Bloch vector as a function of time and as a function of the initial conditions as in figures (6.15) and (6.16), respectively.

The entanglement entropy was also calculated using the von Neumann expression. The result obtained is

[1] For more information on Gell-Mann matrices and its properties we refer to appendix A.9.

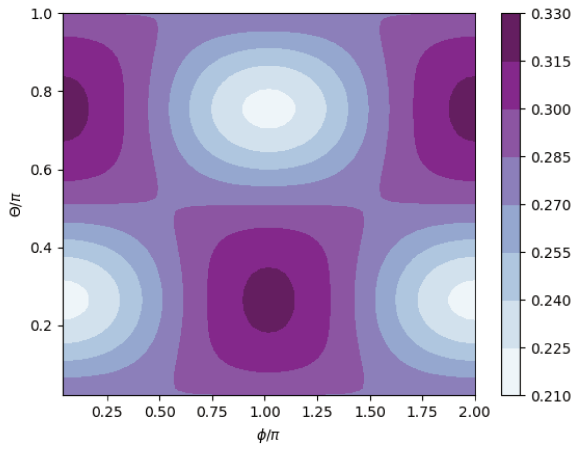

Figure 6.16: Asymptotic norm of the generalized Bloch vector as a function of the initial conditions of the type $|\psi_0^0\rangle = \begin{pmatrix} \cos\theta \\ 0 \\ \sin\theta e^{i\phi} \end{pmatrix} |0\rangle$.

displayed on Figure 6.17. Here we consider initial conditions of the type

$$|\psi_0^0\rangle = \begin{pmatrix} \cos\theta \\ 0 \\ \sin\theta e^{i\phi} \end{pmatrix} |0\rangle . \tag{6.55}$$

However the method could be applied to any possible initial condition. Note that the result of entropy for the asymptotic limit is similar to the two state case, but in this case the peaks of maximum entropy are dislocated by π in ϕ. The localization generated by the walk, i.e, the probability of the walker being at position 0 in the

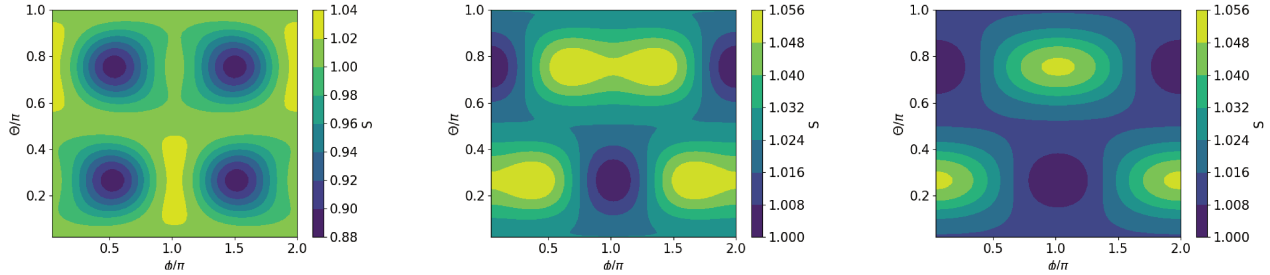

(a) $t = 10$. (b) $t = 100$. (c) Asymptotic limit.

Figure 6.17: Color maps of the entropy of the quantum walk as a function of the initial conditions for different time steps.

asymptotic limit, is given by

$$P(0,t=\infty)=\begin{pmatrix}a^* & b^* & c^*\end{pmatrix}U_1^\dagger U_1\begin{pmatrix}a^*\\ b^*\\ c^*\end{pmatrix}=(5-2\sqrt{6})[(2a+b)a^*+(a+b+c)b^*+(b+2c)c^*], \tag{6.56}$$

where a,b and c are the initial chirality components. Therefore, all the initial conditions of the type (6.55) have localization $10-4\sqrt{6}\approx 0.2$. This means that, although both features depend on the initial condition, there is no direct connection between the localization of the walk and its entanglement entropy.

The energy of the system is given by (Inui et al. (2005))

$$\begin{aligned}E=\langle H\rangle &= \mathrm{Tr}[H\rho_s]=\mathrm{Tr}[-(\mathbf{v}\cdot\lambda)\frac{\mathbf{1}}{\mathbf{3}}(\mathbb{1}\mathrm{d}+\sqrt{\mathbf{3}}\mathbf{B}\cdot\lambda)]\\ &=-\mathrm{Tr}\left[-\frac{(\mathbf{v}\cdot\lambda)}{3}\right]-\frac{1}{\sqrt{3}}\mathrm{Tr}[(\mathbf{v}\cdot\lambda)(\mathbf{B}\cdot\lambda)]=\frac{\mathbf{-1}}{\sqrt{\mathbf{3}}}\sum_{\mathbf{i,j}}\mathbf{v_i}\mathbf{B_j}\mathrm{Tr}[\lambda_\mathbf{i}\lambda_\mathbf{j}]\\ &=\frac{-1}{\sqrt{3}}\sum_{i,j}v_iB_j2\delta_{ij}=\frac{-2}{\sqrt{3}}\mathbf{v}\cdot\mathbf{B}.\end{aligned} \tag{6.57}$$

Hence the entanglement temperature, given by definition, (6.35) is

$$\frac{1}{T_E}=\frac{\partial S_{vN}}{\partial E}=\frac{-\sqrt{3}}{2v}\frac{\partial S_{vN}}{\partial B}\frac{\partial B}{\partial B_{||}}. \tag{6.58}$$

The problem in calculating the entanglement temperature in the case of the three-state quantum walk is that the mean value of another observable, besides the energy, is needed to be used as a constraint, Vallejo et al. (2020b). This means that, unlike the two-state case, we will not be able to calculate the entanglement temperature at any time. In the asymptotic limit, however, this restriction is surpassed and we see that if we assume that the system converges to a Gibbs state, then we can calculate it. We also check that, in this case, the Gibbs temperature also respects the definition 6.58, i.e, it is equivalent to the entanglement temperature.

Let us start by assuming that when the system (chirality) achieves equilibrium with the bath (walker), the eigenvalues of the density matrix are given by

$$\tau_j=\frac{e^{-\beta\epsilon_j}}{Z}=\frac{e^{-\beta\epsilon_j}}{e^{-\beta\epsilon_1}+e^{-\beta\epsilon_2}+e^{-\beta\epsilon_3}}, \tag{6.59}$$

where the index j stands for 1,2 or 3, and the Gibbs temperature per difference of energy can be obtained dividing any two of the three eigenvalues as

$$\frac{T_G}{\epsilon'_j-\epsilon_j}=\frac{1}{\log\left(\frac{\tau_j}{\tau_{j'}}\right)}. \tag{6.60}$$

In this case, however, since there are three different ways of defining the temperature per difference of energy, it is more convenient to define the Gibbs temperature per mean energy. To derive this definition we use the fact that the mean energy is given by

$$E=\mathrm{Tr}[H\rho_s]=\epsilon_1\tau_1+\epsilon_2\tau_2+\epsilon_3\tau_3, \tag{6.61}$$

and that, since we chose to define $H = -\mathbf{v}\cdot\lambda$ as a traceless operator, the sum of the three eigenenergies is zero,

$$\epsilon_1 + \epsilon_2 + \epsilon_3 = 0. \tag{6.62}$$

Dividing expressions (6.59) of τ_1 by the other two eigenvalues we find

$$\begin{aligned} \frac{\tau_1}{\tau_2} &= e^{-\beta(\epsilon_1-\epsilon_2)} = e^{-\beta(2\epsilon_1+\epsilon_3)}, \\ \frac{\tau_1}{\tau_3} &= e^{-\beta(\epsilon_1-\epsilon_3)}, \end{aligned} \tag{6.63}$$

where we used that $1 = \tau_1 + \tau_2 + \tau_3$ in the first line. Then, multiplying both expressions we get

$$\frac{\tau_1^2}{\tau_2\tau_3} = e^{-\beta(3\epsilon_1)} \implies \epsilon_1 = -\frac{T_G}{3}\log\left(\frac{\tau_1^2}{\tau_2\tau_3}\right). \tag{6.64}$$

Following an analogous procedure we obtain the expressions of the other eigenenergies

$$\begin{aligned} \tau_2\epsilon_2 &= -\frac{T_G}{3}\tau_2\log\left(\frac{\tau_2^2}{\tau_1\tau_3}\right), \\ \tau_3\epsilon_3 &= -\frac{T_G}{3}\tau_3\log\left(\frac{\tau_3^2}{\tau_1\tau_2}\right). \end{aligned} \tag{6.65}$$

Now the mean energy (6.61) can be written as a function of the temperature and the eigenvalues of the density matrix only

$$E = -\frac{T_G}{3}\left[\tau_1\log\left(\frac{\tau_1^2}{\tau_2\tau_3}\right) + \tau_2\log\left(\frac{\tau_2^2}{\tau_1\tau_3}\right) + \tau_3\log\left(\frac{\tau_3^2}{\tau_2\tau_1}\right)\right], \tag{6.66}$$

which leads to the final expression for the temperature per mean energy

$$\mathcal{T} = \frac{T_G}{E} = -3\left[\tau_1\log\left(\frac{\tau_1^2}{\tau_2\tau_3}\right) + \tau_2\log\left(\frac{\tau_2^2}{\tau_1\tau_3}\right) + \tau_3\log\left(\frac{\tau_3^2}{\tau_2\tau_1}\right)\right]^{-1}. \tag{6.67}$$

Figure 6.18 shows the result of $|\mathcal{T}|$ for two types of initial conditions.

Manipulating expression (6.66) we can write E as a function of the von Neumann Entropy and of $Z = \mathrm{Tr}[e^{-\beta H}]$, as

$$\begin{aligned} E &= -\frac{T_G}{3}\left[\tau_1\log(\tau_1^2) - \tau_1\log(\tau_2\tau_3) + \tau_2\log(\tau_2^2) - \tau_2\log(\tau_1\tau_3) + \tau_3\log(\tau_3^2) - \tau_3\log(\tau_1\tau_2)\right] \\ &= -\frac{T_G}{3}\left[-2S - \tau_1\log(\tau_2\tau_3) - \tau_2\log(\tau_1\tau_3) - (1-\tau_2-\tau_1)\log(\tau_1\tau_2)\right] \\ &= -\frac{T_G}{3}\left[\,-2S - \tau_1\log(\tau_2) - \tau_1\log(\tau_3) - \tau_2\log(\tau_1) - \tau_2\log(\tau_3) - \log(\tau_1\tau_2)\right. \\ &\quad \left. + \tau_2\log(\tau_1) + \tau_2\log(\tau_2) + \tau_1\log(\tau_1) + \tau_1\log(\tau_2)\,\right] \\ &= -\frac{T_G}{3}\left[-2S - \tau_1\log(\tau_3) - (1-\tau_1-\tau_3)\log(\tau_3) - \log(\tau_1\tau_2) + \tau_2\log(\tau_2) + \tau_1\log(\tau_1)\right] \\ &= -\frac{T_G}{3}\left[-2S - \tau_1\log(\tau_3) - \log(\tau_3) + \tau_1\log(\tau_3) + \tau_3\log(\tau_3) - \log(\tau_1\tau_2) + \tau_2\log(\tau_2) + \tau_1\log(\tau_1)\right] \\ &= -\frac{T_G}{3}\left[-3S + \log\left(\frac{1}{\tau_1\tau_2\tau_3}\right)\right] = -\frac{T_G}{3}\left[-3S + \log\left(\frac{Z^3}{e^{-\beta(\epsilon_1+\epsilon_2+\epsilon_3)}}\right)\right] = -\frac{T_G}{3}\left[-3S + 3\log(Z)\right], \end{aligned} \tag{6.68}$$

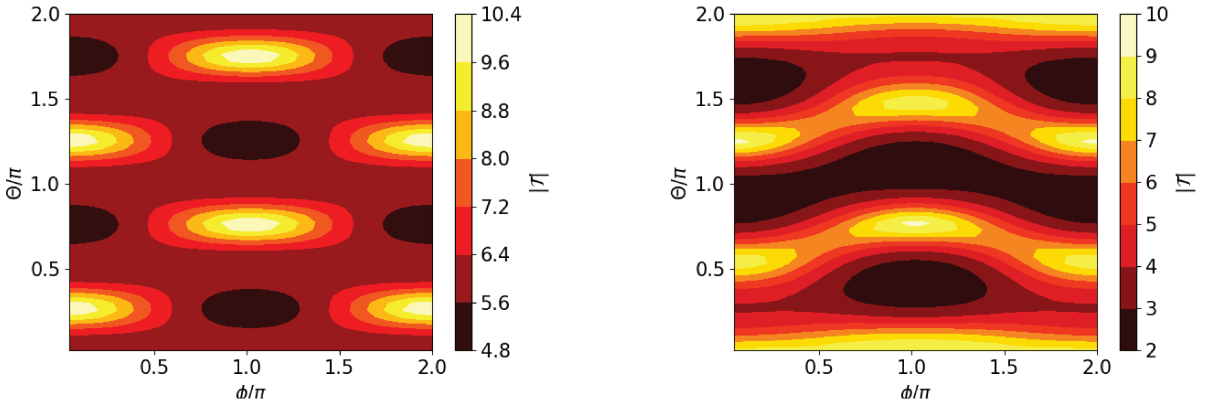

(a) $|\psi_0^0\rangle = \begin{pmatrix} \cos\theta \\ 0 \\ \sin\theta e^{i\phi} \end{pmatrix} |0\rangle.$

(b) $|\psi_0^0\rangle = \begin{pmatrix} \cos\theta/\sqrt{2} \\ 1/\sqrt{2} \\ \sin\theta e^{i\phi}/\sqrt{2} \end{pmatrix} |0\rangle$

Figure 6.18: Color maps of the absolute value of the Gibbs temperature divided by the mean energy.

where we used the fact that $S = \sum_{j=1}^{3} \tau_j \log(\tau_j)$. Now, we conclude that the von Neumann entropy is

$$S = \frac{E}{T_G} + \log(Z) \tag{6.69}$$

and, consequently, the definition (6.58) is valid for the Gibbs temperature.

$$\frac{\partial S}{\partial E} = \frac{1}{T_G} \implies T_E = T_G. \tag{6.70}$$

This was already expected, since we started by assuming that the system would converge to a Gibbs state, however it should be interpreted as a confirmation that our calculations are correct.

6.6 Conclusions

This chapter was devoted to the analyses of quantum walks on an infinite line. Particularly, two and three state quantum walks were analyzed. Our main interests concern the asymptotic limit behavior of the walks, the entanglement between both spaces of the systems, and the definition of temperature in this context.

With respect to the two-state quantum walk, assuming that the reduced system of the coin can be modeled by the master equation of the quantum Brownian motion, we showed that, at equilibrium, the Bloch vector is parallel to the "magnetization " vector of the Hamiltonian ($\mathbf{v}$) and that this means that the effective Hamiltonian of the reduced system depends on the initial conditions. We also calculated the entanglement entropy and temperature of the state for different times, including the asymptotic limit and found that $T_E = T_G$ for the two-state quantum walk in the asymptotic limit.

The last part of the chapter contains our main results. We calculated the asymptotic reduced density matrix for the three-state quantum walk, calculated the von Neumann entropy and the Gibbs temperature. The system only achieves the Gibbs temperature in the asymptotic limit, if it is in thermal equilibrium with the bath. Therefore our assumption is that that the three state quantum walk achieve a state of thermal equilibrium in the asymptotic limit. Questions concerning the reason why, when the system evolves into the thermal equilibrium with the bath, the state is described by the canonical ensemble are a much more fundamental whose answer connects quantum mechanics with the foundation of quantum statistical mechanics. For a more complete discussion on that, we refer to Yuan et al. (2009).

In our calculations we only assumed that the total energy of the system is zero and this does not imply in any loss of generality because the difference between the eigenenergies is the relevant physical quantities, not their absolute value. Hence our expression for the temperature per mean energy extends to the general case of a three-state system that achieves equilibrium with the reservoir, not just the reduced state of the three-state quantum walk. This is in full agreement with the more general result proved by Vallejo et al. (2020b). We also point to the fact that the relation obtained between the energy and entropy for the three-state quantum walk in the asymptotic limit, (6.69), is in accordance with the entropy-energy inequality discussed by Man'ko and Markovich (2016).

This closes our analyses of the entanglement between the two spaces of the quantum walk. In the next section we shall again consider the quantum walk as an open system, but this time we look to the whole space of the quantum walk and consider external influences, not just the reduced space. In other words, in this chapter, we considered the complete system of the quantum walk as an isolated "universe" and analyzed the coin space as our principal system, while the position space was seen as a bath. In the next chapter, we will treat the problem from a different perspective, including the whole system of the quantum walk as the principal system ($\mathscr{H} = \mathscr{H}_C \otimes \mathscr{H}_P$) and the bath is composed by an environment (or uncontrolled degrees of freedom).

CHAPTER 7

Decoherence in Discrete Time Quantum Walks

It is important to clarify a very important difference between random and quantum walks. Randomness plays a clear role at each time step of the random walk, in the sense that we do not know what will be the result of the coin toss. On the other hand, in the quantum walk, the position of the walker is unknown, but the state of the system is always known. The result of the coin toss is perfectly predictable and the dynamics of the system is governed by a unitary evolution, which means that if the initial state is pure it will remain pure. The randomness of the quantum walk is uniquely due to the measurement process. This means that the name "Quantum Walk" is more appropriate to the type of process we were dealing with in the last chapter than "Quantum Random Walk". There is, however, another factor that can add randomness to the quantum walk – the decoherence. Decoherence is a key element to understand the limit between classical and quantum phenomena and it happens when we consider interaction between the environment and the system. Until now we considered the quantum walk as an isolated system, however, sometimes it can be useful to recognize the system we are analyzing to be immersed in an environment, Kendon (2003).

The first reason why is important to consider environmental effects on the quantum walk is that the most important application of this system is on the development of quantum algorithms, and since quantum computers are physical objects they are always subjected to some level of noise and dissipation. Therefore, dealing with decoherence is inevitable to build the quantum computers that will perform the quantum walk. Besides that, another important feature of decoherence is that the evolution of a system under decoherence is not necessarily described by unitary operators, therefore we could use external interactions to control a new class of evolutions that lead to different behaviors of the walk. Decoherence can be physically introduced in the system by many different phenomena, therefore we can account for such interactions by different mathematical ap-

proaches. Here we will consider a Hadamard walk with an initial condition that generates a symmetrical walk, i.e, $\frac{1}{\sqrt{2}}\begin{pmatrix}1 & i\end{pmatrix}^T$ or $\frac{1}{\sqrt{2}}\begin{pmatrix}1 & -i\end{pmatrix}^T$.

This section is subdivided into five parts. At each of the first four parts, we consider one method of accounting for decoherence, and in the last section, we develop a generalization of these models for the three-state quantum walk. In the first part, we introduce the Kraus operator that can be used to model phase and amplitude damping decoherence, in the second part we present the decoherence by unitary noise, and at last, in the third and fourth parts, we analyze decoherence by broken links and periodic measurements and look to the resemblance of those processes with classical Brownian motion. It is important to point out that there are other methods for simulating decoherence, such as changing the coin operator at each time step and the implementation of decoherence via master equations. For more information about other methods to implement decoherence in discrete and continuous-time quantum walks we refer to Kendon (2006).

7.1 Kraus Operators

One method to introduce decoherence on the walk is by adding extra non-unitary operators known as Kraus operators, K_j, to describe the effects of noise and other external effects. Hence, the recurrence relation respected by the evolution of the system becomes

$$\rho(t+1) = \sum_j K_j U \rho(t) U^\dagger K_j^\dagger. \tag{7.1}$$

This expression is completely equivalent to consider a unitary evolution on the total space composed by the system and the environment and taking the partial trace of the environment, Nielsen and Chuang (2010).

The Kraus operators can account for different effects – here we explore the operators associated with phase and amplitude damping on the coin space, Diniz (2016); Nielsen and Chuang (2010). The **phase damping** is modeled by the Kraus operators of the form $K_j = \mathbb{I} \otimes E_j$, where $j = 0, 1$, $\mathbb{I}$ is the identity in the position space and

$$\begin{aligned} E_0 &= \begin{pmatrix} 1 & 0 \\ 0 & \sqrt{1-\gamma} \end{pmatrix}; \\ E_1 &= \begin{pmatrix} 0 & 0 \\ 0 & \sqrt{\gamma} \end{pmatrix}. \end{aligned} \tag{7.2}$$

The parameter $\gamma \in [0,1]$ is the strength of the channel, and the matrices E_0 and E_1 can be obtained if one considers a rotation of a random angle (Gaussian distributed) in the coin space and evaluate the mean over all angles. This noise process describes the quantum loss of information without loss of energy. Physically, the action of this operator on a two-level system can be used to describe the phenomenon where a photon scatters randomly as it travels through a wave guide or the perturbations of electronic states in an atom due to interaction with

distant electrical charges. The energy eigenstates of the quantum system are constant in such a evolution, but as time passes there is an accumulation of phase which is proportional to the eigenvalue. Hence, as the system evolves the information about the relative phase between the energy eigenstates is lost.

Another type of decoherence that can be described by the Kraus operators is the **amplitude damping**. The operators in this case have the same format as the ones presented to phase damping decoherence ($K_j = \mathbb{I} \otimes E_j$), however in this case

$$E_0 = \begin{pmatrix} 1 & 0 \\ 0 & \sqrt{1-\gamma} \end{pmatrix}; \qquad E_1 = \begin{pmatrix} 0 & \sqrt{\gamma} \\ 0 & 0 \end{pmatrix}. \tag{7.3}$$

This type of decoherence describes a process with energy dissipation. For instance, a system with an atom emitting a photon, a spin system at high temperature approaching equilibrium with its environment and a photon on a cavity subjected to scattering and attenuation can be approximately described using the amplitude damping noise. We can see that the difference between this decoherence and the phase damping is in the operator E_1.

To understand the behavior of the walk subjected to those types of decoherence we made the graphics of figure 7.1 that display the probability distribution of the walker's displacement after 100 time steps for different values of the parameter γ. We can see that for both types of damping, as γ increases the distribution approximates to a Gaussian one, and when $\gamma = 0$ the coherent quantum walk behavior is recovered, as expected. The difference between phase and amplitude damping decoherence is in how the transition from quantum to classical behavior occurs. While on the case of phase damping the transitions occur symmetrically, on the amplitude damping decoherence the transition is not symmetric. This is due to the fact that the operator E_1 of eq.(7.3) destroys the left chirality state and changes the right state to a left one as equation (7.4) shows.

$$E_1 |L\rangle = \begin{pmatrix} 0 & \sqrt{\gamma} \\ 0 & 0 \end{pmatrix} \begin{pmatrix} 1 \\ 0 \end{pmatrix} = \begin{pmatrix} 0 \\ 0 \end{pmatrix}, \qquad E_1 |R\rangle = \begin{pmatrix} 0 & \sqrt{\gamma} \\ 0 & 0 \end{pmatrix} \begin{pmatrix} 0 \\ 1 \end{pmatrix} = \begin{pmatrix} \sqrt{\gamma} \\ 0 \end{pmatrix} = \sqrt{\gamma} |L\rangle . \tag{7.4}$$

A parameter that can be used to analyze the distance of the incoherent quantum walk to the quantum or classical walks is the standard deviation. Figure (7.2) shows the standard deviation of the position probability distributions as a function of time. As we expected, for both cases, $\gamma = 0$ gives a line ($\sigma \propto t$) and for $\gamma = 1$ we achieve the classical behavior ($\sigma \propto \sqrt{t}$).

Figure (7.3) displays the evolution of the von Neumann entropy of the coin for the quantum walk with initial

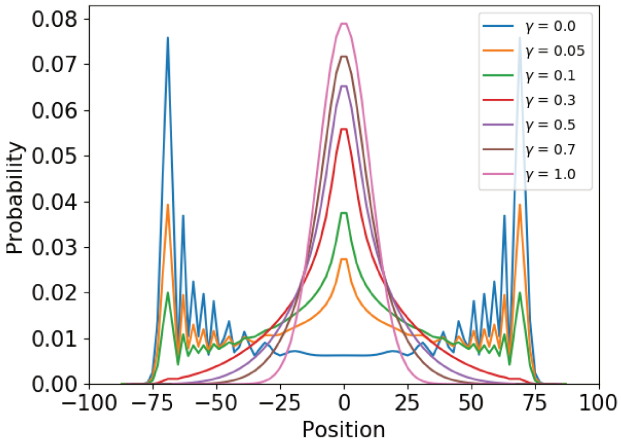

(a) Phase Damping

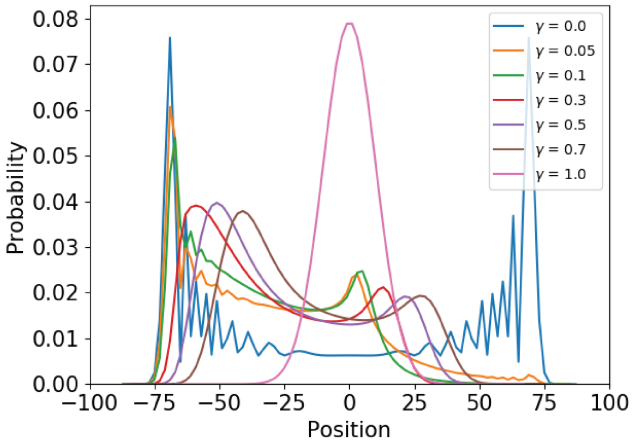

(b) Amplitude Damping

Figure 7.1: The probability distribution of positions of the incoherent quantum walk after 100 time steps for different values of the γ parameter is displayed for Kraus operators corresponding to the phase damping (a) and to the amplitude damping (b).

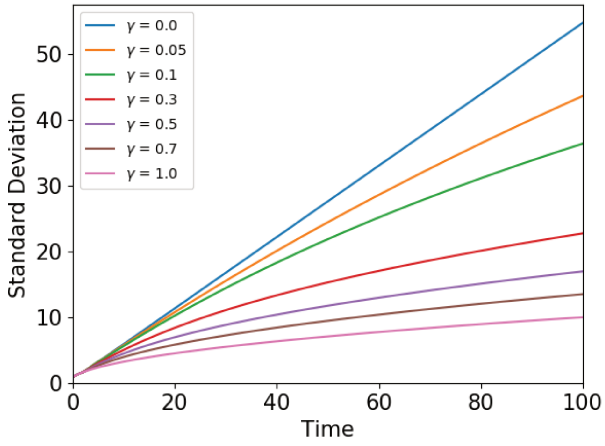

(a) Phase Damping

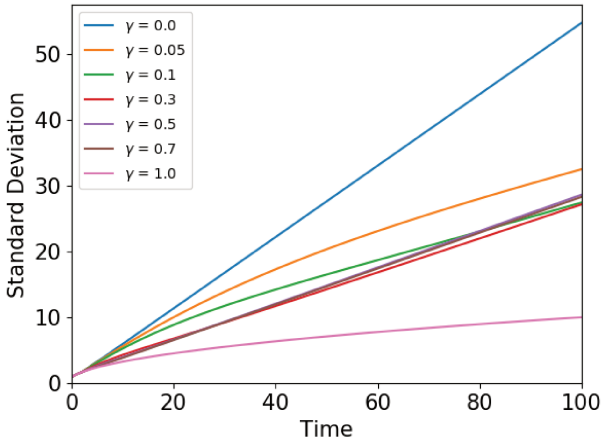

(b) Amplitude Damping

Figure 7.2: The standard deviation as a function of time of the incoherent quantum walk for different values of the γ parameter is displayed for Kraus operators corresponding to the phase damping (a) and to the amplitude damping (b).

condition $\frac{1}{\sqrt{2}}\begin{pmatrix}1 & i\end{pmatrix}^T$. In both graphs, the blue line represents the entropy of a walk without noise, i.e, $\gamma = 0$. In this case, as the whole joint Coin+walker state is pure, this entropy measures the internal entanglement between those two subsystems. We see that even considering noise, the entropy oscillates to a well defined asymptotic value, where it attains a larger or smaller value of entropy, than the noiseless case, for the phase

damping and amplitude damping, respectively. For the process with phase damping, the asymptotic entropy is maximal ($S_{\max} = \log 2 \approx 0.7$) and the walk achieves this value faster for higher strengths of the channel. On the other hand, we see that for the walk with amplitude damping, the asymptotic entropy is smaller than the one of the coherent quantum walk, and as the parameter γ increases the asymptotic von Neumann entropy decreases. This means that the phase damping maximizes the entropy of the coin while the amplitude damping reduces this entropy. Notice however that in this situation , as the global state is not pure, the von Neumann entropy of the coin state is not an entropy of entanglement, but it certainly informs something about the correlation of the systems.

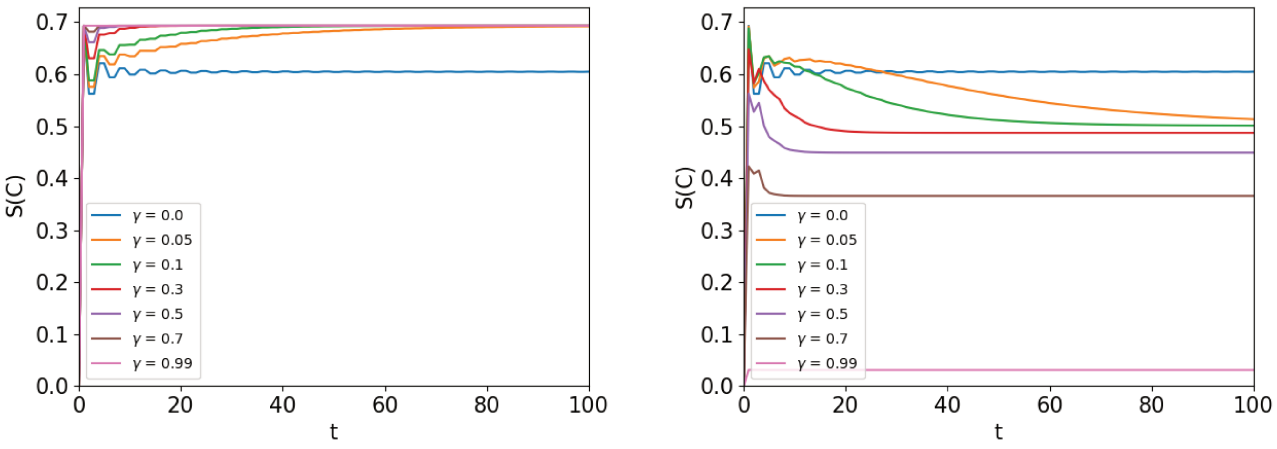

(a) Phase Damping

(b) Amplitude Damping

Figure 7.3: The **von Neumann entropy of the coin state** as a function of time of the incoherent quantum walk for different values of the γ parameter is displayed for Kraus operators corresponding to the phase damping (a) and to the amplitude damping (b).

In this case, where noise is introduced in the walk, the function that can best quantify the correlation between the two subsystems is the mutual information, $I(C;P)$. The mutual entropy between two systems can be interpreted as the information we get from one of the systems from the knowledge of the other, and is mathematically defined as

$$S(C;P) = S(C) + S(P) - S(C,P), \tag{7.5}$$

where $S(C)$ and $S(P)$ are the von Neumann entropies of the coin state and position space, and $S(C,P)$ is the joint entropy. Figure 7.4 shows the evolution of this function for the two types of Kraus operators. We see that for both cases the entropy decreases as γ increases, meaning that the correlation between Coin and position space decreases as an effect of the external noise, as expected.

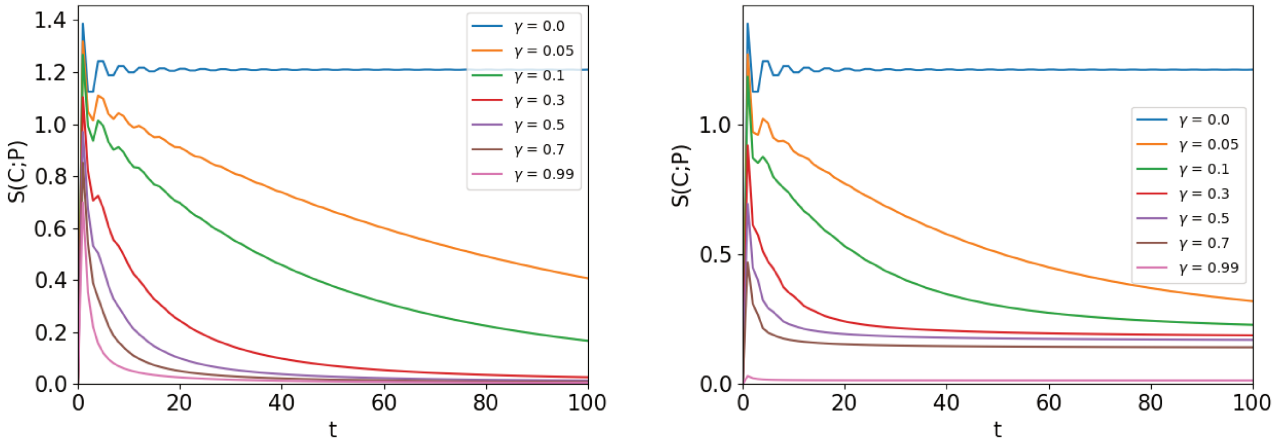

(a) Phase Damping

(b) Amplitude Damping

Figure 7.4: The **mutual entropy** as a function of time of the incoherent quantum walk for different values of the γ parameter is displayed for Kraus operators corresponding to the phase damping (a) and to the amplitude damping (b).

7.2 Unitary Noise

The decoherence described by unitary operators can be caused by fluctuations and drifts in parameters of the system's Hamiltonian. To consider this type of decoherence, a method was developed in the reference Shapira et al. (2003). It consists in changing the evolution operator U in eq. (6.4) to a unitary operator with a stochastic part. This can be interpreted as a random rotation on the coin space at each time step. The dynamics of the system is given by

$$|\psi(t+1)\rangle = \mathrm{Sh}(Ce^{ia(t)} \otimes \mathbb{I})\,|\psi(t)\rangle = Q(t)\,|\psi(t)\rangle\,. \tag{7.6}$$

The operator $a(t)$ is a stochastic and hermitian operator that acts on the coin space. Hence, the new evolution operator, $Q(t)$, is stochastic, but remains unitary. Since the Pauli matrices together with the identity are a basis of the chirality space, we can write

$$a(t) = \sum_{k=x,y,z} \alpha_k(t)\sigma_k, \tag{7.7}$$

with $\alpha_k(t)$ being real components of the expansion. In this case, the identity does not need to be taken into account because it would only add a global phase to the state. Before simulating the effects of this decoherence on the quantum walk we made the following assumptions in the stochastic operator components $a(t)$, i.e,

$$\begin{cases} \langle \alpha_k(t)\alpha_{k'}(t')\rangle = \delta_{k,k'}\delta_{t,t'}\alpha^2 \\ \langle \alpha_k(t)\rangle = 0 \quad ;\mathrm{k} = \mathrm{x,\ y,\ z.} \end{cases} \tag{7.8}$$

This means that there is no correlation between different components of the operator and between different times and that the probability distributions of α are isotropic. In fact, in the simulation, we consider specifically a Gaussian distribution with a standard deviation, σ_a. Figure 7.5 shows the result of the simulations. In the left-hand side figure, there is a graph of the position distribution of the walker after 100 time steps for different values of σ_a. To obtain these distributions the simulation ran 400 times and we took the mean of the results. The line that corresponds to $\sigma_a = 0$ is the limit of the coherent quantum walk, and as σ_a increases we see a tendency of accumulation on the initial state of the distribution. On the right side of the figure, there is a graph of standard deviation as a function of time where we can see that as σ_a increases the walk starts to behave like the classical walk ($\sigma \propto \sqrt{t}$). This graph was also made with a mean of 400 simulation runs.

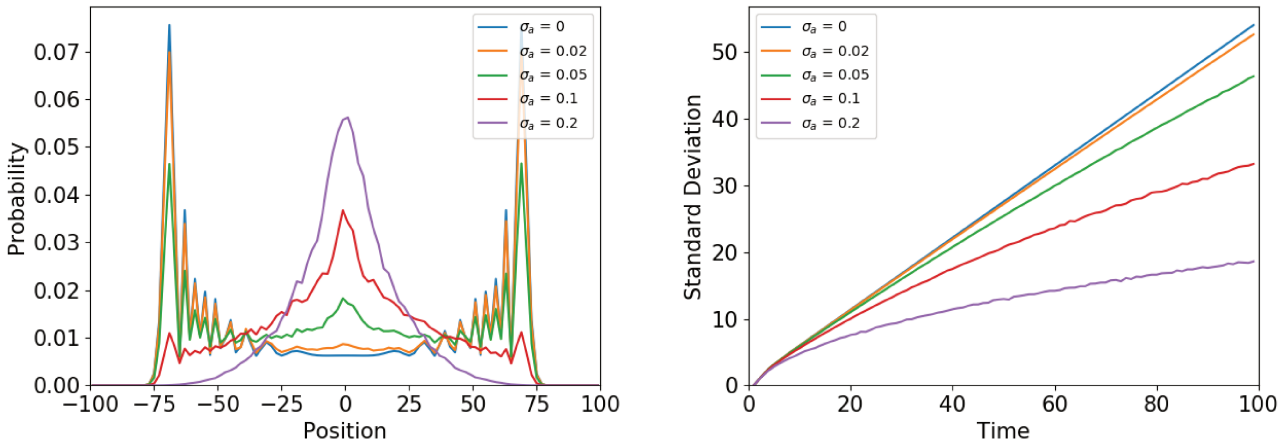

(a) Position distribution.

(b) Standard Deviation.

Figure 7.5: Figure (a) shows the distribution of position probability of the quantum walk with unitary noise after 100 time steps for several values of σ_a. And (b) the evolution of the standard deviation with time.

The von Neumann entropy of the coin and the mutual entropy were also calculated for this type of decoherence. Figure 7.6, made from the mean of 400 simulations, shows the entropys as a function of time for different values of σ_a. Note that in both cases, entropy increases for higher values of σ_a.

From figures 7.5 and 7.6, one can see some resemblances with the behavior of a walk under phase space decoherence. This is due to the fact that the phase space channel is derived considering the mean of a walk with a unitary random rotation in the z axis, while the model we analyzed in this section accounts for random rotations in random directions and the mean is calculated computationally, not analytically. However we see that, in the case of the unitary noise, the mutual information is twice the value of the von Neuamnn entropy – this is due to the fact the evolution of the system is unitary, and, therefore, the entropy of the coin is equal to the entropy of the position state, and the joint entropy is zero (and therefore the joint state remains pure).

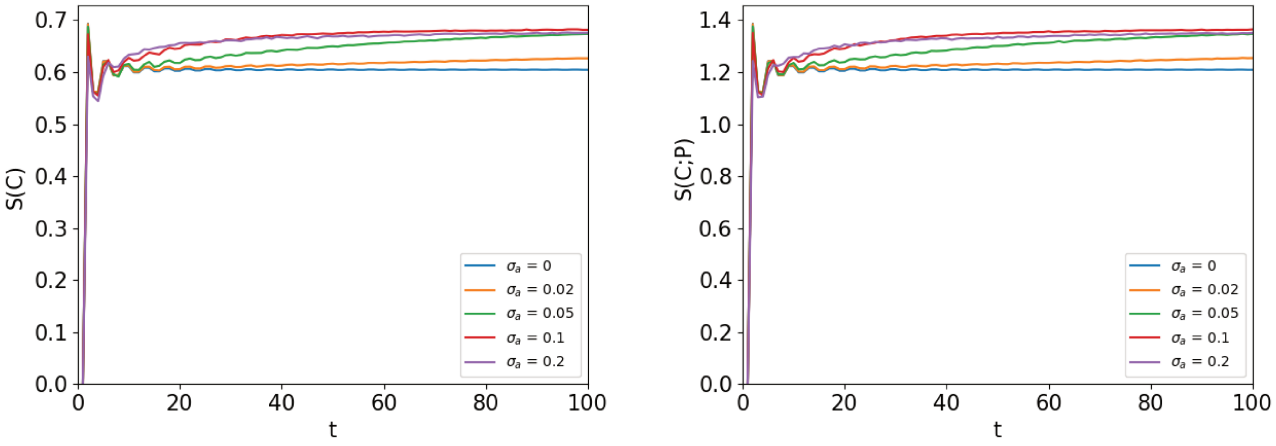

(a) Von Neumann entropy of the coin state.

(b) Mutual Information between coin and position.

Figure 7.6: Entropy and mutual information as a function of time of the incoherent quantum walk for different periods of time between measurements.

7.3 Broken links

Another way of introducing decoherence is by assuming that the links between two sites of the graph have a non-null probability of being broken at each time step, Romanelli et al. (2005). If the link is open, the particle cannot move to the neighbor vertices. Figure 7.7 illustrates the possible motions when one or two of the edges are broken.

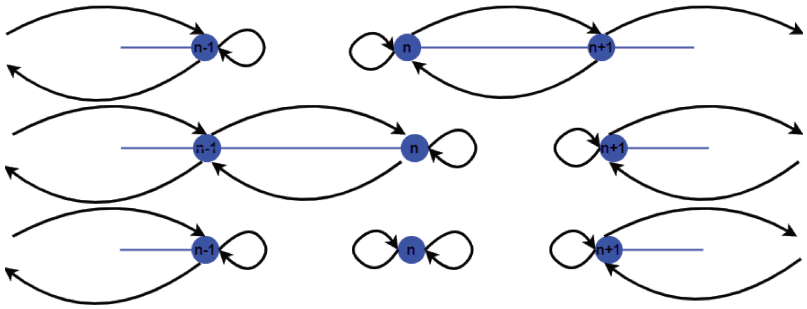

Figure 7.7: Diagram of the walk with broken links on left, right and both sides of the nth vertices.

The recurrence relations (6.8) are correct for the case of no broken links in the neighborhood of site n, however if there is any open link the relation has to be changed. Considering the Hadamard coin, equation (6.8) becomes

$$\begin{aligned} a_n(t+1) &= \frac{1}{\sqrt{2}}(a_{n+1}(t) + b_{n+1}(t)); \\ b_n(t+1) &= \frac{1}{\sqrt{2}}(a_{n-1}(t) - b_{n-1}(t)). \end{aligned} \tag{7.9}$$

If the link on the left side of site n is broken we have

$$\begin{aligned} a_n(t+1) &= \frac{1}{\sqrt{2}}(a_{n+1}(t) + b_{n+1}(t)); \\ b_n(t+1) &= \frac{1}{\sqrt{2}}(a_n(t) + b_n(t)). \end{aligned} \tag{7.10}$$

On the other hand, if the link on the right of position n is open

$$\begin{aligned} a_n(t+1) &= \frac{1}{\sqrt{2}}(a_n(t) - b_n(t)); \\ b_n(t+1) &= \frac{1}{\sqrt{2}}(a_{n-1}(t) - b_{n-1}(t)). \end{aligned} \tag{7.11}$$

At last, if both links are broken the walker doesn't move, but have a change at the coin state

$$\begin{aligned} a_n(t+1) &= \frac{1}{\sqrt{2}}(a_n(t) - b_n(t)); \\ b_n(t+1) &= \frac{1}{\sqrt{2}}(a_n(t) + b_n(t)). \end{aligned} \tag{7.12}$$

In this case, the evolution occurs with unitary operations, however, the operators change randomly according to the topology of the graph. Note that the decoherence comes from a stochastic process - i.e, the changes on the graph - that change the evolution operator, U, to another unitary operator, just like in the case of the unitary noise model.

Figure 7.8 displays graphs of the probability distribution of the position of the walker after 50, 200 and 500 time steps obtained by a simulation of the quantum walk with broken links for three different probabilities of broken link and figure 7.9 shows the same distributions, but for the mean value of 1000 simulations. As we can see, as the probability of broken links increases, the probability distribution starts to look more like a Gaussian. There is a characteristic time, t_c, associated with the transition between quantum to classical behavior that

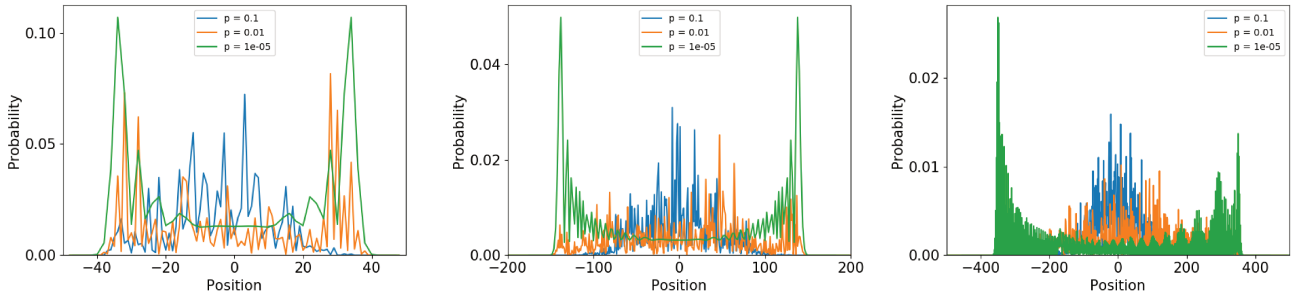

(a) $t = 50$. (b) $t = 200$. (c) $t = 500$.

Figure 7.8: Probability distribution of the position of the walker after 50, 200 and 500 time steps obtained by one simulation of the quantum walk with broken links for three different probabilities of broken link.

depends on the probability of broken links p. At the initial time, the walker is at position 0, therefore there are only two relevant links to the walk, the ones connecting position 0 with ± 1. As the walk evolves the wave

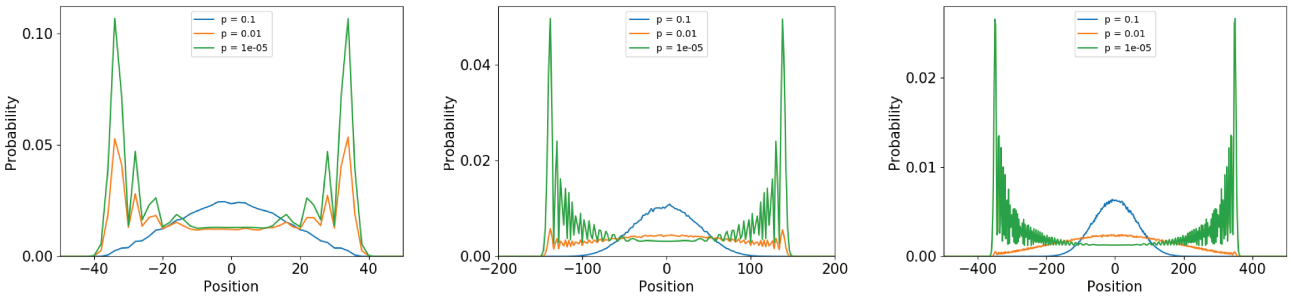

(a) $t = 50$. (b) $t = 200$. (c) $t = 500$.

Figure 7.9: Probability distribution of the position of the walker after 50, 200 and 500 time steps, from left to right, obtained by the mean values of 1000 simulations of the quantum walk with broken links for three different probabilities of broken link.

function spreads through the line covering a range of $\sqrt{2}t$. Hence, the mean number of broken links per time step is proportional to the time, $p\sqrt{2}t$. The classical behavior starts to emerge when the mean number of broken links per time step is of order one, so $t_c = \dfrac{1}{p\sqrt{2}}$ and for $t >> t_c$ the distribution tends to a Gaussian. The transition is also reflected on the standard deviation, the spread for early times is ballistic and for $t >> t_c$ the classical spread is dominant. For instance, the values of probabilities we used in the simulations have the following characteristic time

$$\begin{aligned} p = 0.1 &\implies t_c \approx 7 \text{ time steps;} \\ p = 0.01 &\implies t_c \approx 71 \text{ time steps;} \\ p = 10^{-5} &\implies t_c \approx 70711 \text{ time steps.} \end{aligned} \tag{7.13}$$

This can be observed on figure 7.10. All three curves start looking like a straight line but approximately at t_c, the ballistic feature stops to be the dominant behavior. This happens approximately at the 7th time step for the blue curve and at the 70th time for the orange one. The green curve remains with quantum behavior through all the time accounted .

The diffusion coefficient can be calculated as $D_{bl} = \dfrac{1}{2}\lim_{t\to\infty}\dfrac{\partial\sigma^2}{\partial t}$, which give us the result of Romanelli et al. (2005)

$$D_{bl} = K\frac{1-p}{p}, \tag{7.14}$$

where K is a constant.

The mean von Neumann entropy of the coin and the mutual information of the quantum walk with broken links, of 400 simulations, are depicted in figure 7.11. Like in the case of unitary noise, we see that the decoherence increases both quantities. Specially, from figure 7.11 (b) we can infer that the induced decoherence causes an increase in the correlation between the two sub-spaces of the system – something not expected in the usual

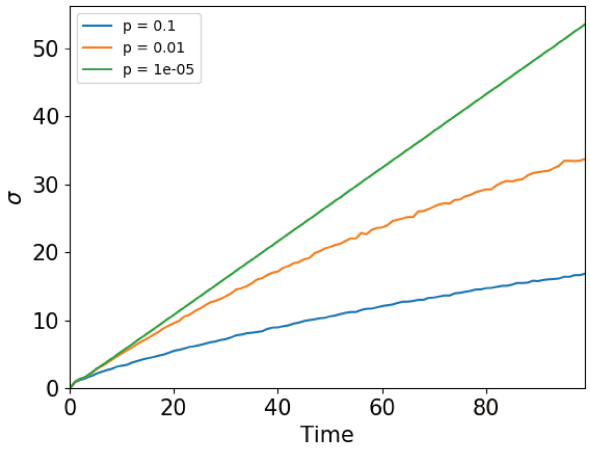

Figure 7.10: Standard deviation as a function of time of the quantum walk with broken links for different probabilities of open edges. The values of standard deviation were obtained by the mean of 400 simulations.

system-reservoir treatment of decoherence, as we saw in the case of amplitude and phase damping.

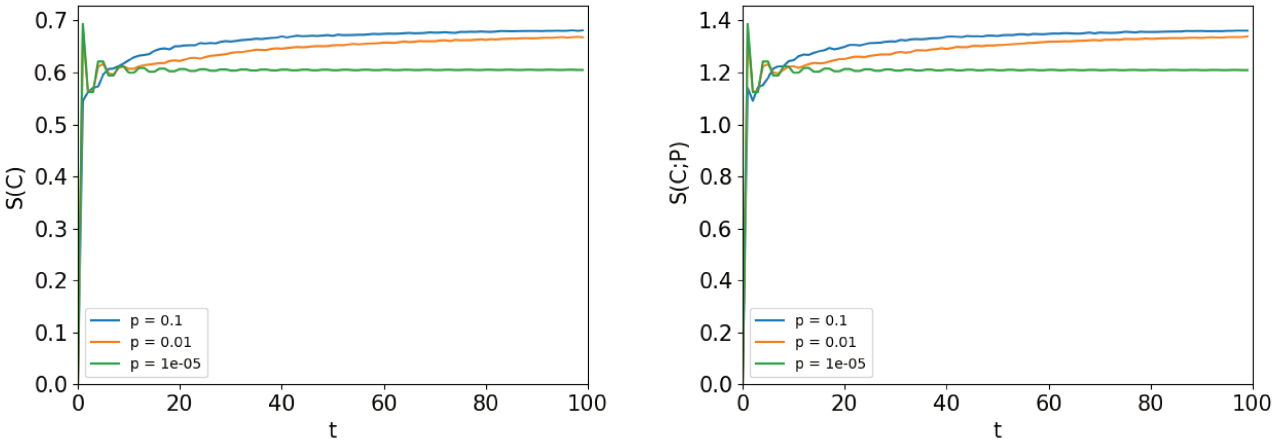

(a) Von Neumann entropy of the coin state.

(b) Mutual information.

Figure 7.11: Entropy and mutual information as a function of time of the quantum walk with broken links for different probabilities of open edges.

7.4 Periodic measurement

It is clear that if the position or coin state is measured at each time step of the quantum walk evolution there is no interference in the dynamics of the system and the quantum walk has the same behavior as the random walk. But what would happen if the state of the walker is measured only some times during the process? We

can imagine that the answer is that the behavior will be something in the way between the quantum walk and its classical counterpart. To analyze the transition behavior between both walks Romanelli et al. (2005) proposed a model where periodic measurements are made, i.e, the state is measured after every T time steps. The measurement of the coin state is made by a projection with the σ_y operator to preserve the symmetry of the evolution.

Let us consider a Hadamard walk with an initial condition that generates a symmetric walk, e.g, $\frac{1}{\sqrt{2}}(1,i)^T$. After the first period of T time steps the probability that the position measurement results in n is $q_n = P_n(T)$. Then the wave function collapses to the measurement value and evolves again in a unitary way. The probability density function repeats itself, however, now, centered on the measured position.

We will consider that measurements are performed on the times $t = T, 2T, 3T, .., \tau T$. On the interval between any two consecutive measurements the position probability distribution respects the following master equation

$$P_n(t+T) = \sum_{j=n-T}^{n+T} q_{n-j} P_j(t). \tag{7.15}$$

Using the definitions of the first, M_1, and second moments, M_2, presented on section 2 and eq. (7.15) we find

$$\begin{cases} M_1(t+T) = M_1(t) + M_{1q}(T); \\ M_2(t+T) = M_2(t) + 2M_1(t)M_{1q}(T) + M_{2q}(T), \end{cases} \tag{7.16}$$

where $M_{1q}(T) = \sum_{-T}^{T} nq_n$ and $M_{2q}(T) = \sum_{-T}^{T} n^2 q_n$ are the moments associated with the unitary evolution between measurements. Hence, if the associated variance is $\sigma_q^2(T) = M_{2q}(T) - M_{1q}^2(T)$, the variance is

$$\sigma^2(t+T) = \sigma^2(t) + \sigma_q^2(T). \tag{7.17}$$

Since the diffusion coefficient is $D_{pm} = \frac{\Delta\sigma^2}{2\Delta t}$, considering the time interval as $\Delta t = \tau T$, we have that

$$D_{pm} = \frac{\sigma_q^2(T)}{2T} = \frac{KT}{2}, \tag{7.18}$$

where K is a constant. This means that the diffusion coefficient depends inversely on the frequency of measurements $f = \frac{1}{T}$.

Figure (7.12) shows the variance of the walk as a function of time for different frequencies of measurements. Note that between measurements the walker spreads ballistically, however taking into account only the values of variance on times that measurements occurred the variance seams to evolve classically. On the limit where the measurement is performed at each time step, $T = 1$, we have that $\sigma^2 \propto t$, and when no measurement is performed at the time interval considered, $T = 120$, the quantum feature is recovered. Note that this result is independent of how the chirality measurement is done because the variance of the quantum walk does not depend on the initial chirality condition, just on the parameters of the coin.

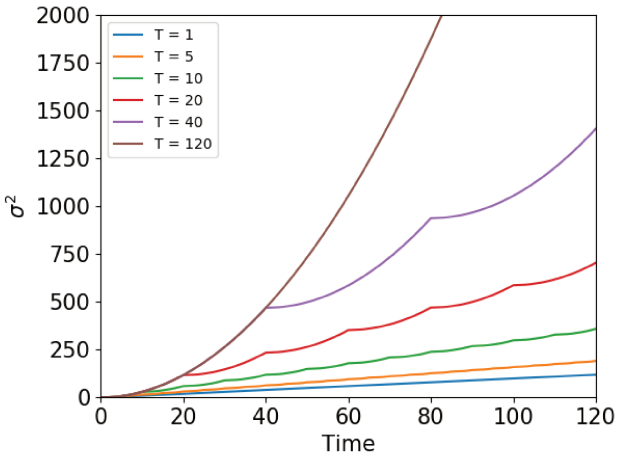

Figure 7.12: Variance as a function of time of the incoherent quantum walk for different periods of time between measurement.

This model can be generalized to the case where the intervals between measurements are randomly distributed, Romanelli et al. (2005). Then the diffusion coefficient is given by

$$D_{pm} = \frac{C\langle T^2\rangle}{2\langle T\rangle}, \tag{7.19}$$

where $\langle T\rangle$ is the mean time between measurements. In this case, the process is analogous to the classical Brownian motion discussed in section 3. The collisions of the Brownian motion can be associated with the quantum measurement process, and the free movement of the Brownian particle can be associated with the evolution between measurements. From the equation obtained for the diffusion coefficient of the Brownian motion, D_2, in section 3 we know that the coefficient is proportional to the inverse of the viscosity coefficient, k,

$$D_2 = \frac{C'}{k} \tag{7.20}$$

where C' is a constant. This coefficient can be compared with the one for the quantum walk with periodic measurements at long times obtained in eq. (7.18), therefore we have that

$$k \propto \frac{2}{T} = 2f. \tag{7.21}$$

This shows that the quantum walk with disrupting events such as measurements can be interpreted as a dissipative process. In fact, a similar argument can be used to interpret the broken link model as a dissipative process as well, however in this case the frequency of measurements would have to be substituted by the frequency of broken links. Those interpretations are in accordance with the view of decoherence as the loss of information from a system into the environment.

7.5 Three-state Quantum Walk

In this section, we extend the methods explained in the last sections to the case of a discrete-time quantum walk with a three-state coin. Since the main difference between the behavior of this walk and the two-state quantum walk is the localization generated by some initial conditions, we extend the methods and simulate the decoherent walk with and without localization. The initial conditions chosen to represent both behaviors are the same ones used to graphic the position probability distribution in figures 6.14, i.e, $|\psi(0)\rangle = \frac{1}{\sqrt{2}}(i,0,1)^T$ and $|\psi(0)\rangle = \frac{1}{\sqrt{6}}(1,-2,1)^T$.

7.5.1 Kraus Operators

The first methods we use to introduce decoherence in the two-state quantum walk consisted in apply Kraus operators on the evolution of the system, as exposed in equation (7.1). In this case, since we are dealing with a three level system, we will need Kraus operators of a single qutrit. The **phase damping** operators of a qutrit are (C.f. Ramzan and Khan (2011))

$$E_0 = \sqrt{1-\gamma}\begin{pmatrix} 1 & 0 & 0 \\ 0 & 1 & 0 \\ 0 & 0 & 1 \end{pmatrix}; \qquad E_1 = \sqrt{\gamma}\begin{pmatrix} 1 & 0 & 0 \\ 0 & \omega & 0 \\ 0 & 0 & \omega^2 \end{pmatrix}, \tag{7.22}$$

where $\omega = e^{2\pi i/3}$. The walk with and without localization was simulated considering the phase damping operators, result is presented in figure 7.13. In both cases the effect of the decoherence is similar to the effect in the two-state walk in the sense that there is a transition to the classical behavior. The main difference in the case of the three-state walk is that the transition occurs as the strength parameter, γ, increases, but the Gaussian curve is achieved for $\gamma = 0.5$, instead of 1 and for $\gamma > 0.5$ the distribution starts to transit back to the quantum behavior. This means that the distribution of walks with $\gamma = 0.5 - x$ and $\gamma = 0.5 + x$ are equal ($0 < x < 0.5$).

On the other side, the **amplitude damping** operators of a qutrit are (C.f. Ramzan and Khan (2011))

$$E_0 = \begin{pmatrix} 1 & 0 & 0 \\ 0 & \sqrt{1-\gamma} & 0 \\ 0 & 0 & \sqrt{1-\gamma} \end{pmatrix}; \qquad E_1 = \begin{pmatrix} 0 & \sqrt{\gamma} & 0 \\ 0 & 0 & 0 \\ 0 & 0 & 0 \end{pmatrix} \qquad E_2 = \begin{pmatrix} 0 & 0 & \sqrt{\gamma} \\ 0 & 0 & 0 \\ 0 & 0 & 0 \end{pmatrix}. \tag{7.23}$$

Figure 7.14 shows the resultant distribution of the three-state quantum walk with amplitude damping for the two initial conditions we are considering in this section. In this case, the transition to a Gaussian shape distribution occurs in a similar way to the two-state case. The walk with strength $\gamma = 0$ represents the walk with no decoherence and as γ increases the classical distribution is recovered, but with a shift in the position lattice.

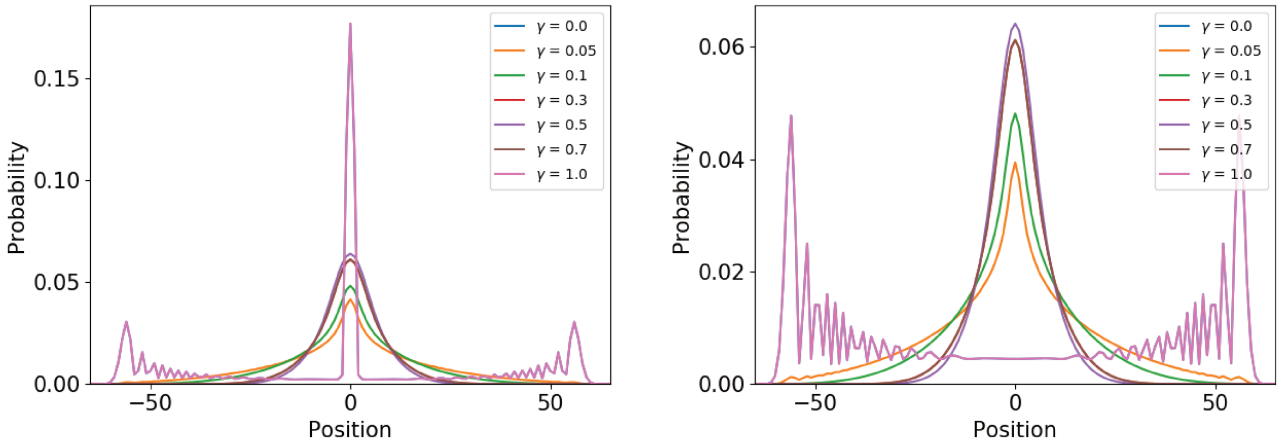

(a) $|\psi(0)\rangle = \frac{1}{\sqrt{2}}(i,0,1)^T$ (b) $|\psi(0)\rangle = \frac{1}{\sqrt{6}}(1,-2,1)^T$.

Figure 7.13: The probability distribution of positions of the three-state quantum walk with phase damping after 100 time steps for different values of the γ parameter is displayed for two initial conditions, one that generates localization and one that doesn't .

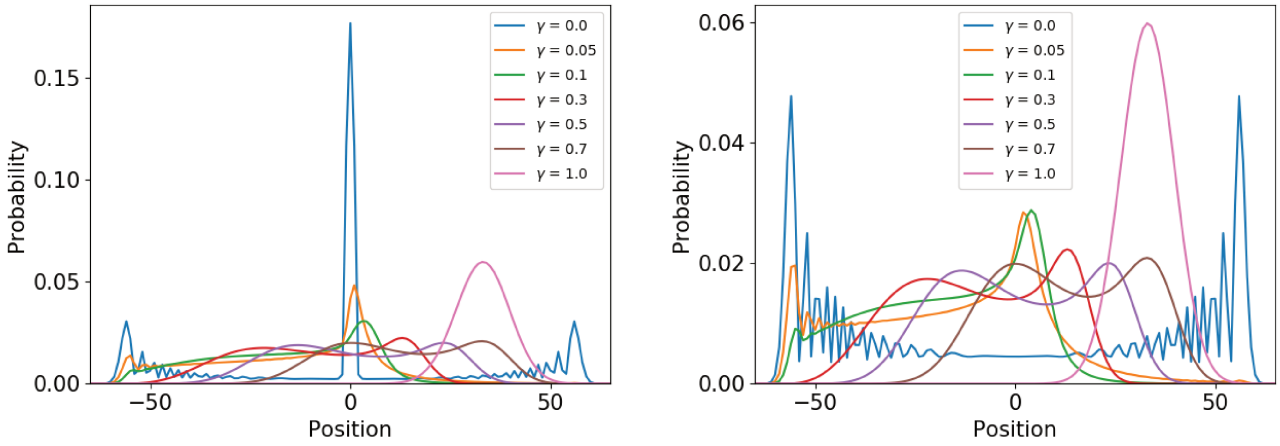

(a) $|\psi(0)\rangle = \frac{1}{\sqrt{2}}(i,0,1)^T$. (b) $|\psi(0)\rangle = \frac{1}{\sqrt{6}}(1,-2,1)^T$.

Figure 7.14: The probability distribution of positions of the three-state quantum walk with amplitude damping after 100 time steps for different values of the γ parameter is displayed for two initial conditions, one that generates localization and one that doesn't .

7.5.2 Unitary Noise

The procedure used to numerical implement a unitary noise in a three-state quantum walk is very similar to the one explained in 7.2, however, in this case the stochastic operator $a(t)$ is written in terms of the Gell-Mann

matrices (A.9), instead of the Pauli matrices

$$a(t) = \sum_{k=1}^{8} a_k(t)\lambda_k. \tag{7.24}$$

$a_k(t)$ are real components of the expansions and the assumptions made about them are considered again. Following that procedure we simulated the decoherent walk for a localized and a non localized initial condition $\frac{1}{\sqrt{2}}(i,0,1)^T$ and $\frac{1}{\sqrt{6}}(1,-2,1)^T$. Figure 7.15 show the resultant probability density function of positions obtained by the mean values of 400 simulations. The blue curve represents the walk without noise and, as σ_a increases the classical behavior starts to emerge for both cases.

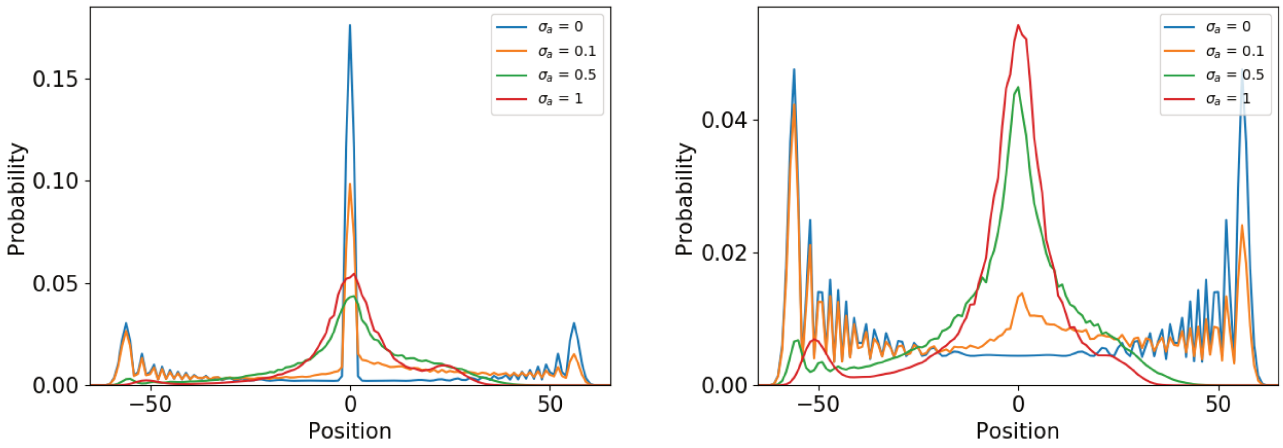

(a) $|\psi(0)\rangle = \frac{1}{\sqrt{2}}(i,0,1)^T$.

(b) $|\psi(0)\rangle = \frac{1}{\sqrt{6}}(1,-2,1)^T$.

Figure 7.15: Distribution of position probability of the three-state quantum walk with unitary noise after 100 time steps for several value of σ_a, for a localized and a non localized walk.

7.5.3 Broken Links

To extend the model of decoherence by broken links to the three-state quantum walk, the recursion relations for the chirality components must be rewritten. The recurrence relation for the regular walk - i.e, with no broken links - is

$$\begin{aligned} a_n(t+1) &= \frac{1}{3}(-a_{n+1}(t) + 2b_{n+1}(t) + 2c_{n+1}(t)); \\ b_n(t+1) &= \frac{1}{3}(2a_n(t) - b_n(t) + 2c_n(t)); \\ c_n(t+1) &= \frac{1}{3}(2a_{n-1}(t) + 2b_{n-1}(t) - c_{n-1}(t)). \end{aligned} \tag{7.25}$$

If the link on the left side of position n is broken, then the upper component of the spinor at n receives probability flux from $n+1$. To conserve the probability flux, the outgoing flux must be passed to component c at the

same site. The resultant expressions are

$$\begin{aligned} a_n(t+1) &= \frac{1}{3}(-a_{n+1}(t) + 2b_{n+1}(t) + 2c_{n+1}(t)); \\ b_n(t+1) &= \frac{1}{3}(2a_n(t) - b_n(t) + 2c_n(t)); \\ c_n(t+1) &= \frac{1}{3}(-a_n(t) + 2b_n(t) + 2c_n(t)). \end{aligned} \tag{7.26}$$

Analogous the recurrences relations in the case that there is a broken link on the right of site n are

$$\begin{aligned} a_n(t+1) &= \frac{1}{3}(2a_n(t) + 2b_n(t) - c_n(t)); \\ b_n(t+1) &= \frac{1}{3}(2a_n(t) - b_n(t) + 2c_n(t)); \\ c_n(t+1) &= \frac{1}{3}(2a_{n-1}(t) + 2b_{n-1}(t) - c_{n-1}(t)). \end{aligned} \tag{7.27}$$

Finally, if both links that connect site n with its neighbors are broken, the relations became

$$\begin{aligned} a_n(t+1) &= \frac{1}{3}(2a_n(t) + 2b_n(t) - c_n(t)); \\ b_n(t+1) &= \frac{1}{3}(2a_n(t) - b_n(t) + 2c_n(t)); \\ c_n(t+1) &= \frac{1}{3}(-a_n(t) + 2b_n(t) + 2c_n(t)). \end{aligned} \tag{7.28}$$

Using those relations to simulate the three-state quantum walk with decoherence we calculate the position probability distribution of the walk after 50 and 200 and time steps. Figures 7.16 and 7.18 show the mean result of 1000 simulations for two initial conditions, one that generates localization, $\frac{1}{\sqrt{2}}(i,0,1)^T$, and one that does not $\frac{1}{\sqrt{6}}(1,-2,1)^T$. As in the other cases of decoherence, we see a transition from the quantum distribution to a Gaussian, however in this case and interesting feature differentiates the effect of the decoherence. When the initial conditions generate localization, the broken links conserve the localization, changing only the other regions of the distribution. Figure 7.17 is a zoom of the left-hand side graph in figure 7.16, where we can see clearly that outside the localization region the blue and orange curves approach a Gaussian shape and in the central region of the three curves present the localized shape.

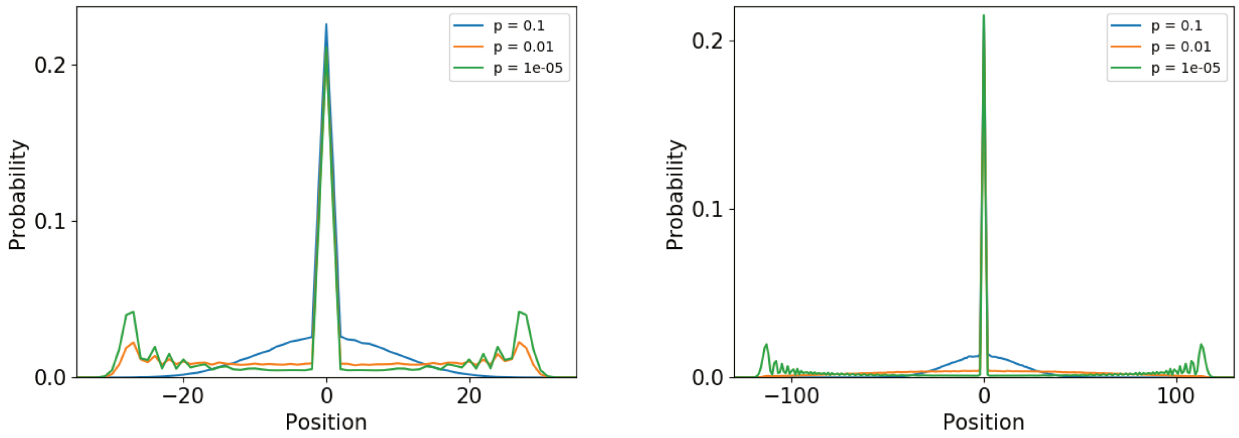

(a) $t = 50$. (b) $t = 200$.

Figure 7.16: Probability distribution of the position of the walker after 50 and 200 time steps obtained by the mean values of 1000 simulations of the three-state quantum walk with broken links for three different probabilities of broken link. The initial condition considered is $\frac{1}{\sqrt{2}}(i,0,1)^T$.

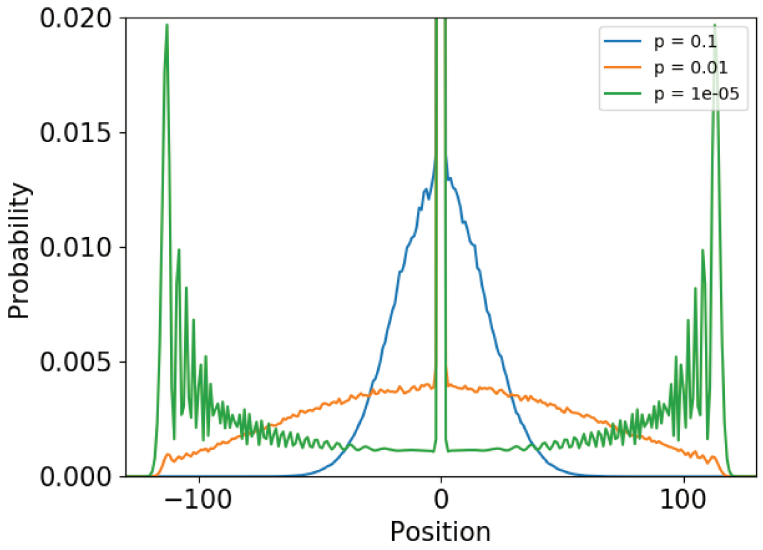

Figure 7.17: Zoom of the graph on the right side of fig. 7.16, that is, the distribution of position probability's of the decoherent walk after 200 time steps.

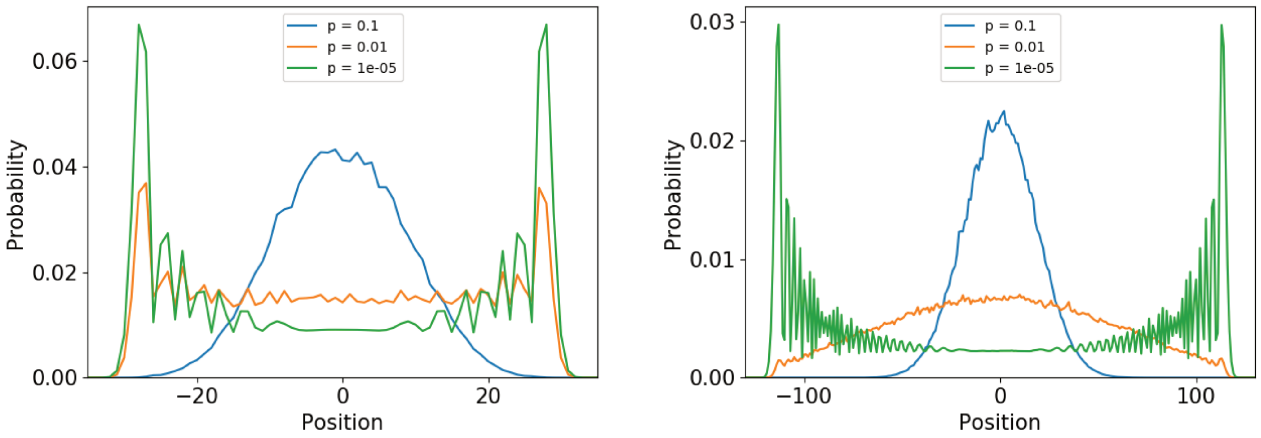

(a) $t = 50$.

(b) $t = 200$.

Figure 7.18: Probability distribution of the position of the walker after 50 and 200 time steps obtained by the mean values of 1000 simulations of the three-state quantum walk with broken links for three different probabilities of having a broken link. The initial condition considered is $\frac{1}{\sqrt{6}}(1,-2,1)^T$.

CHAPTER 8

Continuum Limit of the Discrete Time Quantum Walk

8.1 Continuum Limit of the Quantum Walk without Interference

As it was already demonstrated in chapter 6, the recurrence relations of the discrete-time quantum walk can be manipulated in a way that separates the term responsible for interference. In this section we are going to consider the continuum limit of the discrete time quantum walk without taking into account those interference terms, C.f. Romanelli et al. (2003). If we remind the recurrence expressions (6.8) for the right and left components of the state of the system

$$\begin{aligned} a_n(t+1) &= a_{n+1}(t)\cos\gamma + b_{n+1}(t)\sin\gamma \\ b_n(t+1) &= a_{n-1}(t)\sin\gamma - b_{n-1}(t)\cos\gamma, \end{aligned},$$

and if we define $P_L(n,t) = |a_n(t)|^2$ and $P_R(n,t) = |b_n(t)|^2$ as the probability of finding the walker at position n, at time t and the coin in state left or right, respectively, the recurrence relations can be written as

$$\begin{aligned} P_L(n,t+1) &= P_L(n+1,t)\cos^2\gamma + P_R(n+1,t)\sin^2\gamma + q(n+1,t)\sin 2\theta, \\ P_R(n,t+1) &= P_L(n-1,t)\sin^2\gamma + P_R(n-1,t)\cos^2\gamma - q(n-1,t)\sin 2\theta, \end{aligned} \tag{8.1}$$

where $q(n,t) = \mathbb{R}e[a_n(t)b_n^*(t)]$ is the interference term. Again, we easily manage to identify it in the equation, so, as stated above we are not going to consider this term. Since $P(n,t) = P_L(n,t) + P_R(n,t)$, summing both equations we have that the recurrence relation for the position probability defines a second order Markov process

$$P(n,t+1) = [P(n+1,t) + P(n-1,t)]\cos^2\gamma - P(n,t-1)\cos 2\gamma. \tag{8.2}$$

Before taking the continuum limit, we manipulate the expression by adding and subtracting $2P(n,t)\cos^2\gamma$ and $P(n,t)\sin^2\gamma$, in addition to replacing the distance between two positions on the lattice by Δn and the time between two steps by Δt. We find

$$\begin{aligned} 0 =& [P(n,t+\Delta t)-P(n,t)]\sin^2\gamma + [P(n,t)-P(n,t-\Delta t)]\sin^2\gamma \\ &+ [P(n,t+\Delta t)-2P(n,t)+P(n,t-\Delta t)]\cos^2\gamma - [P(n+\Delta n,t)-2P(n,t)+P(n-\Delta n,t)]\cos^2\gamma. \end{aligned} \tag{8.3}$$

Dividing both sides of the equation by $(\Delta t\Delta n)^2$ we end up with

$$\begin{aligned} 0 =& \frac{[P(n,t+\Delta t)-P(n,t)]}{\Delta t}\frac{\sin^2\gamma}{\Delta t\Delta n^2} + \frac{[P(n,t)-P(n,t-\Delta t)]}{\Delta t}\frac{\sin^2\gamma}{\Delta t\Delta n^2} \\ &+ \frac{[P(n,t+\Delta t)-2P(n,t)+P(n,t-\Delta t)]}{\Delta t^2}\frac{\cos^2\gamma}{\Delta n^2} - \frac{[P(n+\Delta n,t)-2P(n,t)+P(n-\Delta n,t)]}{\Delta n^2}\frac{\cos^2\gamma}{\Delta t^2}. \end{aligned} \tag{8.4}$$

Now, we can take the continuum limit in two different ways. If the limits $\Delta t \to 0$ and $\Delta n \to 0$ are taken in such a way that the velocity $v = \Delta n/\Delta t$ and the ratio $\sin\gamma^2/\Delta t$ are considered constants we find the **Telegraph equation**

$$\frac{\partial P}{\partial t} = \frac{\Delta t\ \cot^2\gamma}{2}\left[v^2\frac{\partial^2 P}{\partial n^2} - \frac{\partial^2 P}{\partial t^2}\right]. \tag{8.5}$$

On the other hand, if we consider $(\Delta x)^2/\Delta t$ constant, the limit leads to the **Diffusion equation**

$$\frac{\partial P}{\partial t} = \frac{\Delta t\ \cot^2\gamma}{2}v^2\frac{\partial^2 P}{\partial n^2}. \tag{8.6}$$

Note that, in this case, the diffusion coefficient is $D = \frac{\Delta t\ \cot^2\gamma}{2}v^2$. The diffusion coefficient obtained in chapter 3 was $D_2 = \frac{K_B T}{mk}$, hence, due to the equipartition theorem $D_2 = \frac{\langle v^2\rangle}{k}$. We want to use this system to simulate the Brownian motion, so we compare both expressions and identify the viscosity coefficient with $\frac{2\tan^2\gamma}{\Delta t}$. For the Hadamard walk with position and time increment equals to 1, the classical value of the diffusion coefficient for the random walk is recovered, $D = \dfrac{1}{2}$.

8.2 Mathematical Resemblance with Relativistic Quantum Mechanics

The dynamics of the quantum walk is very simple and easy to implement computationally. Therefore it can be used to simulate analogous systems. In this section, we present some resemblances between the mathematical structure of quantum walks and relativistic quantum mechanics. This makes it possible to relate some relativistic problems with the discrete-time quantum walk and, furthermore, to simulate them using quantum walks.

We divided this section in three parts. In the first one, we demonstrate, by taking the continuum limit, that the decoupled form of the equation of motion of the quantum walk is equivalent to the Klein-Gordon equation of a free particle with spin 0. In the second part, we show that the coupled form for the dynamics of the quantum walk is analogous to the Dirac equation of a particle of spin 1/2. In the third part, we analyze the

resemblance between the Dirac Hamiltonian and the Hamiltonian of the discrete-time quantum walk. Those demonstrations were first derived by Chandrashekar et al. (2010) and to a more detailed calculation, we refer to Diniz (2016).

First let us introduce a different notation for the discrete time quantum walk than the one used in chapter 6. Both notations are very similar, however in this one the coin operator has complex elements which can generate different inferences from the ones on the quantum walk with a real coin. The state of the system at time t and position n is composed by the left ($a(n,t)$) and right ($b(n,t)$) components

$$\psi(n,t) = \begin{pmatrix} a(n,t) \\ b(n,t) \end{pmatrix}. \tag{8.7}$$

With the coin operator of the form

$$C(\theta) = \begin{pmatrix} \cos\theta & -i\sin\theta \\ -i\sin\theta & \cos\theta \end{pmatrix}, \tag{8.8}$$

and the shift operator is defined by the pair of operators $e^{\pm i\hat{P}}$ as

$$S = \begin{pmatrix} e^{i\hat{P}} & 0 \\ 0 & e^{-i\hat{P}} \end{pmatrix}, \tag{8.9}$$

where $e^{\pm i\hat{P}}\psi(n,t) = \psi(n\pm,t)$. Once the shift and coin operators are well defined, the evolution of the state (8.7) on one time step is given by equation (6.4), i.e,

$$\begin{pmatrix} a(n,t+1) \\ b(n,t+1) \end{pmatrix} = \begin{pmatrix} \cos\theta e^{i\hat{P}} & -i\sin\theta e^{i\hat{P}} \\ -i\sin\theta e^{-i\hat{P}} & \cos\theta e^{-i\hat{P}} \end{pmatrix} \begin{pmatrix} a(n,t) \\ b(n,t) \end{pmatrix}. \tag{8.10}$$

Then, we obtain the following recurrence relations

$$\begin{aligned} a(n,t+1) &= a(n+1,t)\cos\theta - ib(n+1,t)\sin\theta \\ b(n,t+1) &= b(n-1,t)\cos\theta - ia(n-1,t)\sin\theta. \end{aligned} \tag{8.11}$$

In next sections we use relations (8.11) to show how the quantum walk relates with the Klein-Gordon and the Dirac equations.

8.2.1 Decoupled discrete-time Quantum Walk equation in Klein-Gordon form

To decouple the variables a and b in equation (8.11), let us start by isolating the left component of the second line of the recurrence relation,

$$a(n-1,t) = \frac{i}{\sin\theta}[b(n,t+1) - \cos\theta\, b(n-1,t)]. \tag{8.12}$$

By making the transformations $(n,t)\rightarrow(n+1,t+1)$ and $(n,t)\rightarrow(n+2,t)$ we find

$$\begin{cases} a(n,t+1) &= \frac{i}{\sin\theta}[b(n+1,t+2)-\cos\theta\, b(n,t+1)]; \\ a(n+1,t) &= \frac{i}{\sin\theta}[b(n+2,t+1)-\cos\theta\, b(n+1,t)]; \end{cases} \tag{8.13}$$

that can be substituted in the first line of the recurrence relation to get an equation that depends only on the right chirality components,

$$b(n,t+1)+b(n,t-1)=\cos\theta[b(n+1,t)+b(n-1,t)]. \tag{8.14}$$

If the same procedure had been done to get the decoupled equation with respect to a, the result would be completely analogous,

$$a(n,t+1)+a(n,t-1)=\cos\theta[a(n+1,t)+a(n-1,t)]. \tag{8.15}$$

Therefore, from now on, instead of carrying two identical equations we define the variable $\Lambda(n,t)$ that can represent $a(n,t)$ or $b(n,t)$ and write

$$\Lambda(n,t+1)+\Lambda(n,t-1)=\cos\theta[\Lambda(n+1,t)+\Lambda(n-1,t)]. \tag{8.16}$$

Subtracting $2\Lambda(n,t)+2\cos\theta\Lambda(n,t)$ from both sides of the equation above we find

$$[\Lambda(n,t+1)-2\Lambda(n,t)+\Lambda(n,t-1)]-2\cos\theta\Lambda(n,t)=\cos\theta[\Lambda(n+1,t)-2\Lambda(n,t)+\Lambda(n-1,t)]-2\Lambda(n,t). \tag{8.17}$$

Now, the decoupled equations are in the format we need to take the continuum limit. Since the first and second differential operators of an arbitrary function, f, are

$$\begin{aligned} \nabla_y f(x,y) &= \frac{f(x,y+\epsilon/2)-f(x,y-\epsilon/2)}{\epsilon}, \\ \nabla_y^2 f(x,y) &= \frac{f(x,y+\epsilon)-2f(x,y)+f(x,y-\epsilon)}{\epsilon^2}, \end{aligned} \tag{8.18}$$

where for $\epsilon=1$, $\nabla_y=\dfrac{\partial}{\partial y}$ and $\nabla_y^2=\dfrac{\partial^2}{\partial y^2}$, the continuum limit of eq. (8.17) is

$$\left[\cos\theta\frac{\partial^2}{\partial n^2}-\frac{\partial^2}{\partial t^2}\right]\Lambda(n,t)=2[1-\cos\theta]\Lambda. \tag{8.19}$$

Comparing it with the Klein-Gordon equation

$$\left[\nabla^2-\frac{1}{c^2}\frac{\partial^2}{\partial t^2}\right]\phi=\mu^2\phi, \tag{8.20}$$

where c is the velocity of light, $\mu=\frac{mc}{\hbar}$ and m is the mass, the analogy is clear. Making the following associations

$$c=\sqrt{\cos\theta}; \qquad m=\sqrt{\frac{2(\sec\theta-1)}{\cos\theta}}; \tag{8.21}$$

and considering $\hbar=1$, we see that the chirality components $a(n,t)$ and $b(n,t)$ have a free spin-0 particle character. Note that $c=1$ corresponds to $\theta=0$, and consequently, $m=0$ as is required by the relativity theory. The condition $\theta=0$ corresponds to the case where two peaks move away from each other without interference, i.e, there is no coin.

8.2.2 Coupled discrete-time quantum walk equation in Dirac form

To show the mathematical equivalence between the discrete-time quantum walk and the Dirac equation we start again from the expressions (8.11), but without decoupling them this time. In the matrix form we have

$$\begin{aligned}\begin{pmatrix} a(n,t+1) \\ b(n,t+1) \end{pmatrix} &= \cos\theta \begin{pmatrix} 1 & 0 \\ 0 & 1 \end{pmatrix} \begin{pmatrix} a(n+1,t) \\ b(n-1,t) \end{pmatrix} + \sin\theta \begin{pmatrix} 0 & -i \\ -i & 0 \end{pmatrix} \begin{pmatrix} a(n-1,t) \\ b(n+1,t) \end{pmatrix} \\ &= (\cos\theta\, \mathbb{I} + \sin\theta\sigma_z\sigma + y) \begin{pmatrix} a(n+1,t) \\ b(n-1,t) \end{pmatrix} - \sin\theta\sigma_y \begin{pmatrix} a(n+1,t) - a(n-1,t) \\ b(n+1,t) - b(n-1,t) \end{pmatrix}.\end{aligned} \tag{8.22}$$

Subtracting $\begin{pmatrix} a(n,t) \\ b(n,t) \end{pmatrix} + (\cos\theta\, \mathbb{I} + \sin\theta\sigma_z\sigma + y) \begin{pmatrix} a(n,t) \\ b(n,t) \end{pmatrix}$ from both sides of the expression we obtain

$$\begin{aligned}\begin{pmatrix} a(n,t+1) - a(n,t) \\ b(n,t+1) - b(n,t) \end{pmatrix} =& (\cos\theta\, \mathbb{I} + \sin\theta\sigma_z\sigma + y) \begin{pmatrix} a(n+1,t) - a(n,t) \\ b(n-1,t) - b(n,t) \end{pmatrix} \\ &+ (\cos\theta\, \mathbb{I} + \sin\theta\sigma_z\sigma + y - \mathbb{I}) \begin{pmatrix} a(n,t) \\ b(n,t) \end{pmatrix} \\ &- \sin\theta \begin{pmatrix} a(n+1,t) - a(n-1,t) \\ b(n+1,t) - b(n-1,t) \end{pmatrix}.\end{aligned} \tag{8.23}$$

Finally, to take the continuum limit we use the same approach as used in the last section, which led us to

$$\left[\frac{\partial}{\partial t} - (\cos\theta\sigma_z - 3\sin\theta\sigma_y) \frac{\partial}{\partial n} - (\cos\theta\, \mathbb{I} + \sin\theta\sigma_z\sigma_y - \mathbb{I}) \right] \psi(n,t) = 0. \tag{8.24}$$

Now considering $\theta = 0$, i.e, $\cos\theta = 1$, and multiplying both sides of the equation by $i\hbar$ we find

$$\left[i\hbar \frac{\partial}{\partial t} - i\hbar\sigma_z \frac{\partial}{\partial n} \right] \psi(n,t) = 0. \tag{8.25}$$

Therefore, we can compare it with the 1+1 dimensional Dirac equation which is given by

$$\left[i\hbar \frac{\partial}{\partial t} - i\hbar c\hat{\alpha} \frac{\partial}{\partial x} - \hat{\beta} mc^2 \right] \psi(x,t) = 0, \tag{8.26}$$

where m is the rest mass, c is the speed of light, $i\hbar\partial/\partial x$ is the momentum operator, x and t are the space and time coordinates and the matrices $\hat{\alpha}$ and $\hat{\beta}$ are Hermitians, satisfying the following properties

$$\begin{aligned}\hat{\alpha}^2 = \hat{\beta}^2 = \mathbb{I}d; \\ \hat{\alpha}\hat{\beta} = -\hat{\beta}\hat{\alpha}.\end{aligned} \tag{8.27}$$

Comparing equation (8.25) with the Dirac equation, we see that the coupled equations of the quantum walk are mathematically equivalent to the massless spin-1/2 particle Dirac equation if $\theta = 0$, $c = 1$ and $\hat{\alpha} = -\sigma_z$. This is again the case of the quantum walk without interference, that is, without the coin. It is important to mention that for other values of θ the matrix $\hat{\beta}$ does not respect conditions (8.27), therefore the resemblance is not valid anymore.

8.2.3 The Hamiltonian of the Walk

In this section the resemblance of the discrete time quantum walk with the Dirac equation is explored by the analysis of the Hamiltonian of the system. The following discussion is based on the work of Diniz (2016). To find the Hamiltonian of the walk we consider the base of eigenstates of σ_z (we also change the notation making $n = z$) and recall equation (6.4) that describes the dynamics of the walk,

$$|\psi(t)\rangle = (\mathrm{Sh}(C \otimes \mathbb{I}))^t |\psi(0)\rangle = Q^t |\psi(0)\rangle . \tag{8.28}$$

The Hamiltonian is associated to the evolution operator by $Q = e^{-iH}$, and therefore we can find an expression for H by taking the logarithm of this expression

$$H = i \log Q = iV \log \Lambda V^{-1}, \tag{8.29}$$

where Λ is the diagonal form of Q and V is the matrix composed of the eigenvalues of Q as its columns. Then the operator responsible for one time step is

$$Q = \mathrm{Sh}(C \otimes \mathbb{I}) = \sum_z \begin{pmatrix} \cos\gamma & \sin\gamma \\ 0 & 0 \end{pmatrix} \otimes |z-1\rangle\langle z| + \begin{pmatrix} 0 & 0 \\ -\sin\gamma & \cos\gamma \end{pmatrix} \otimes |z+1\rangle\langle z| . \tag{8.30}$$

If we use the momentum operators P_z to rewrite the shift operators we find

$$Q = \begin{pmatrix} \cos\gamma e^{-iP_z} & \sin\gamma e^{-iP_z} \\ -\sin\gamma e^{iP_z} & \cos\gamma e^{iP_z} \end{pmatrix}, \tag{8.31}$$

Now, to find the Hamiltonian of the system, the only thing left for us to do is to find the eigenvalues and eigenvectors of Q and use equation (8.29). The eigenvalues are

$$\Lambda = \cos\gamma\cos P_z \pm \sqrt{\cos^2\gamma\cos^2 P_z - 1} = \cos\omega_z \pm i\sin\omega_z = e^{\pm i\omega_z}, \tag{8.32}$$

where we have defined the operator $\cos\omega_z = \cos\gamma\cos P_z$. Hence the matrices $\log\Lambda$, V and V^{-1} are

$$\begin{aligned} \log\Lambda &= \begin{pmatrix} -i\omega_z & 0 \\ 0 & i\omega_z \end{pmatrix} \\ V &= \frac{1}{\sin\gamma e^{iP_z}} \begin{pmatrix} \cos\gamma e^{iP_z} - e^{-i\omega_z} & \cos\gamma e^{iP_z} - e^{i\omega_z} \\ \sin\gamma e^{iP_z} & \sin\gamma e^{iP_z} \end{pmatrix}, \\ V^{-1} &= \frac{1}{2i\sin\omega_z} \begin{pmatrix} \sin\gamma e^{iP_z} & e^{i\omega_z} - \cos\gamma e^{iP_z}, \\ -\sin\gamma e^{iP_z} & -e^{-i\omega_z} + \cos\gamma e^{iP_z} \end{pmatrix}. \end{aligned} \tag{8.33}$$

Finally we can write the Hamiltonian as

$$H = \frac{\omega_z}{\sin\omega_z} \begin{pmatrix} \cos\gamma\sin P_z & -i\sin\gamma e^{-iP_z} \\ -i\sin\gamma e^{iP_z} & -\cos\gamma\sin P_z \end{pmatrix} \tag{8.34}$$

Now we perform the continuous approximations part by part of the Hamiltonian. This is done by studying the effect of the operators $e^{\pm iP_z}$ and $\sin P_z$ on the state $a/b(z,t) = \psi(z,t)$:

$$\begin{aligned}\sin P_z \psi(z,t) &= i\frac{e^{-iP_z} - e^{+iP_z}}{2}\psi(z,t) = \frac{-i}{2}(\psi(z+1,t) - \psi(z-1,t)) \approx -i\frac{\partial\psi(z,t)}{\partial z} \equiv P_z\psi(z,t),\\ e^{\pm iP_z}\psi(z,t) &= \psi(z\pm 1,t) = \psi(z\pm 1,t) - \psi(z,t) + \psi(z,t) \approx \left(\pm\frac{\partial}{\partial z} + 1\right)\psi(z,t).\end{aligned} \tag{8.35}$$

Hence

$$\begin{aligned}\sin P_z &\approx -i\frac{\partial}{\partial z} \equiv P_z,\\ e^{\pm iP_z} &\approx \left(\pm\frac{\partial}{\partial z} + 1\right).\end{aligned} \tag{8.36}$$

Those expressions can be seen as first-order expansions. Ignoring higher order terms in the expansion of $\sin P_z$, we find

$$\frac{\omega_z}{\sin\omega_z} \approx 1. \tag{8.37}$$

Substituting the expansions on (8.34) leads to the following Hamiltonian

$$H = -i\begin{pmatrix}\cos\gamma & \sin\gamma\\ \sin\gamma & -\cos\gamma\end{pmatrix}\frac{\partial}{\partial z} - \begin{pmatrix}0 & -i\\ i & 0\end{pmatrix}\sin\gamma = -i\alpha_z\frac{\partial}{\partial z} + \sin\gamma\beta_z, \tag{8.38}$$

where

$$\begin{aligned}\alpha_z &= \cos\gamma\sigma_z + \sin\gamma\sigma_x;\\ \beta_z &= -\sigma_y.\end{aligned} \tag{8.39}$$

The Dirac Hamiltonian is

$$H_D = -i\hbar c\alpha\frac{\partial}{\partial z} + \beta mc^2, \tag{8.40}$$

where c is the speed of light, m is the mass of the particle and the matrices are Hermitian and satisfy the conditions (8.27). Although α_z and β_z are hermitian and also satisfy (8.27), the comparison would be more consistent if α and β were Pauli matrices. To solve this issue and be able to compare both Hamiltonians, without loss of generality, we can perform a rotation $R_y(\gamma/2) = e^{-i\frac{\gamma}{2}\sigma_y}$

$$\bar{H} = R_y^\dagger(\gamma/2)HR_y(\gamma/2) = -i\sigma_z\frac{\partial}{\partial z} - \sin\gamma\sigma_y. \tag{8.41}$$

Identifying $m = -\sin\gamma$ and $c = 1$ we see that $\bar{H}$ and the Dirac Hamiltonian are identical.

CHAPTER 9

Conclusions

This work can be divided into three main parts that describe the classical, relativistic, and quantum aspects of random walks and Brownian motion. In the first part, we introduced stochastic methods, random walks, Brownian motion, and analyzed the mathematical limit between the simple random walk and the Brownian motion. As mentioned before, the tools introduced in this part of the dissertation have applications in different areas of human knowledge, such as physics, chemistry, biology, mathematics, engineering, and sociology.

The second part of the dissertation concerns the relativistic regime of the Brownian motion. The probability distribution of positions, found by the methods of chapter 3, implies that the Brownian particle has a non-null probability of being outside the light cone, i.e., of having a speed larger than the speed of light. Therefore, the main goal of chapter 4 is to find a probability distribution that is in agreement with the relativistic theory. Finding the PDF that better describes the relativistic Brownian motion has applications in astrophysics, the physics of the early universe, and in the analysis of the collisions of heavy particles.

A natural guess at how to proceed generalizing the Brownian motion to the relativistic regime is to repeat the approach of chapter 2, that is, propose a relativistic random walk and analyze its continuum time limit. Unfortunately, there are two problems with this approach. First, since random walks are mathematical discrete dynamic systems, assign physical properties to it, such as bath temperature, and generalize them does not make much sense. Besides that, it was proved by Dunkel et al. (2006) that it is impossible to find a nontrivial, continuous, relativistic Markov process in Minkowski space.

The restriction that the Markov hypotheses cannot be used is very strong and there are two strategies to overcome the issue. One can try to find a relativistic diffusion non-Markovian propagator in Minkowski space or derive a Markov model in phase space. Regarding the first strategy, we analyzed the telegraph's propagator,

the generalization of the diffusion propagator proposed by Dunkel et al. (2006), and proposed our approach to derive a propagator. The solution to the telegraph equation excludes superluminal positions but implies sharp fronts of particles traveling with the speed of light, therefore we conclude that the propagator derived by the method of maximization of entropy and Dunkel's propagator give the best probability distributions. Both propagators are almost equal, the only difference is the subtraction of a constant term, which is negligible in the range of times that the assumption that the system has maximum entropy is valid. This means that after a transition period of time, when the probability distribution of position of the Brownian particle achieves a stationary regime, our solution is correct, and in accordance with Dunkel's propagator.

The second strategy was to discuss the generalization of Langevin's equation. This approach is useful because the information about the heat bath is less hidden, therefore it can be more easily suited to describe the Brownian motion in different mediums. The Relativistic Langevin equation derived by Dunkel and Hanggi (2005) provides a reasonable distribution of velocities for the Brownian particle and, if Hanggi's discretization rule is considered, it is in accordance with Jüttner's velocity distribution. The microscopic model that considers elastic collisions between the Brownian particle and the molecules of the bath was also analyzed, with other assumptions about the fluid it is immersed in a relativistic Langevin equation can also be derived using the model. Particularly, we made simulations assuming that the interval between the collisions of the Brownian particle is constant and calculated the velocity of the particle after a fixed number of collisions. The results of the simulations provided histograms of probability of finding the particle with certain velocity that are in accordance with Jüttner's distribution as well.

In the last part of the relativistic analyses (chapter 5), we discussed the following connections by analytic continuation

$$\text{Diffusion equation} \longleftrightarrow \text{Schrödinger equation}$$

$$\text{"Relativistic Diffusion equation"} \longleftrightarrow \text{Relativistic Schrödinger equation}$$

$$\text{Telegraph equation} \longleftrightarrow \text{Dirac equation.}$$

We concluded that the methods based on analytic continuation should only be considered as mathematical tools to deal with the simulation of analogous systems and to increase the comprehension of the mathematical resemblances between the three regimes covered in this dissertation.

In the third, and last, part of this work we studied quantum walks – systems that have been of great interest to researchers in the field of quantum computation, because the spread of a quantum walk is faster than the random walk and this makes it an important tool in the development of quantum search algorithms.

First, we analyzed the asymptotic limit of quantum walks, reaching the counter-intuitive conclusion that the Hamiltonian of the reduced coin system depends on the initial conditions. Then we calculated the entanglement entropy and temperature of the two-state quantum walk, discussed the meaning of those variables

and concluded that the entanglement temperature has a thermodynamic meaning, in the sense that, in the asymptotic limit, it is in accordance with the temperature derived assuming that the reduced system of the coin respects a Gibbs distribution. The analysis was extended to the three-state quantum walk. We calculated the Gibbs temperature of the three-state quantum walk and, as expected, this led to an equivalence with the entanglement temperature. This conclusion is in accordance with other results in the literature, Vallejo et al. (2020b); Man'ko and Markovich (2016), and applies to other three-state systems, besides the quantum walk.

The limit between the random and quantum walk in an infinite line was analyzed in chapter 7 using four types of decoherence: Kraus Operators, Unitary Noise, Broken Links, and Periodic measurements. In all four types of decoherences, we showed the transition behavior for the displacement variance and the position distribution of the walk. The study of these types of phenomena is important for two reasons: to deal with the dissipations in real systems (quantum computers), since it is impossible to completely exclude external interaction in real systems, and to control non-unitary evolutions. The original result of this part of the work is the analysis of decoherence in three-state quantum walks. We generalize the models of decoherence by Kraus Operators, Unitary Noise and Broken Links to a three-state system (qutrit) and calculated the probability distribution of the position of the walker for different parameters of decoherence. In all cases, we saw that the introduction of the decoherence causes a transition to classical behavior, but the transitions are different for each model. The most interesting result was obtained by the generalization of the model of broken links. We observed that, in the case where an initial condition that generates localization is considered, the localization is preserved in the system with decoherence.

In the last chapter of the dissertation, we analyzed the mathematical resemblance of the discrete-time quantum walk and Dirac and Klein Gordon equations. Despite being only a revision of the literature, this part was introduced in the dissertation for completeness. In some sense, those results connect the second and third parts of this work, since, because of that connection, quantum walks can be used to simulate a relativistic system.

Bibliography

G. Abal, R. Siri, A. Romanelli, and R. Donangelo. Quantum walk on the line: Entanglement and nonlocal initial conditions. *Physical Review A*, 73, 07 2005. doi: 10.1103/PhysRevA.73.042302.

B. Baeumer, M. Meerschaert, and M. Naber. Stochastic models for relativistic diffusion. *Physical review. E, Statistical, nonlinear, and soft matter physics*, 82:011132, 07 2010. doi: 10.1103/PHYSREVE.82.011132.

M. Bazant. 18.366 random walks and diffusion. fall 2006. https://ocw.mit.edu. License: Creative Commons BY-NC-SA, 2000.

R. Brown. A brief account of the microscopical obsevations made in the mounths of june and july of 1827,on the particles contained in the pollen of plants and on the general existence of active molecules in organic and inorganic bodies. *Edinburg nem Philosophical Journal*, 1828.

H. Callen and G. Horwitz. Relativistic thermodynamics. *American Journal of Physics*, 39, 01 1971. doi: 10.1119/1.1986330.

C. M. Chandrashekar, S. Banerjee, and S. Radhakrishna. Relationship between quantum walk and relativistic quantum mechanics. *Physical Review A*, 81, 07 2010. doi: 10.1103/PhysRevA.81.062340.

A. Childs. Universal computation by quantum walk. *Physical review letters*, 102:180501, 06 2009. doi: 10.1103/PhysRevLett.102.180501.

G. Crispin W. *Hanbook of Stochastic Methods:for Physics, Chemistry and the Natural Sciences*. Springer Series in Synergetics, 1994.

D. Cubero, J. Casado-Pascual, J. Dunkel, P. Talkner, and P. Hanggi. Thermal equilibrium and statistical thermometers in special relativity. *Physical review letters*, 99:170601, 11 2007. doi: 10.1103/PhysRevLett.99.170601.

F. Debbasch. A diffusion process in curved space–time. *Journal of mathematical physics*, 45(7):2744–2760, 2004.

F. Debbasch. Always look back. *Nature Physics*, 5:708–709, 2009.

F. Debbasch, K. Mallick, and J. Rivet. Relativistic ornstein–uhlenbeck process. *Journal of statistical physics*, 88 (3-4):945–966, 1997.

E. Desurvire. *Classical and quantum information theory: an introduction for the telecom scientist*. Cambridge university press, 2009.

J. F. D. Diniz. Implementation of two-dimensional quantum walks = Implementação de passeios quânticos em duas dimensões. Master's thesis, UNICAMP, 2016. URL http://repositorio.unicamp.br/jspui/handle/REPOSIP/305748.

R. M. Dudley. Lorentz-invariant markov processes in relativistic phase space. *Arkiv för Matematik*, 6(3):241–268, 1966.

J. Dunkel. *Relativistic Brownian Motion and Diffusion Processes*. PhD thesis, Universitat Augsburg, 11 2008.

J. Dunkel and P. Hanggi. Theory of relativistic brownian motion: The (1+1)-dimensional case. *Physical review. E, Statistical, nonlinear, and soft matter physics*, 71:016124, 02 2005. doi: 10.1103/PhysRevE.71.016124.

J. Dunkel and P. Hanggi. Relativistic brownian motion. *Physics Reports*, 471:1–73, 02 2009. doi: 10.1016/j.physrep.2008.12.001.

J. Dunkel, P. Talkner, and P. Hanggi. Relativistic diffusion processes and random walk models. *Physical Review D*, 75, 09 2006. doi: 10.1103/PhysRevD.75.043001.

D. Eimerl. On relativistic thermodynamics. *ANNALS OF PHYSICS*, 08 1975.

A. Einstein. On the movement of small particles suspended in stationary liquids required by the molecular-kinetic theory of heat. *Annalen der Physikl*, 1905.

A. Einstein. The collected papers of albert einstein, vol. 2, the swiss years: Writings, 1900–1909 (english translation supplement), 1989.

A. Einstein et al. On the electrodynamics of moving bodies. *Annalen der physik*, 17(10):891–921, 1905.

S. Falkner and S. Boettcher. Weak limit of the 3-state quantum walk on the line. *Physical Review A*, 90, 04 2014. doi: 10.1103/PhysRevA.90.012307.

C. Farías, V. Pinto, and P. Moya. What is the temperature of a moving body? *Scientific Report*, 12 2017. doi: 10.1038/s41598-017-17526-4.

R. P. Feynman, A. R. Hibbs, and D. F. Styer. *Quantum mechanics and path integrals*. Courier Corporation, 2010.

R. P. Feynman, R. B. Leighton, and M. Sands. *The Feynman lectures on physics, Vol. I: The new millennium edition: mainly mechanics, radiation, and heat*, volume 1. Basic books, 2011.

A. Gamba. Physical quantities in different reference systems according to relativit. *American Journal of Physics*, pages 83–89, 05 1966. doi: 10.1119/1.1973974.

J. L. García-Palacios. Introduction to the theory of stochastic processes and brownian motion problems-lecture notes for a graduate course,, 2004.

B. Gaveau, T. Jacobson, M. Kac, and L. S. Schulman. Relativistic extension of the analogy between quantum mechanics and brownian motion. *Phys. Rev. Lett.*, 53:419–422, Jul 1984. doi: 10.1103/PhysRevLett.53.419. URL https://link.aps.org/doi/10.1103/PhysRevLett.53.419.

J. Güémez. Relativistic thermodynamics: A modern 4-vector approach. *Physics Research International*, 2011. doi: 10.1155/2011/387351.

R. Hakim. Relativistic stochastic processes. *Journal of Mathematical Physics*, 9(11):1805–1818, 1968.

P. Hanggi, J. Dunkel, and S. Hilbert. Non-localobservables and light cone-averaging in relativistic thermodynamic. *Nature physics*, pages 741–747, 2009. doi: 10.1038/NPHYS1395.

W. R. Inc. Mathematica, Version 12.1, 2020. URL https://www.wolfram.com/mathematica. Champaign, IL, 2020.

N. Inui, N. Konno, and E. Segawa. One-dimensional three-state quantum walk. *Physical review. E, Statistical, nonlinear, and soft matter physics*, 72:056112, 12 2005. doi: 10.1103/PhysRevE.72.056112.

W. Israel. Nonstationary irreversible thermodynamics: A causal relativistic theory. *ANNALS OF PHYSICS*, pages 310–331, 02 1976.

F. Jüttner. Das maxwellsche gesetz der geschwindigkeitsverteilung in der relativtheorie. *Annalen der Physik*, 339:856 – 882, 03 2006. doi: 10.1002/andp.19113390503.

N. Kampen. Relativistic thermodynamics of moving systems. *Physical Review - PHYS REV X*, 173:295–301, 09 1968. doi: 10.1103/PhysRev.173.295.

N. Kampen. A model for relativistic heat transport. *Physica*, 46, 03 1970. doi: 10.1016/0031-8914(70)90231-4.

V. Kendon. Decoherence can be useful in quantum walks. *Phys. Rev. A*, 67, 04 2003. doi: 10.1103/PhysRevA.67.042315.

V. Kendon. Decoherence in quantum walks - a review. *Mathematical Structures in Computer Science*, 17, 07 2006. doi: 10.1017/S0960129507006354.

T. Kibble. Relativistic transformation laws for thermodynamic variables. *Il Nuovo Cimento B Series 10*, 41:72–78, 10 1966. doi: 10.1007/BF02711119.

G. Kimura and A. Kossakowski. The bloch-vector space for n-level systems: the spherical-coordinate point of view. *Open System Information Dynamics*, 12, 09 2004. doi: 10.1007/s11080-005-0919-y.

G. Landsberg, P.T.and Matsas. The impossibility of a universal relativistic temperature transformation. *Physica A*, pages 92–94, 2004.

P. Landsberg and G. Matsas. Laying the ghost of the relativistic temperature transformation. *Physics Letters A*, 223:401–403, 10 1996. doi: 10.1016/S0375-9601(96)00791-8.

G. F. Lawler and V. Limic. *Random Walk: A Modern Introduction*. Cambridge University Press, 2010.

N. Lovett, S. Cooper, M. Everitt, M. Trevers, and V. Kendon. Universal quantum computation using the discrete time quantum walk. *Physical Review A*, 81, 10 2009. doi: 10.1103/PhysRevA.81.042330.

H. M. Schwartz. Einstein's comprehensive 1907 essay on relativity, part iii. *American Journal of Physics - AMER J PHYS*, 45:899–902, 01 1977. doi: 10.1119/1.10743.

L. Mandel and E. Wolf. *Optical Coherence and Quantum Optics*, volume 1. Cambridge University Press, September 1995.

V. Man'ko and L. Markovich. Entropy - energy inequality for superconducting qutrit. *arXiv preprint arXiv:1608.01821*, 2016.

J. Masoliver and G. Weiss. Finite-velocity diffusion. *European Journal of Physics*, 17:190, 01 1999. doi: 10.1088/0143-0807/17/4/008.

A. Montakhab, M. Ghodrat, and M. Barati. Statistical thermodynamics of a two-dimensional relativistic gas. *Physical review. E, Statistical, nonlinear, and soft matter physics*, 79:031124, 04 2009. doi: 10.1103/PhysRevE.79.031124.

T. K. Nakamura. Three views of a secret in relativistic thermodynamics. *European Physical Journal Progress of Theoretical Physics*, 128:463–475, 2012.

A. Nayak and A. Vishwanath. Quantum walk on the line, 2000.

M. A. Nielsen and I. L. Chuang. *Quantum Computation and Quantum Information*. Cambridge University Press, 2010.

H. Ott. Lorentz-transformation der warme und der temperatur. *European Physical Journal A*, 175:70–104, 02 1963. doi: 10.1007/BF01375397.

M. Ozols and L. Mancinska. Generalized bloch vector and the eigenvalues of a density matrix, Accessed in 08/2020. URL http://home.lu.lv/~sd20008/papers/Bloch%20Vectors%20and%20Eigenvalues.pdf.

M. Planck. Zur dynamic bewegter systeme (on the dynamics of moving systems). sitzungsber. d. kgl. *Preuss. Akad. d. Wissensch*, 1907.

R. Portugal. *Quantum walks and search algorithms*. Springer, 2013.

M. Ramzan and m. k. Khan. Decoherence and entanglement degradation of a qubit-qutrit system in non-inertial frames. *Quantum Information Processing - QUANTUM INF PROCESS*, 11, 01 2011. doi: 10.1007/s11128-011-0257-7.

H. Risken. *The Fokker-Planck Equation: Methods of Solutions and Applications*. Springer Series in Synergetics, 1996.

A. Romanelli. Distribution of chirality in the quantum walk: Markov process and entanglement. *Physical Review A*, 81, 04 2010. doi: 10.1103/PHYSREVA.81.062349.

A. Romanelli. The quantum walk temperature. *arXiv preprint arXiv:1108.5730*, 2011.

A. Romanelli, A. Schifino, R. Siri, G. Abal, A. Auyuanet, and R. Donangelo. Quantum random walk on the line as a markovian process. *Physica A: Statistical Mechanics and its Applications*, 338:395–405, 10 2003. doi: 10.1016/j.physa.2004.02.061.

A. Romanelli, R. Siri, G. Abal, A. Auyuanet, and R. Donangelo. Decoherence in the quantum walk on the line. *Physica A: Statistical Mechanics and its Applications*, 347:137–152, 03 2005. doi: 10.1016/j.physa.2004.08.070.

H. Rudberg. *On the Theory of Relativistic Diffusion/The Compactification of a Lorentz Space Some Remarks on the Foundation of the Theory of Conformal Relativity*. PhD thesis, Almqvist & Wiksell, 1957.

Rudnick and G. Gaspari. *Elements of the Random Walk*. Cambridge University Press, 2004.

G. L. Sewel. On the question of temperature transformations under lorentz and galilei boosts. *JOURNAL OF PHYSICS A: MATHEMATICAL AND THEORETICAL*, 2008. doi: 10.1088/1751-8113/41/38/382003.

D. Shapira, O. Biham, A. Bracken, and M. Hackett. One-dimensional quantum walk with unitary noise. *Physical Review A*, 68, 12 2003. doi: 10.1103/PhysRevA.68.062315.

C. Silberhorn. Integrated Quantum Optics website. Prof. Dr. Christine Silberhorn (Accessed: 2020-07-16)., 2020. URL https://physik.uni-paderborn.de/en/silberhorn/forschung/quantum-networking/quantum-walks.

F. Spitzer. *Principles of Random Walk*. Springer, 1970.

M. Toda, R. Kubo, N. Saitō, N. Hashitsume, et al. *Statistical physics II: nonequilibrium statistical mechanics*, volume 2. Springer Science & Business Media, 1991.

A. Vallejo, A. Romanelli, and R. Donangelo. Out-of-equilibrium quantum thermodynamics in the bloch sphere: Temperature and internal entropy production. *Physical Review E*, 101, 04 2020a. doi: 10.1103/PhysRevE.101.042132.

A. Vallejo, A. Romanelli, and R. Donángelo. Temperature of a finite-dimensional quantum system. *arXiv preprint arXiv:2005.00261*, 2020b.

N. van Kampen. Relativistic thermodynamics of moving systems. *THE PHYSICAL REVIEW*, pages 70–104, 05 1968.

C. Y. Wang. Thermodynamics since einstein. *Advances in Natural Science*, pages 13–17, 2013. doi: 10.3968/j.ans.1715787020120602.2121.

Q. Wang. Action principle and jaynes' guess method. *arXiv preprint cond-mat/0407515*, 2004.

Q. Wang. Maximum path information and the principle of leas action for chaotic systems. *Chaos, Solitons and Fractals, 23(2004)1253*, 2005a.

Q. Wang. Non-quantum uncertainty relations of stochastic dynamics. *Chaos, Solitons and Fractals*, 26:1045–1052, 11 2005b. doi: 10.1016/j.chaos.2005.03.012.

Q. Wang. Maximum entropy change and least action principle for nonequilibrium systems. *Astrophysics and Space Science 305 (3), 273-281*, 2006.

S. Weinberg. *Gravitations and Cosmology: Principles and Applications of the General Theory of Relativity*. Willey, 1972.

N. Wiener. The homogeneous chaos. *American Journal of Mathematics*, 60(4):897–936, 1938.

S. Yuan, M. I. Katsnelson, and H. De Raedt. Origin of the canonical ensemble: thermalization with decoherence. *Journal of the Physical Society of Japan*, 78(9):094003, 2009.

APPENDIX A

Appendix

A.1 Kramers-Moyall Expansion

The Kramers-Moyall expansion, 2.80, has infinite order,

$$\frac{\partial \rho(R,t)}{\partial t} = \sum_{n=1}^{\infty} (-1)^n D_n \frac{\partial^n}{\partial R^n}[\rho_N(R,t)].$$

However, it can be finite if $D_r = 0$ to $r > N$, $N \in \mathbb{N}$. In this section we show that if Kramers-Moyall expansion has finite order, then it has order 1 or 2. To show that we start from Schwarz inequality (Mandel and Wolf (1995)), that states that for any two integers r_1 and r_2,

$$\begin{aligned}\left[\int (\Delta x)^{r_1} (\Delta x)^{r_2} P(x+\Delta x, t+\delta t|x,t) d\Delta x\right]^2 \leq & \int (\Delta x)^{2r_1} P(x+\Delta x, t+\delta t|x,t) d\Delta x \\ & \times \int (\Delta x)^{2r_2} P(x+\Delta x, t+\delta t|x,t) d\Delta x.\end{aligned} \tag{A.1}$$

Using the definition of the coefficients D_r we see that the Schwarz inequality implies that

$$D_{r_1+r_2}^2 \leq D_{2r_1} D_{2r_2}, \tag{A.2}$$

for any r_1, r_2. Therefore if we chose if $r_1 = 1$ and $r_2 = N-1$

$$D_N^2 \leq D_2 D_{2N-2}. \tag{A.3}$$

Suppose that for $r > N$, D_r vanishes. Then the Kramers-Moyall equation becomes a expansion of N order. Particularly if $N \geq 3$, since $2N-2 \geq N+1$, both D_{N+1} and D_{2N-2} vanish. However, from the inequality (A.3) we see that if $D_{2N-2} = 0$, then $D_N = 0$. It follows that if the coefficient $D_N = 0$, then D_{N-1} also vanishes. Repeating

this argument recursively we conclude that all terms of the expansion are zero. Only if $N = 1$ or $N = 2$ the argument breaks down. The conclusion is that the Kramers-Moyall expansion has order 1, 2 or ∞. When $N = 2$ the equation is known as **Fokker-Planck equation**.

A.2 Lagrange Multipliers

The method of Lagrange multipliers is a technique used to find the local extremes (maximum and minimum) of a function subjected to constraints. In other words, the goal of the method is to maximize or minimize a function $f(x_1,...,x_n)$ knowing that $g_i(x_1,...,x_n) = 0$, for $i = 1,...m$, where m is the number of constraints. The Lagrange multipliers method uses the fact that if a direction is perpendicular to all gradients of the constraints than it will also be perpendicular to the gradient of the function.

To demonstrate how to use the method let's take as an example the Shannon entropy of a source $X = (x_1, x_2, ..., x_n)$, Desurvire (2009),

$$S(X) = -\sum_{i=1}^{n} p(x_i) \log p(x_i) \tag{A.4}$$

If we consider the normalization condition, $\sum p(x_i) = 1$, as the only constraint then the method consists in defining the functions f with the parameter λ, known as Lagrangian multipliers

$$f = S(X) + \lambda \sum_i p(x_i). \tag{A.5}$$

To find the extreme value of f we take the derivative with respect to $p(x_i)$

$$\begin{aligned} \frac{df}{dp(x_j)} &= \frac{d}{dp(x_j)} \left(-\sum_i p(x_i) \log p(x_i) + \lambda \sum_i p(x_i) \right) \\ &= -\log p(x_j) - 1 + \lambda = 0 \end{aligned} \tag{A.6}$$

This implies that $p(x_j) = e^{\lambda - 1}$, which is the uniform distribution, since λ is a constant.

If, we wanted two consider another constraint such as the mean value of the distribution, $\sum_i x_i p(x_i) = N$ definition of function f would need to have one more term

$$f = S(X) + \lambda_1 \sum_i p(x_i) + \lambda_2 \sum_i x_i p(x_i). \tag{A.7}$$

Again we take the derivative with respect to $p(x_j)$

$$\begin{aligned} \frac{df}{dp(x_j)} &= \frac{d}{dp(x_j)} \left(-\sum_i p(x_i) \log p(x_i) + \lambda_1 \sum_i p(x_i) + + \lambda_2 \sum_i x_i p(x_i) \right) \\ &= -\log p(x_j) - 1 + \lambda + \lambda_2 x_j = 0 \end{aligned} \tag{A.8}$$

The probability distribution that satisfies this equality is

$$p(x_j) = \frac{e^{\lambda_2 x_j}}{e^{1-\lambda_1}}, \tag{A.9}$$

which under certain circumstances is the Bose Einstein distribution.

A.3 Jüttner Distribution

Because of velocity limit imposed by relativity theory it is clear that Maxwell Boltzmann velocity distribution is not appropriate. One of the first attempts to solve this inconsistency was made by Jüttner Jüttner (2006) in 1911. The method used to derive the distribution was the maximization of Boltzmann entropy,

$$S = K_B \log W. \tag{A.10}$$

K_B is the Boltzmann Constant and W the number of micro-states. The constraints considered on the maximization were the total number of molecules

$$N = \int F dw \tag{A.11}$$

of the gas an the total energy

$$E = mc^2 \int \gamma F dw, \tag{A.12}$$

where F is a distribution function, $dw = dxdydzdv_x dv_y dv_z$, $\gamma = (1 - \dot{\mathbf{r}}^2/c^2)^{-1/2}$, $\mathbf{r} = (x, y, z)$ and $v_x = \dot{x}\gamma$, $v_y = \dot{y}\gamma$, $v_z = \dot{z}\gamma$.

The final expression obtained by Jüttner's for the relativistic generalization of Maxwell velocity distribution was

$$F = \frac{m^d \gamma^{2+d}}{Z} e^{-\beta mc^2 \gamma}. \tag{A.13}$$

with $\beta = \frac{1}{K_B T}$, where T is the temperature.

Figure (A.1) shows the distribution for different masses. The dotted line is the distribution of the heaviest one and the solid of the lightest one. It can be seen that for heavy particles it approximates to Maxwell Boltzmann distribution, while for small masses it approximates to the solution of the wave equation.

Jüttner distribution can also be written in terms of momentum as

$$\frac{1}{Z'} exp[-\beta c\sqrt{m^2c^2 + \mathbf{p}^2}], \tag{A.14}$$

where Z is the normalization constant. Now, if one use the distribution (A.1) to rewrite entropy and calculate $\left(\frac{\partial S}{\partial V}\right)_E = \frac{P}{T}$, we get

$$PV = K_B NT. \tag{A.15}$$

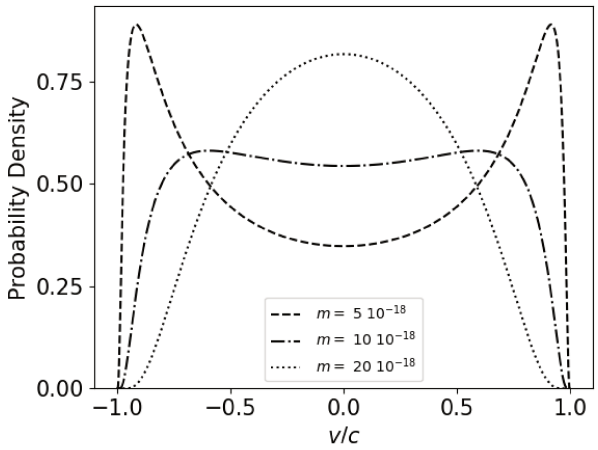

Figure A.1: Jüttner distribution for particles with different masses.

Therefore , for Jüttner, the law of ideal gas remain valid for a relativistic gas.

Another useful result is how probability distribution (A.1) changes for a referential frame that is moving with respect to the lab frame with velocity u. Figure (A.2) depicts this result for several masses values.

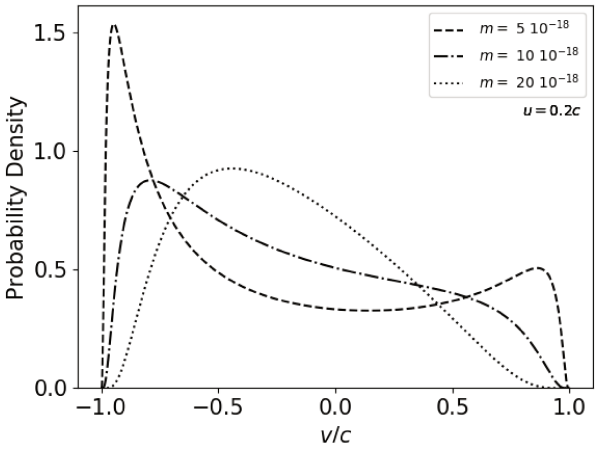

Figure A.2: Jüttner distribution for particles with 9 different masses,on the view point of an observer on a referential frame moving with respect to the lab frame.

As it was already mentioned, Jüttner was one of the first attempts to derive a velocity distribution that is consistent with special relativity impositions. Thereafter other distributions were proposed. However, since molecular-dynamics simulations in one and two dimensions favored Jüttner distribution (Cubero et al. (2007); Montakhab et al. (2009)), in this work consider this as the right one.

A.4 Temperature Transformations

Soon after Einstein et al. (1905) published his article about relativity, questions about how this would affect other areas of physics emerged. In thermodynamics, since we deal with extensive quantities, the adaptation of the theory to a relativistic regime is not trivial. In fact, several authors tried to formulate it - Güémez (2011); Hanggi et al. (2009); Nakamura (2012); Debbasch (2009); Wang (2013) - in different ways, but unfortunately different formulations many times causes contradictory results. For example, how temperature should be redefined on the relativistic regime is a question that still open today -Ott (1963); M. Schwartz (1977); Kibble (1966); Farías et al. (2017); Callen and Horwitz (1971); Eimerl (1975); Israel (1976); van Kampen (1968). Figure (A.3) shows a table made by Nakamura (2012) that summarizes transformation rules proposed in the 1960s.

	P	ΔQ	T	PV/T	E	ΔW
Toleman Pauli Schwars	P_0	$\frac{\Delta Q}{\gamma}$	$\frac{T_0}{\gamma}$	$\frac{P_0V_0}{T_0}$	$\gamma(E_0+v^2P_0V_0)$	$\Delta W_0\gamma^{-1}+\gamma v^2\Delta H_0$
Ott	P_0	$\Delta Q_0\gamma$	$T_0\gamma$	$\frac{P_0V_0}{T_0\gamma^2}$	γE_0	-
Arzelies	P_0	$\Delta Q_0\gamma$	$T_0\gamma$	$\frac{P_0V_0}{T_0\gamma^2}$	γE_0	$\gamma\Delta W_0$
Gamba	-	$\Delta Q_0\gamma$	$T_0\gamma$	-	γE_0	-
Sutcliffe	$P_0\gamma^2$	$\Delta Q_0\gamma$	$T_0\gamma$	$\frac{P_0V_0}{T_0}$	γE_0	-
Børs	-	$\Delta Q_0\gamma$	$T_0\gamma$	-	-	-
Kibble	P_0	$\Delta Q_0\gamma$	$T_0\gamma$	$\frac{P_0V_0}{T_0\gamma^2}$	$\gamma(E_0+v^2P_0V_0)$	$\gamma[\Delta W_0+v^2\Delta(P_0V_0)]$
Penney	P_0	$\frac{\Delta Q}{\gamma}$	$\frac{T_0}{\gamma}$	$\frac{P_0V_0}{T_0}$	-	$\Delta W_0\gamma^{-1}+\gamma v^2\Delta H_0$
Pathria	P_0	$\frac{\Delta Q}{\gamma}$	$\frac{T_0}{\gamma}$	$\frac{P_0V_0}{T_0}$	$\gamma(E_0+v^2P_0V_0)$	-
Landsberg	P_0	-	T_0	$\frac{P_0V_0}{T_0\gamma}$	γE_0	-
Landsberg & Jones	P_0	$\frac{\Delta Q}{\gamma}$	T_0	$\frac{P_0V_0}{T_0\gamma}$	$\gamma(E_0+v^2P_0V_0)$	$\Delta W_0\gamma^{-1}+\gamma v^2\Delta H_0$
	P_0	$\frac{\Delta Q}{\gamma}$	T_0	$\frac{P_0V_0}{T_0\gamma}$	γE_0	$\Delta W_0\gamma^{-1}+\gamma v^2\Delta H_0$

Figure A.3: Transformation rules proposed in the 1960s.

Since our goal here isn't to present arguments in favor of all proposals, we preset only the three following

proposals and arguments with the most historical relevance.

$$T = T_0 \begin{cases} \frac{1}{\gamma}; & \text{Planck and Einstein} \\ 1; & \text{Lansberg and van Kampen} \\ \gamma; & \text{Ott} \end{cases} \tag{A.16}$$

where T_0 is the rest temperature and $\gamma(u) = \dfrac{1}{\sqrt{1-u^2}}$ is the Lorentz factor. In the next sections we consider natural units $c = 1$.

A.4.1 Einstein's result

The approach presented here is based on Einstein's proof of temperature transformation (Einstein (1989); M. Schwartz (1977)). Suppose a system is in rest with respect to the reference frame Σ and moving with velocity v with respect to the reference frame Σ'. The heat supplied, dQ, is given by the total energy increased dE minus the work produced by pressure, $dW = PdV$, and by the increase in momentum,$d\mathbf{p}$:

$$dQ = dE + PdV - \mathbf{v}\cdot\mathbf{dp} = \mathbf{dE} + \mathbf{dW_V}, \tag{A.17}$$

where $dW_V = dW - dW_u$ is the work due to the gas expansion, dW the total work and dW_u the work due to velocity change.

To establish relations between, entropy, heat exchange, and temperature, S, dQ, T on Σ' reference frame with respect to the same quantities on the system rest frame, S_0, dQ_0, T_0, let us consider the cyclic reversible process presented in figure A.4.

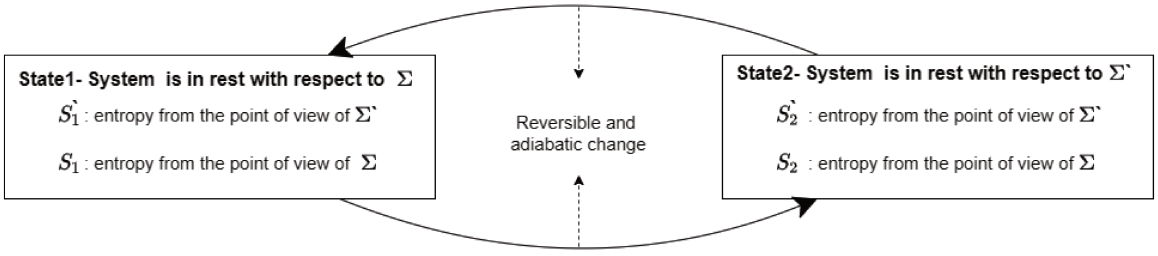

Figure A.4: A cyclic process alternates the system from state 1 to state 2.

The cycle consists of a reversible process taking the body from state 1, where it is in rest with respect to Σ, to the state 2, where it is in rest with respect to Σ' and then the other way around. Since the process is reversible and adiabatic we have that entropy doesn't change either in Σ or in Σ' points of view, i.e.

$$\begin{cases} S_1 = S_2 \\ S_1' = S_2'. \end{cases} \tag{A.18}$$

At this point, to prove that entropy is invariant under change of reference, Einstein cites a verbatim of the work of Planck (1907) where he argues that if we suppose, for example, that $S_1' > S_1$, this would mean that the entropy of a body is bigger for a moving observer. If this is true, then it also must be true that $S_2' < S_2$, but this contradicts equality (A.18). Using an analogous argument supposing $S_1' < S_1$ we find that the only possible alternative is that

$$S_1' = S_1$$

, i. e. $S = S_0$.

Since we are talking about a reversible process, it holds that $dS = \frac{dQ}{T}$, which means that dQ and T have to change according to the same transformation law. To find out such a transformation we substitute on (A.17) the known transformations of p, dV, dE and dp

$$\begin{aligned} P &= P_0 \\ dV &= \frac{dV_0}{\gamma} \\ dE &= \gamma\left[mc^2 + dE_0 + \left(\frac{v}{c}\right)^2 P_0 dV_0\right] \\ dp &= \gamma v\left[m + \left(\frac{dE_0 + P_0 dV_0}{c^2}\right)\right] \end{aligned} \tag{A.19}$$

This leads to

$$dQ = \frac{1}{\gamma}(dE_0 + P_0 dV_0) = \frac{dQ_0}{\gamma}, \tag{A.20}$$

and consequently

$$T = \frac{T_0}{\gamma}. \tag{A.21}$$

Thus, the temperature of a body appears to be **colder** from the point o view of a moving observer.

A.4.2 Ott's result

One of the first attempts to reconsider relativistic thermodynamics after Planck and Einstein's approach was made by Ott (1963) in 1963. In his work he also considered that first (Eq.(A.17)) and second law of thermodynamics are correct for any referential frame. The difference in this approach is that he argued that if the rest energy of a system is E_0, then the amount of work required to accelerate it to a velocity u is

$$d\left[\frac{E_0}{(1-u^2)^{1/2}}\right] = E_0 d\gamma. \tag{A.22}$$

Then he choose the natural extension of the definition of internal energy to be

$$E = \gamma E_0(V_0, P_0). \tag{A.23}$$

Since the work, dW_V, is the work done when the system expands and such work is typically measured as the increase of mechanical energy of a second system, we have that

$$dW_V = \gamma dW_{V0}. \tag{A.24}$$

For the reason explained in the previous section Ott agrees that $S_0 = S$. Therefore T and dQ transform according to the same law. Substituting (A.23) and (A.24) on first law (A.17) we conclude that

$$dQ = \gamma dQ_0 \tag{A.25}$$

And therefore

$$T = \gamma T_0, \tag{A.26}$$

that is, the of a body appears to be **hotter** from the point of view of a moving observer.

A.4.3 Van Kampen's result

In his work, Kampen (1968) argued that the difference between Einstein's and Ott's approaches is that Ott's is valid for the gas inside a box and Einstein's for the gas alone. When the box is at rest these considerations doens't change the result, but for a moving system, it does.

Van Kampen proposed a third form of relativistic thermodynamics by replacing the first Law with a covariant form expressing energy and momentum conservation. Here we summarize his demonstration.

Let $u_\mu = (\gamma; \gamma\mathbf{u})$ be the four-velocity of the system and $E_\mu = u_\mu E_0 = (m\gamma; \gamma m\mathbf{u})$ its energy-momentum four-vector. Then the first law can be replaced by the following covariant equation

$$dQ_\mu = dE_\mu + dW_\mu, \tag{A.27}$$

with dQ_μ being defined as the "thermal energy-momentum transfer". Thus, the "heat supply" is defined as the component of the four vector along the four-velocity $dQ = u_\mu dQ_\mu$. Therefore it is a scalar which implies it is invariant under reference change. The second law, again, implies that the heat supply and temperature have the same transformation law, so the temperature is also invariant.

After demonstrating this result, van Kampen also verifies it for heat transfers between systems with the same velocity (Homotachic) and between systems with different velocities (Heterotachic).

Another interesting proposition that, besides being completely different from this one, also arrive at invariant temperature was derived using Jüttner's velocity distribution by Dunkel (2008). This approach consists in define a microcanonic temperature, τ^{MC} using the mean of $\mathbf{p}\cdot\mathbf{v}$. Considering the Hamiltonian $H = \sum^N (m^2c^4 + \mathbf{p}^2c^2)^{1/2}$ and calculating the mean on the microcanonic ensemble we get

$$< \mathbf{p}\cdot\mathbf{v} > = < p\frac{\partial H}{\partial p} > = \left[\frac{\partial \log\Omega}{\partial e}\right]^{-1} = K_B\tau^{MC}. \tag{A.28}$$

Now considering two relativistic gases in thermodynamic equilibrium, but moving with respect to each other, using the distributions depicted in figures (A.1) and (A.2) to calculate the temperature. The conclusion is that, when defined this way, it is a Lorentz invariant. Figure (A.5) shows this result.

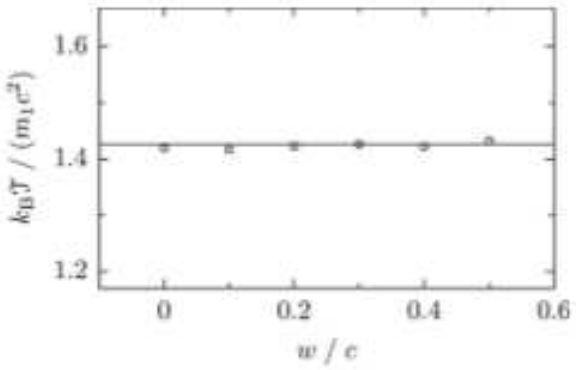

Figure A.5: Microcanonic temperature calculated for different velocities. Figure taken from Dunkel (2008).

A.4.4 Remarks

Although the four-vector formalism, proposed by van Kampen, might look more elegant from the mathematical point of view, this should not be considered as a complete proof that the invariant temperature result is the right one. As showed by Nakamura (2012), a similar formalism can be used to derive all three results.

The main problem of trying to find the right temperature transformation is in the fact that temperature is not well defined in the relativistic regime. This means that some thermodynamic definitions that might seem well established in the rest frame generate ambiguity for moving frames. Here we list some of this ambiguities

- The transfer of heat and work between moving systems implies a transfer of mass, and as a consequence, momentum.
- In the relativistic case the internal energy can't be decomposed in a term of kinetic energy and one term that depends only on the internal state of the gas because the mass also depends on the velocity ($m = m_0\gamma$).
- The definition of three-dimensional volume in the Minkowski space is frame-dependent, therefore the total energy-momentum within the volume depends on the choice of the frame when there is an energy-momentum flow. This difference is relevant when the gas is inside a finite container under pressure Gamba (1966).

All the debate generated by questions such as 'what's the best way to define temperature?' And 'how does the temperature change for a moving observer?' still not a consensus among the researchers.

There are some authors, such as Landsberg (2004); Landsberg and Matsas (1996); Sewel (2008), that defend the idea that there is no universal relativistic temperature transformation. Landsberg's argument for that is that a moving observer in a heat reservoir can't detect a black-body spectrum and hence can't identify a parameter like a temperature. However, this didn't stop researchers from trying to find a transformation to other systems. The problem remains open.

A.5 Path Integrals or Wiener Integrals

The method of path integrals used to sum over all possible paths were first introduced by Norbert Wiener to solve problems related to Brownian motion, Wiener (1938). However, since the Schrodinger equation can be obtained by an analytic continuation of the diffusion equation it is possible to obtain the solution of quantum mechanical problems using an analytic continuation of the method proposed by Wiener. This among other factors made possible to Richard Feynman the creation of a new way of interpreting quantum mechanics, Feynman et al. (2010).

In this section, we give a brief explanation —with an example— of the method of functional integration used to account the integral of a variable over all possible paths that go from a fixed initial point to a fixed final point.

Lets suppose we want to find out the sum of some arbitrary variable , $\phi(x(t))$, over all possibles paths that goes from an initial point x_0 to a final point x_N in the time interval $[t_0, t_N]$. The number of paths from x_0 to x_N are, of course, infinite; however, with the path integral method this calculation is possible. First, we chose a subset of all possible paths by dividing the time interval in small intervals of size $[t_i, t_{i+1}(= \epsilon$ and addressing a point x_i to each t_i, $i = 0, 1, ..., N$. The path is constructed by connecting all the points (x_i, t_i). Then, to define the sum over all paths we integrate over all values of x_i and take the limit of $\epsilon \to 0$, as shown in eq. (A.29)

$$\lim_{\epsilon\to 0}\int\cdots\int\int \phi(x(t))dx_1dx_2\ldots dx_{N-1}, \tag{A.29}$$

the only values of x that are not integrated in are the initial and final point, since both of them are fixed. Figure (A.6) illustrates the procedure of construction of the path integral.

To illustrate the idea of the path integral method we take as an example the integral calculated in section 4.1.3 to find the mean on equation (4.22),

$$A_{AB} = \sum_k p_{AB}(k)A_{AB}(k) = \frac{\sum_k A_{AB}(k)e^{-\eta A_{AB}(k)}}{\sum_k e^{-\eta A_{AB}(k)}} = \frac{M}{Q}, \tag{A.30}$$

where the letter k represents the possible paths. Lets start by calculating the normalization constant, Q,

$$Q = \lim_{\epsilon\to 0}\int\int\cdots\int_{-\infty}^{\infty}\prod_{i=1}^{N}\exp\Big(\frac{-\eta m}{2\epsilon}(x_i - x_{i-1})^2\Big)dx_1dx_2\ldots dx_{N-1} \tag{A.31}$$

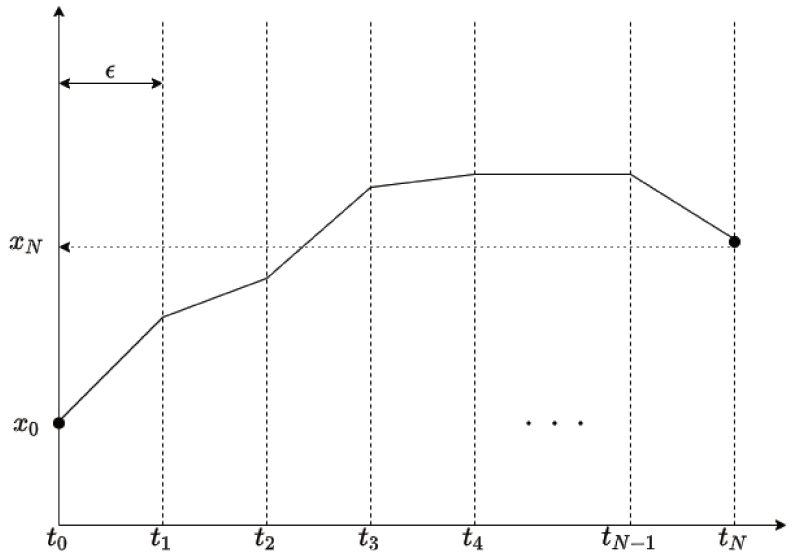

Figure A.6: Illustration of the construction of the idea of path integrals. Time is divided in intervals of size ϵ, then integrate over all possible values of x_i, $i = 1, ..., N-1$, and taking the limit of $\epsilon \to 0$ is the same as summing over all paths.

Since the integral of a Gaussian is also a Gaussian, we may carry out the integrations on one variable after the other. Starting by x_1 we have

$$\int_{-\infty}^{\infty} \exp\left(\frac{-\eta m}{2\epsilon}(x_1 - x_0)^2\right) \exp\left(\frac{-\eta m}{2\epsilon}(x_2 - x_1)^2\right) dx_1 = \sqrt{\frac{\pi\epsilon}{\eta m}} \exp\left(\frac{-\eta m}{2(2\epsilon)}(x_2 - x_0)^2\right) \tag{A.32}$$

Then we have to replace this result on eq. (A.31) and follow with the integral on x_2. After doing this procedure some times is easy to deduce that the result is

$$Q = \lim_{\epsilon \to 0} \left(\frac{2\pi\epsilon}{m\eta}\right)^{\frac{N-1}{2}} \exp\left(\frac{-\eta m}{2(N\epsilon)}(x_N - x_0)^2\right). \tag{A.33}$$

A similar procedure is done to obtain the numerator, M,

$$M = \lim_{\epsilon \to 0} \int\int \cdots \int_{-\infty}^{\infty} \frac{m}{2\epsilon} \left[\sum_{i=1}^{N} (x_i - x_{i-1})\right] \prod_{i=1}^{N} \exp\left(\frac{-\eta m}{2\epsilon}(x_i - x_{i-1})^2\right) dx_1 dx_2 \ldots dx_{N-1} \tag{A.34}$$

After the calculations we find

$$\frac{M}{Q} = \frac{(N-1)}{2\eta} + \frac{m(x_N - x_0)^2}{2(t_N - t_0)}. \tag{A.35}$$

The second term is the least action from x_0 to x_N.

A.6 Stochastic integrals: Itô, Stratonovich and Hänggi dilemma

The Langevin equation presented in section 3 is part of a larger class of stochastic equations of the type

$$\frac{dx}{dt} = a(x,t) + b(x,t)\Gamma(t), \tag{A.36}$$

where $a(x,t)$ and $b(x,t)$ are known functions and Γ is a fluctuation term that obeys the following requirements

$$\langle \Gamma(t) \rangle = 0; \tag{A.37}$$

$$\langle \Gamma(t)\Gamma(t') \rangle = \delta(t = t'). \tag{A.38}$$

This second requirement states that there is no correlation at different times, however it also has the odd implication that the noise has infinite variance. This is, of course, impossible, so we need a model to deal with this noise. The standard way is to interpret the integral of the noise with respect to time as a Wiener process (Crispin W. (1994)), i.e,

$$\int_0^t \Gamma(t')dt' = W(t), \tag{A.39}$$

hence

$$dW(t) = W(t+dt) - W(t) = \Gamma(t)dt. \tag{A.40}$$

Therefore, the solution of the Langevin equations (A.36) would be obtained by integration

$$x(t) - x(0) = \int_0^t a(x,t')dt' + \int_0^t b(x,t')dW(t'). \tag{A.41}$$

The problem with this approach is that $W(t)$ is not differentiable, however we can redefine the integral dW to try to move across this issue. To define the stochastic integral $\int b(x(t'),t')dW(t') = \int b(t')dW(t')$ the same approach as the one used to define usual Riemann integrals is considered. We divide the integration interval $[t_0, t]$ in n part and choose intermediate points, τ_i, as exemplified in figure (A.7)

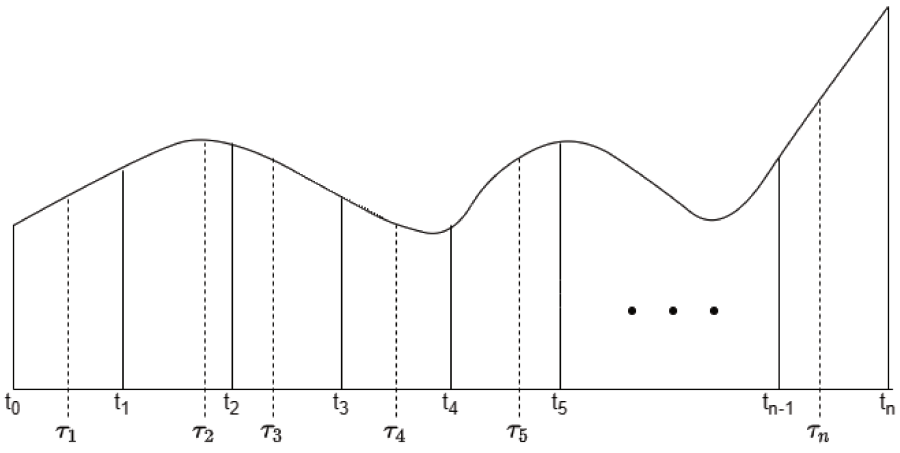

Figure A.7: Diagram of the intervals of integration used to calculate the stochastic integral.

Then the stochastic integral is defined as

$$\int_{t+0}^t b(t')dW(t') = \text{ms} - \lim_{n\to\infty}\left[\sum_{i=1}^n b(\tau_i)(W(t_i) - W(t_{i-1}))\right], \tag{A.42}$$

where ms – lim is the mean square limit that is defined such that

$$\text{ms} - \lim_{n\to\infty} X_n = X \Leftrightarrow \lim_{n\to\infty} \langle (X_n - X)^2 \rangle = 0. \tag{A.43}$$

The dilemma here emerges from the fact that the choice of τ_i can generate different results. While Itô's interpretation is based on a pre-point discretization rule, $\tau_i = t_{i-1}$, i.e,

$$\int_{t+0}^{t} b(t')dW(t') = \text{ms} - \lim_{n\to\infty} \left[\sum_{i=1}^{n} b(t_{i-1})(W(t_i) - W(t_{i-1})) \right], \tag{A.44}$$

Stratonovich's approach considers a midpoint discretization rule, $\tau_i = \dfrac{t_i + t_{i-1}}{2}$, i.e,

$$\int_{t+0}^{t} b(t')dW(t') = \text{ms} - \lim_{n\to\infty} \left[\sum_{i=1}^{n} b((t_i + t_{i-1})/2)(W(t_i) - W(t_{i-1})) \right]. \tag{A.45}$$

Both interpretations lead to the same Fokker-Plank equation for constant b, however if b is not constant the results diverge. Those are the two most common interpretations of the dilemma; Stratonovich's is usually more used in physical procedures while Itô's is usually used in mathematics and financial problems. Another possible interpretation is the one presented on chapter 4, named Hänggi-Klimontovich approach, that is based on a post-point discretization rule, i.e, $\tau_i = t_i$. With this interpretation the definition of the stochastic integral becomes

$$\int_{t+0}^{t} b(t')dW(t') = \text{ms} - \lim_{n\to\infty} \left[\sum_{i=1}^{n} b(t_i)(W(t_i) - W(t_{i-1})) \right]. \tag{A.46}$$

A.7 Simulations of the binary collision models

In sections 3.2 and 4.2.2 we made simulations of the Brownian motion considering the model of binary collisions. The simulations were made in the simplest possible way. On the non-relativistic case, we considered that, at each time step of the simulation, the particle suffers a collision with one of the molecules of the fluid, having it's momentum changed as expressed in equation (3.19). The momentum of the molecule of the fluid that suffers the collision is drawn from Maxwell's distribution. The code used to make the histograms of section 3.2 is presented below.

```
import matplotlib.pyplot as plt
import numpy as np
from scipy import stats

M = 10**(-15)#mass of the molecule of the fluid
m = 10**(-22)#mass of the Brownian particle
a = 100 #(KB*T/m)**0.5
N = 50 #number of collisions
num = 10000 #number of simulations used to make the histogram
```

```
F = []
k = 0

class deterministic_gen(stats.rv_continuous):
    def _pdf(self, v):
        return (np.exp(-(v**2)/(2*a**2))/(a*np.sqrt(2*np.pi)))

Max = deterministic_gen(name="deterministic") # Defining Maxwell's distribution

for particula in range(num):
    Px = [0]
    px = 0
    x = [0]
    print(particula)
    #theta = random([N]) * 2 * np.pi
    for i in range (N):
        if (i > 0):

            v =  Max.rvs()
            px= v * m
            DeltaPx = ((2*M*px) - (Px[i-1]*2*m))/(M+m)
            Px.append(Px[i-1] +DeltaPx)

    #print(Px[i])
    F.append(Px[i]/M)

print(len(F))
(values, bins, _) = plt.hist(F, int(np.sqrt(num)), histtype='step' , color= 'black', lw = 2, density=True)

mean = np.mean(F)
variance = np.var(F)
sigma = np.sqrt(variance)

bin_centers = 0.5*(bins[1:] + bins[:-1])
pdf = stats.norm.pdf(x = bin_centers, loc=mean, scale=sigma) #Compute probability density function
plt.plot(bin_centers, pdf, label="PDF",color='r') #Plot PDF

plt.xlabel('v[m/s]', size = 15)
#plt.ylabel('Occurrences', size = 15)
plt.locator_params(axis='x', nbins=4)
plt.locator_params(axis='y', nbins=4)
plt.xticks(size = 15)
plt.yticks(size = 15)
cur_axes = plt.gca()
#cur_axes.axes.get_yaxis().set_ticks([])

plt.show()
```

Tho run the relativistic simulations, the procedure is very similar, the main differences are that the equation used to quantify the momentum increment at each collision is 4.41 and that the speed of the molecules of the fluid are distributed according with Jüttner's distribution.The code used to make the histograms of section 4.2.2 is presented below.

```
from scipy import stats
import matplotlib.pyplot as plt
import numpy as np
from scipy import special
from scipy import integrate

c = 1
beta = 10
m = 10**(-6)
M = 1
dt = 1

Zd = 2*m*special.kv(1, beta*m) # Normalization constant

def gamma(v):
    return (1/np.sqrt(1 - v ** 2))


class deterministic_gen(stats.rv_continuous):
    def _pdf(self, p):
        return (np.exp(-beta*np.sqrt(m**2 + p**2))/Zd)

J = deterministic_gen(name="deterministic")

N = 100 #Number of collisions
num = 1000 # Number of simulations used to make the histogram
luz = [0]
F = []
for j in range(num):
    print(j)
    Px = []
    px = []
    x = [0]
    e =[]
    E = []
    tempo = [0]

    for i in range(0,N,1):
        if(i == 0):
            Px.append(0)
```

```
        p = J.rvs() #momentum of the molecules of the fluid
        px.append(p)

        E.append(np.sqrt(M**2 + Px[i]**2))
        e.append(np.sqrt(m ** 2 + px[i] ** 2))
        u = (Px[i]+px[i])/(E[i]+e[i])
        DeltaPx = ((-2*(gamma(u)**2)*e[i]*Px[i])+(2*(gamma(u)**2)*E[i]*px[i]))/(E[i]+e[i])
        Px.append(Px[i] + DeltaPx)
        if(Px[i+1] > 0):
            v = 1/np.sqrt(1 + (M/Px[i+1])**2)
        elif(Px[i + 1] < 0):
            v = - 1 / np.sqrt(1 + (M / Px[i + 1]) ** 2)
        x.append(x[i] + v * dt)
        F.append(v)


(values, bins, _) = plt.hist(F, int(np.sqrt(num)), histtype='step' , color= 'black',
lw = 2, density= True, label = ' $\\beta$ = %i' %beta)
plt.legend()
var1 = np.var(F)

M = (M + m)/2

def f(v):
    return (M * (gamma(v) ** 3) * np.exp(-beta *M * gamma(v)))

def m2(v):
    return (M * (gamma(v) ** 3) * np.exp(-beta *M * gamma(v)))*(v**2)

norm, er = integrate.quad(f, -c, c)
var2 = integrate.quad(m2, -c, c)[0] /norm
print(var1,var2)
x = np.arange(-1.1, 1.1, 0.001)
plt.plot(x,f(x)/norm,color='r')
x = np.arange(-1.1, 1.1, 0.001)
plt.plot(x,(2*M * (gamma(x) ** 3) * np.exp(-beta *2*M * gamma(x)))/norm,color='g')

plt.xlabel('v', size = 15)
plt.ylabel('Occurrences', size = 15)
plt.locator_params(axis='x', nbins=4)
plt.locator_params(axis='y', nbins=4)
plt.xticks(size = 15)
plt.yticks(size = 15)

plt.show()
```

A.8 Continuous-time QW

Just like in the discrete case, the continuous quantum walk is also defined using a classical random process as a base. In this case, the definition is based on the continuous-time version of the random walk, i.e, on a continuous-time Markov chain.

The continuous time Markov process can be described by a transition matrix M, such that the probability distribution at time t depend on $M(t)$ and the initial distribution, that is,

$$p(t) = M(t)\,p(0) \tag{A.47}$$

the elements of M are

$$M_{ij}(\epsilon) = \begin{cases} 1 - d_j\gamma\,\epsilon + \mathcal{O}(e^2), \text{ if } i = j; \\ \gamma\,\epsilon + \mathcal{O}(e^2), \text{ if } i \neq j \text{ and adjacent;} \\ 0, \text{ if } i \neq j \text{ and non- adjacent,} \end{cases} \tag{A.48}$$

where γ is the transition rate from vertex x_j to vertex x_i, when the vertexes are neighbors and d_j is the degree of vertex x_j. Since the elements, M_{ij}, are the probabilities of going from x_j to x_i the sum of the elements of a row is 1.

Assuming the initial condition $M(0) = \delta_{ij}$ it is easy to prove, Portugal (2013), that

$$M(t) = e^{-Ht}. \tag{A.49}$$

H is an auxiliary matrix called generating matrix, defined as

$$H_{ij}(\epsilon) = \begin{cases} d_j\gamma \text{ if } i = j; \\ -\gamma, \text{ if } i \neq j \text{ and adjacent;} \\ 0, \text{ if } i \neq j \text{ and non- adjacent.} \end{cases} \tag{A.50}$$

To define the continuous time Quantum Walk we convert the probability distribution to a state vector, $p(t) \to |\psi(t)\rangle$, and the transition matrix to an equivalent unitary, $M \to U$. Looking to equation (A.49) we see that M is not unitary. So to make it be unitary we simply multiply H by the imaginary number i. Therefore

$$U(t) = e^{-iHt}. \tag{A.51}$$

The operator H can be called Hamiltonian with no lost of generality. And the dynamics of the system is described by the equation analogous to (A.47)

$$|\psi(t)\rangle = U(t)\,|\psi(0)\rangle \tag{A.52}$$

Considering the special case of our interest where the graph is an infinity line, than the degree of each vertex is 2 and equation (A.50) becomes

$$H_{ij}(\epsilon) = \begin{cases} 2\gamma \text{ if } i = j; \\ -\gamma, \text{ if } i \neq j \text{ and adjacent;} \\ 0, \text{ if } i \neq j \text{ and non- adjacent.} \end{cases} \tag{A.53}$$

The probability distribution of positions is depicted in figure (A.8), together with a graphic that shows how standard deviation changes with time. It can be observed that as in the discrete case the spread of distribution is ballistic ($\sigma \propto t$), but in this case, the proportionality constant depends on the γ parameter. The results are in accordance with the intuition that a bigger transition rate would imply a faster spread.

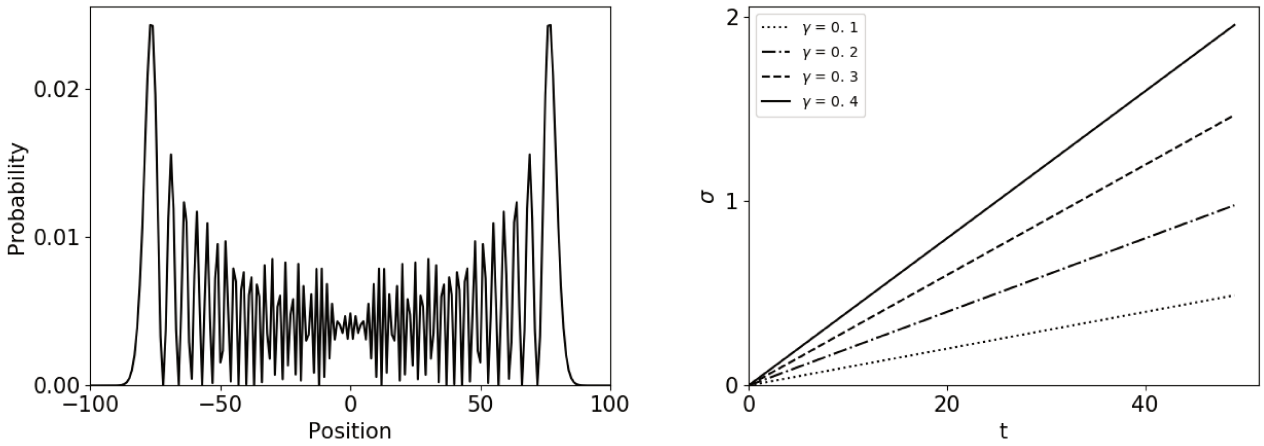

Figure A.8: The probability distribution of positions is displayed at the left side figure. The γ parameter used to calculate this distribution was 0.4. The right side figure depicts the spread of the distributions for different values of transition rate.

The questions that naturally arises at this point usually concerns the differences between discrete and continuous quantum walks. An important difference to point out is that while the first one has a space of dimension $2N$ - N is the number of nodes on the line - the second one has dimension N. This difference is due to the introduction of the coin space in the discrete case. Both distributions have ballistic spread, so both can be used to make quantum algorithms that are faster than the classical ones. On the matter of what would be the best one to use on this search algorithms the answer is not clear to the scientific community yet.

A.9 Gell-Mann matrices

The Gell-Mann matrices are a set of eight linear independent square matrices that together with the Identity span the space of $3x3$ matrices. In physics and information theory, these matrices are usually used as a generalization of the Pauli matrices. The matrices are presented at eq. (A.54), bellow

$$\begin{aligned}
&\lambda_1 = \begin{pmatrix} 0 & 1 & 0 \\ 1 & 0 & 0 \\ 0 & 0 & 0 \end{pmatrix}; \quad \lambda_2 = \begin{pmatrix} 0 & -i & 0 \\ i & 0 & 0 \\ 0 & 0 & 0 \end{pmatrix}; \quad \lambda_3 = \begin{pmatrix} 1 & 0 & 0 \\ 0 & -1 & 0 \\ 0 & 0 & 0 \end{pmatrix}; \quad \lambda_4 = \begin{pmatrix} 0 & 0 & 1 \\ 0 & 0 & 0 \\ 1 & 0 & 0 \end{pmatrix}; \\
&\lambda_5 = \begin{pmatrix} 0 & 0 & -i \\ 0 & 0 & 0 \\ i & 0 & 0 \end{pmatrix}; \quad \lambda_6 = \begin{pmatrix} 0 & 0 & 0 \\ 0 & 0 & 1 \\ 0 & 1 & 0 \end{pmatrix}; \quad \lambda_7 = \begin{pmatrix} 0 & 0 & 0 \\ 0 & 0 & -i \\ 0 & i & 0 \end{pmatrix}; \quad \lambda_8 = \frac{1}{\sqrt{3}} \begin{pmatrix} 1 & 0 & 0 \\ 0 & 1 & 0 \\ 0 & 0 & -2 \end{pmatrix}.
\end{aligned} \tag{A.54}$$

The main features that influenced the choice of this set to be the generalization of the Pauli matrices are that they are Hermitian, traceless and obey the following trace orthonormality condition

$$\mathrm{Tr}(\lambda_i \lambda_j) = 2\delta_{ij}. \tag{A.55}$$

A important property of Gell-Mann matrices, used in the demonstration of equation (6.54), is that commutator relation of two elements of the set is give by

$$[\lambda_1, \lambda_j] = 2i \sum_k f^{ijk} \lambda_k, \tag{A.56}$$

where f^{ijk} are structure constants, asymmetric in all indexes. Most of the constants are null, except from the ones in eq (A.57) and their corresponding permutations

$$\begin{aligned}
&f^{123} = 1 \\
&f^{147} = f^{165} = f^{246} = f^{257} = f^{345} = f^{376} = \frac{1}{2} \\
&f^{458} = f^{678} = \frac{\sqrt{3}}{2}.
\end{aligned} \tag{A.57}$$

A.10 Asymptotic reduced density matrix of the three-state QW

Here we present the asymptotic reduced density matrix of the three-state quantum walk calculated with Wolfram Mathematica, Inc. (2020) with the help of the complement material of Falkner and Boettcher (2014) paper. This matrix was used to calculate the asymptotic results of the three-state quantum walk shown in chapter 6. The reduced density matrix has the following form

$$\rho_{c,\infty} = \begin{pmatrix} \rho_{\infty,11} & \rho_{\infty,12} & \rho_{\infty,13} \\ \rho_{\infty,21} & \rho_{\infty,22} & \rho_{\infty,23} \\ \rho_{\infty,31} & \rho_{\infty,32} & \rho_{\infty,33} \end{pmatrix}. \tag{A.58}$$

where the matrix elements are presented in equation (A.59)

$$
\begin{aligned}
\rho_{\infty,11} &= \frac{1}{48}(((48-11\sqrt{6})a+6(-8+3\sqrt{6})b+(-48+19\sqrt{6})c)a^* \\
&\quad +2(3(-8+3\sqrt{6})a+\sqrt{6}(3b+c))b^* \\
&\quad +((-48+19\sqrt{6})a+\sqrt{6}(2b+5c))c^*) \\
\rho_{\infty,12} &= \frac{1}{24}((3(-8+3\sqrt{6})a+96b-39\sqrt{6}b+144c-59\sqrt{6}c)a^* \\
&\quad +(3*\sqrt{6}a+24b-10\sqrt{6}b+48c-19\sqrt{6}c)b^* \\
&\quad +\sqrt{6}(a-b+c)c^*) \\
\rho_{\infty,13} &= \frac{1}{48}(((-48+19\sqrt{6})a+288b-118\sqrt{6}b+576c-235\sqrt{6}c)a^* \\
&\quad +2(\sqrt{6}a+48b-19\sqrt{6}b+144c-59\sqrt{6}c)b^* \\
&\quad +(5\sqrt{6}a+2\sqrt{6}b-48c+19\sqrt{6}c)c^*) \\
\rho_{\infty,21} &= \frac{1}{24}((3(-8+3\sqrt{6})a+\sqrt{6}(3b+c))a^* \\
&\quad -(-96a+39\sqrt{6}a-24b+10\sqrt{6}b+\sqrt{6}c)b^* \\
&\quad +(144a-59\sqrt{6}a+48b-19\sqrt{6}b+\sqrt{6}c)c^*) \\
\rho_{\infty,22} &= \frac{1}{24}((3\sqrt{6}a+24b-10\sqrt{6}b+48c-19\sqrt{6}c)a^* \\
&\quad +2((12-5\sqrt{6})a-3(-4+\sqrt{6})b+(12-5\sqrt{6})c)b^* \\
&\quad +(48a-19\sqrt{6}a+24b-10\sqrt{6}b+3\sqrt{6}c)c^*) \\
\rho_{\infty,23} &= \frac{1}{24}((\sqrt{6}a+48b-19\sqrt{6}b+144c-59\sqrt{6}c)a^* \\
&\quad -(\sqrt{6}a-24b+10\sqrt{6}b-96c+39\sqrt{6}c)b^* \\
&\quad +(\sqrt{6}a+3\sqrt{6}b-24*c+9\sqrt{6}c)c^*) \\
\rho_{\infty,31} &= \frac{1}{48}(((-48+19\sqrt{6})a+\sqrt{6}(2b+5c))a^* \\
&\quad +2(144a-59\sqrt{6}a+48*b-19\sqrt{6}b+\sqrt{6}c)b^* \\
&\quad +(576a-235\sqrt{6}a+288b-118\sqrt{6}b-48c+19\sqrt{6}c)c^*) \\
\rho_{\infty,32} &= \frac{1}{24}(\sqrt{6}(a-b+c)a^* \\
&\quad +(48a-19\sqrt{6}a+24b-10\sqrt{6}b+3\sqrt{6}c)b^* \\
&\quad +(144a-59\sqrt{6}a+96b-39\sqrt{6}b-24c+9\sqrt{6}c)c^*) \\
\rho_{\infty,33} &= \frac{1}{48}((5\sqrt{6}a+2\sqrt{6}*b-48c+19\sqrt{6}c)a^* \\
&\quad +2(\sqrt{6}a+3\sqrt{6}b-24c+9\sqrt{6}c)b^* \\
&\quad +((-48+19\sqrt{6})a+6(-8+3\sqrt{6})b+(48-11*\sqrt{6})c)c^*)
\end{aligned}
\tag{A.59}
$$

Where a, b and c are the chirality initial conditions

$$|\psi(0)\rangle = \begin{pmatrix} a_n(t) \\ b_n(t) \\ c_n(t) \end{pmatrix} |0\rangle . \tag{A.60}$$

As expected, the matrix is Hermitian and $\mathrm{Tr}(\rho_{c,\infty}) = |a|^2 + |b|^2 + |c|^2 = 1$.